Perturbative QCD in Exclusive Processes

by

Huayi Zhang

Dissertation submitted to the Faculty of the
Virginia Polytechnic Institute and State University
in partial fulfillment of the requirements for the degree of
Doctor of Philosophy
in
Physics

APPROVED:

L. David Roper, Chairman

Lay Nam Chang

Richard A. Arndt

Hsiung Chia Tze

Tetsuro Mizutani

August 18, 1987

Blacksburg, Virginia

Perturbative QCD in Exclusive Processes

by

Huayi Zhang

L. David Roper, Chairman

Physics

(ABSTRACT)

A computer program that symbolically generates and evaluates all Feynman diagrams required for scattering amplitude for exclusive processes is tested, corrected, extended, and brought to operational status. The sensitivity of perturbative QCD predictions for the nucleon form factors, $\psi \to p\bar{p}$, and $\gamma\gamma \to p\bar{p}$, to the theoretical uncertainties of the nucleon wave function and the form of the running coupling constant is investigated. A new prediction for the cross section for $\gamma\gamma \to \Delta^{++}\bar{\Delta}^{++}$ with sum-rule wave functions is presented. As a product of the development of the computer program, the quark amplitudes for meson-baryon scattering are obtained. Integrations of the quark amplitudes over wave functions are carried out by cutting off singularities. The numerical reliability of the integration and its sensitivity to the cut-off's and the choice of wave function are investigated.

Dedicated

in memory of my father and mother.

Acknowledgements

This dissertation has profited from many people: David Roper, Glennys Farrar, Lay Nam Chang, Richard Arndt, Chia Tze, and Tetsuro Mizutani. I would like to thank them all for their support and encouragement and for being my committee members.

Thanks are especially due to David Roper, my adviser, for his generous support in many aspect; to Glennys Farrar for her guidance and collaboration; and to Lay Nam Chang, for his help in almost all areas.

Most of all, I would like thank my loved wife, for her support and concern over the years and for her help both directly and indirectly for this work.

Table of Contents

List of Illustrations

List of Tables

Chapter I

Introduction

The deep inelastic electron-proton scattering [1] has exposed the internal structure of the proton. Once seemingly "elementary" particles, (proton, neutron, for example) were evidently no longer elementary anymore. Instead, they must consist of more fundamental constituents. The parton model [2] was then proposed, which introduced point-like, free particles – partons – as the constituents of hadrons. On the other hand, experiments showed that hadrons were grouped in multiplets, each of which could be characterized by a distinct quantum flavor. The quark model [3] successfully constructed the hadron family, which consists of mesons and baryons, by correctly yielding the multiplets of hadrons and their quantum numbers: electric charge, spin, baryon number, etc.. The diversity of the hadron family was then organized by quarks of several different "flavors" and three "colors".

Flavor is a quantum number that differentiates quark species. It is generally accepted that there are six flavors grouped in three generations, namely, u (up) and d (down); c (charm) and s (strange); b (bottom) and t (top), where the t quark has not been found experimentally. To form a proton,

for example, two u quarks and one d quark are needed, and, by exchanging u and d quarks, a neutron is formed.

Color is the charge of the strong interaction just as the electric charge is the charge of the electromagnetic interaction, except that there are three different types of color charges; namely, red, green, and blue. While the naming of the colors is purely artificial and conventional, the number of the colors is physical and gives the degrees of freedom of the interaction. Just as the photon is the mediator of the electromagnetic interaction, the gluon is the mediator of the strong interaction. One of the differences is that, to mediate strong interactions among three different types of color charges, $3^2 - 1 = 8$ types of gluons are needed. Quantum chromodynamics (QCD) is the theory that describes the interaction among quarks and gluons and is generally believed to be the best available theory of the strong interaction.

QCD, similar to the extremely successful quantum eletrodynamics (QED), is a gauge field theory. In the theory of gauge fields the first principle is the local symmetry of the physical system. A symmetry is said to be local if the system is invariant under a group of transformations that are dependent on space-time, and it is said to be global if the transformation is independent of space-time. There are space-time symmetries and internal *isotopic* symmetries. The Lorentz group is an example of global symmetry of space-time. Physical systems should be invariant under Lorentz transformations as required by the principle of special relativity. For internal symmetries, the invariance under a global U(1) transformation represents, for example, charge conservation. Both space-time symmetry and isotopic symmetry can be local. Local space-time symmetry yielded general relativity, about a half century before the isotopic symmetries were made local and yielded the theory of gauge fields. A globally invariant system is generally not invariant under a certain group of local transformations. To obtain local invariance additional compensating fields have to be introduced. These fields play the role of interacting fields in the theory and are called gauge fields. It should be emphasized that the gauge fields or the interactions are not assumptions inserted

into the theory; instead, they are the natural results of and required by the symmetry principle. Given the symmetry group under which the transformations of system are required to be invariant, gauging the theory then gives the the interactions.

What is then the symmetry group for colors? In order to transform a three-component color state, a 3×3 matrix is required. This leads naturally to the SU(3) group which has a triplet contravariant representation that describes a unitary triplet of particles and a triplet covariant representation that describes a unitary triplet of anti-particles. It should not be any surprise that QCD is just the gauge theory obtained from localizing the SU(3) symmetry. SU(3) is a non-Abelian group because its $3^2 - 1 = 8$ generators (they are 3×3 matrices known as Gell-Mann matrices) do not commute. One of the significant features of non-Abelian groups is that the associated gauge theory is asymptotically free. This is to say, that the effective color charge decreases to zero when the distance goes to zero.

Asymptotic freedom was first discovered by Gross and Wilczek [4] and Politzer [5]. Its derivation from the renormalization group can be found elsewhere in the literature [6]. A field theory usually contains divergences when one or more loops in the Feynman diagrams are encountered. In order to remove the divergences, the theory has to be renormalized. Clearly, a theory is useful only if it is renormalizable. QCD is a such theory. The effective charge, or the coupling constant $\bar{g}^2$, satisfies the equation (see, for example, ref. 6)

$$\frac{d\bar{g}^2}{dt} = \beta(\bar{g})\bar{g}\,, \quad \bar{g}(t=0) = g\,, \quad t = \ln\frac{Q^2}{\mu^2}, \tag{1.1}$$

where $Q^2 = -q^2$ and q is the momentum transfer, which is also frequently referred to as the transverse momentum and denoted by p_t; g is the renormalized coupling constant and μ^2 is the subtraction scale whereby the theory is normalized. Following the renormalization group equations, the function β can be calculated perturbatively:

$$\beta(g) = -\beta_0\frac{g^3}{16\pi^2} - \beta_1\frac{g^5}{(16\pi^2)^2} - \cdots,$$
$$\beta_0 = 11 - \frac{2}{3}n_f, \quad \beta_1 = 102 - \frac{38}{3}n_f, \tag{1.2}$$

where n_f is the number of flavors. It should be pointed out here that a negative $\beta(g)$ is a characteristic of the non-Abelian group and is true for the leading term as long as $n_f < \frac{33}{2} < 17$. Keeping only the leading term of $\beta(g)$, Eq. (1.1) leads to

$$\bar{g}^2(Q^2) = \frac{g^2}{1 + \frac{\beta_0}{16\pi^2}g^2}. \tag{1.3}$$

The plus sign in the denominator reflects the negativity of $\beta(g)$ and ensures that $\bar{g}^2(t \to \infty) \to 0$, i.e., asymptotic freedom. With this discovery, the perturbative method is then permitted for large Q^2.

Introducing a new parameter Λ defined by

$$\Lambda^2 = \mu^2 \exp[-(16\pi^2/\beta_0 g^2)], \tag{1.4}$$

Eq. (1.3) can then be rewritten as

$$\bar{g}^2(Q^2) = \frac{16\pi^2}{\beta_0 \ln(Q^2/\Lambda^2)}. \tag{1.5}$$

Because of the Q^2-dependence, it is commonly referred to as the running coupling constant. Furthermore,

$$\alpha_s(Q^2) \equiv \frac{\bar{g}^2(Q^2)}{4\pi} \tag{1.6}$$

is very often referred to, in place of $\bar{g}^2$, as the running coupling constant. Also it should be noticed that Λ absorbs both μ and g and becomes the only free parameter of the theory.

Perturbative QCD was first applied to inclusive processes such as deep inelastic electron-proton scattering and hadron production from e^+e^- annihilation. The theory gave very good agreement with experiments on scaling violation [7], and the ratio R of the total cross section of hadronic production and the cross section of $\mu^+\mu^-$ production [8]. Only after the discovery of asymptotic freedom, was it realized that a very much wider range of hadronic processes are at least partially calculable by perturbative QCD at short distances or large momentum transfer. Among them are exclusive processes of hadronic magnetic form factors, large angle scattering, strong and electromagnetic decays of heavy quarkonia, etc.. Unlike the inclusive case where the momenta of the final particles are not measured, the asymptotic behavior of the exclusive hadronic processes is governed not only by the short distance perturbative physics, but also by the large distance non-perturbative physics. Experimentally observed hadrons are always color singlets and on the mass shell. The physics underlying the color confinement and the formation of hadrons is non-perturbative since the hadronic size is large compared to the strong interaction range. Therefore, in order to completely predict an exclusive hadronic process, and not just some features such as energy dependence of it, assessments of both the perturbative hard process part and the non-perturbative fragmentation and formation of hadrons are required.

In chapter 2 the procedure of factorization is reviewed. As indicated above, the amplitude of an exclusive hadronic process generally depends on both hard scattering and soft hadron fragmentation and formation. The factorization procedure separates the soft part from the hard part into a factor which can be identified as the quark momentum distribution amplitude or the hadronic wave function and leaves the hard part in a factor called the hard scattering amplitude. The result that emerges from this procedure gives a very simple picture for exclusive processes and makes the calculation possible to any order of the coupling constant. For example, the magnetic form factor of the proton G_M^p is then a product of three factors [9]: the wave function φ of the incident proton, the hard-scattering amplitude T_H for the three quark state scattered by a virtual photon into the final state and the wave function for the final proton φ^*. It can be written as

$$G_M(Q^2) = \int_0^1 d_3x d_3y\, \varphi^*(y, \tilde{Q}_y)\, T_H(x,y,Q)\, \varphi(x, \tilde{Q}_x), \tag{1.7}$$

where $d_3x = dx_1 dx_2 dx_3\, \delta(1 - x_1 - x_2 - x_3)$ and $\tilde{Q}_x = \min(x_i Q)$.

To the leading order of $\alpha_s(Q^2)$ the hard-scattering amplitude T_H is the sum of all Born diagrams, i.e., tree diagrams with the incident and outgoing protons replaced by three free quarks. One of the characteristic of exclusive processes is that the number of diagrams grows factorially as the number of quark lines increases, even at the lowest order. For a relatively simple case $\gamma\gamma \to B\bar{B}$, there are already $\sim$ 1000 diagrams involved in predicting the unpolarized cross section. It has been practically impossible to calculate processes that are more complicated. As part of this research a computer program has been developed which is specialized to generate and evaluate all the Born diagrams for any given process that involves quarks, gluons, and photons. Chapter 3 discusses the development and the applications of the computer program.

Gauge invariance plays a vital role in developing the computer program because, for an amplitude involving a large number of diagrams, it is the most effective means to check the correctness of the calculation. In chapter 4 the theory of gauge fields is reviewed and the Feynman rules for QCD are rederived with the focus on gauge invariance. The implementation of the gauge invariance testing of the computer program is also presented.

Perturbative QCD can only be used to calculate the quark scattering amplitudes. To obtain the physical hadron scattering amplitudes these quark scattering amplitudes must be integrated over the wave functions of the hadrons. Although the asymptotic forms of the meson and baryon wave functions are determined by perturbative QCD, and in the case of pion, the normalization of its asymptotic wave function is determined by its decay constant, at momentum scales relevant for

feasible experiments, both meson and baryon wave functions are determined by non-perturbative physics. Attempts to determine these wave functions from lattice QCD are in their infancy, and, at present, QCD sum rules provide the best determination of these wave functions. The sum rule technique [10] permits determination of a few low moments of the wave functions in terms of non-perturbative quantities such as quark and gluon condensates, which have been fixed in previous applications of the sum rule technique to such problems as the hadron masses and widths. Since only a small number of moments are determined, some further ansatz must be made to fix the wave function. The simplest choice, truncating the wave function as a polynomial of sufficiently low degree that is completely determined by the known moments, yields quite reasonable order-of-magnitude predictions for the nucleon magnetic form factors and the branching ratio of $\psi \to p\bar{p}$. Exploring systematically and quantitatively the sensitivity of the predictions to this assumption is another part of this research. The cross sections for $\gamma\gamma \to \Delta^{++}\bar{\Delta}^{++}$ is predicted with sum-rule derived wave functions [11]. Attempts were also made to improve the wave functions. Chapter 5 discusses this part of the research.

Due to the large number of diagrams, the only exclusive processes for which the quark amplitudes have been calculated to one-loop accuracy are the pion form factor and $\gamma\gamma \to \pi^+\pi^-$. Since processes involving baryons have many more diagrams contributing to the quark scattering amplitude for a given number of loops, for baryons only Born approximations are available. For a long time even this Born approximation was calculated only for relatively simple cases of, e.g., the magnetic form factors, $\psi \to p\bar{p}$, $\gamma\gamma \to B\bar{B}$, and Compton scattering. As a consequence, the dependence of the baryon predictions on Λ_{QCD} is unknown, and one does not know *a priori* what value of the strong coupling should be used at a particular value of the energy and momentum transfer. As still another part of this research, the Λ_{QCD} dependence is studied through the running coupling constant. The sensitivity of the predictions to the choices of running coupling constant is also quantitatively studied and the "best" choice is obtained by a simultaneous fit to the data of the nucleon magnetic form factor and $\psi \to p\bar{p}$. This study is presented in Chapter 6.

In Chapter 7, the calculations of the meson-baryon (MB) scattering amplitudes are presented. Singularities of the quark amplitudes are regulated by cut-off's and integrations are carried out. The sensitivity of the predictions to the cut-off, to the choice of wave functions is studied and the comparison with experiment is discussed. Finally a summary is given in chapter 8 for what has been done and what still needs to be done.

Chapter II

Factorization

Factorization plays an essential role in perturbative QCD. Although asymptotic freedom principally grants the applicability of the perturbative QCD at short distances, the actual calculation for exclusive hadronic processes is made possible and valid only after the hard scattering part is factored out. Consider the example of the pion form factor: A highly virtual photon comes in and is converted into a pair of $q\bar{q}$ pairs moving in opposite directions. In the vicinity of the point where the quarks are produced, the quarks are also of high virtuality. They then lose their virtuality by exchanging gluons and finally evolve into pions. As depicted in Figure 1 on page 10 many gluons can be exchanged between both $q\bar{q}$ pairs. There is no *a priori* way to tell which gluons are hard (those with high virtuality) and which are soft. Therefore, a theoretical method must be developed that systematically separates the perturbative part and the non-perturbative part to any order of the coupling constant g^2. In the inclusive case the Wilson's method of operator expansion gives a rigorous proof [12] that the factorization is valid. In the exclusive case there are various approaches to the question of validity of factorization in the literature. One of the common strategies is to

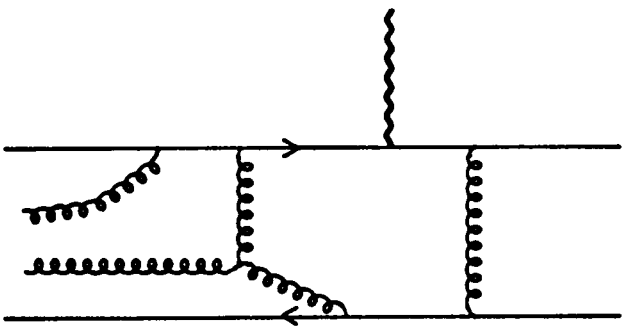

Figure 1. The Meson Form Factor

calculate the exclusive processes perturbatively and then show that the non-perturbative part can be factored out and absorbed into the hadronic wave functions [9]. Another approach is to use operator expansion and renormalization equations [7,13]. There is a third type of approach which has features of the first two [14, 15].

In the following factorization will be discussed by using the third approach. Before proceeding, some discussion on the operator expansion is necessary.

2.1 Operator Expansion

The method of operator expansion was first introduced into particle physics by Wilson [16]. It was successfully used in deep inelastic scattering [12] and other fields. In deep inelastic scattering the fundamental amplitude is

$$W_{\mu\nu} = \frac{1}{4\pi}\sum_{spin}\int d\xi e^{iq\xi} < p|J_\mu(\xi)J_\nu(0)|p > . \tag{2.1}$$

Defining the following variables:

$$\nu = \frac{pq}{M}, \quad \text{and} \quad x = \frac{-q^2}{2\nu M};$$

then in the proton rest frame,

$$p = (M,0,0,0) \quad \text{and} \quad q = (\nu,0,0,\sqrt{\nu^2 - q^2}),$$

where q is the momentum transfer and M is the proton mass. The product that appears in the exponential of Eq. (2.1) is then

$$q\xi \cong \nu(\xi_0 - \xi^3) - Mx\xi_3.$$

In the deep inelastic region, (i.e., $\nu \to \infty$, $-q^2 \to \infty$ and x remains finite) the factor $\exp(iq\xi)$ is rapidly oscillating, so that the significant contribution to the integral of Eq. (2.1) comes only when

$$\xi_0 - \xi_3 = O(\frac{1}{\nu}), \tag{2.2}$$

in other words, in the vicinity of the light-cone.

Following Wilson, the product of currents, $J_\mu(x)J_\nu(y)$, can be expanded as a series of products of local operators in the vicinity of the light-cone:

$$J(x)J(y) \cong \sum_{n,i} C_n^i(\xi)\xi_{\mu 1}\xi_{\mu 2}\ldots\xi_{\mu n}O_i^{\mu_1\mu_2\ldots\mu_n}(R), \tag{2.3}$$

where $\xi = x - y$ and $R = \frac{1}{2}(x + y)$. The superscript i denotes the type of the operator which can be fermion or gluon, singular or non-singular. The operators $O_i^{\mu_1\ldots\mu_n}$ are of definite spin n and the functions C_n^i are coefficient functions of the expansion. In this scheme twist-two operators give dominant contributions, where twist is a quantity that equals dimension minus spin. Contributions from high twist operators are suppressed by powers of Q^2 relative to the twist two operators.

For inclusive processes the operator expansion separates the non-perturbative matrix elements of local operators from the perturbative coefficient functions, and assures that the factorization is valid to all orders of the coupling constant g^2. The Q^2 dependence of the coefficient functions can then be found by using renormalization group equations.

The operator expansion method can also be used in exclusive processes such as hadron form factors. In this case the amplitude to be calculated is $<p|J_\mu|p'>$. In a simplified form, where the spin of the operators are not explicitly given, the current has the following expansion:

$$\begin{aligned} J(0) &= [\overline{\psi}(0)\psi(0)] + g^2\int dz_1 dz_2 [\overline{\psi}\psi]|0><C_1><0|[\overline{\psi}\psi] \\ &+ g^3\int dz_1 dz_2 dz_3 [\overline{\psi}\psi G]|0><C_2><0|[\overline{\psi}\psi] \\ &+ g^4\int dz_1 dz_2 dz_3 dz_4 [\overline{\psi}\psi\overline{\psi}\psi]|0><C_3><0|[\psi\psi\psi] + \ldots \end{aligned} \tag{2.4}$$

The meson form factor, as shown in Figure 1 on page 10, can be written as

$$\begin{aligned} <p|J_\mu|p'> &= \int d^4z_1 d^4z_2 <p|\{\overline{\psi}_a(x)\exp(ig\int_{z_2}^{z_1} d\sigma_\mu G_\mu(\sigma))\psi_\beta(z_2)\}_{ij}|0> \\ &\times T^{ijkl}_{\alpha\beta\gamma\delta} <0|\{\overline{\psi}_\gamma(z_2)\exp(ig\int_0^{z_2} d\sigma_\nu G_\nu(\sigma))\psi_\delta(0)\}_{kl}|p'>, \end{aligned} \tag{2.5}$$

where $T^{ijkl}_{\alpha\beta\gamma\delta}$ is the amplitude of the virtual photon transforming into two $q\overline{q}$ pairs, ψ is the quark field and G is the gluon field. It can be immediately verified that Eq. (2.5) is the second term in the expansion series of Eq. (2.4).

It should be pointed out that Eq. (2.4) shows the method to obtain the corresponding operator expansion for a certain process. As to how operator expansion leads to factorization for hadron form factors, the next section will demonstrate in full detail.

2.2 Verification

Factorization can be made more explicit by taking π^+ as an example and calculate Eq. (2.5). The twist-two local operator that dominants the π^+ form factor is $\gamma_\rho\gamma_5(\overline{d}\gamma_\rho\gamma_5 u)$. Substituting it for the quark field operators $\overline{\psi}\psi$ in Eq. (2.5), the matrix element takes the form:

$$<0|\{\bar{\psi}_\gamma(z_2)\exp(ig\int)\psi_\delta(z_1)\}_{ij}|\pi(p)> \cong \frac{\delta^{ij}}{3}\{-\frac{1}{4}(\gamma_\rho\gamma_5)_{\delta\gamma}<0|\bar{d}\exp(ig\int)\gamma_\rho\gamma_5 u|\pi>\}. \qquad (2.6)$$

By Fourier transformation and some algebra it reduces to

$$\begin{aligned}&<0|\bar{d}(z_2)\exp(ig\int)\gamma_\rho\gamma_5 u(z_1)|\pi(p)> \\ &\quad \cong ip_\rho\int dx_1 dx_2\delta(1-x_1-x_2)\exp[-ix_1(z_1p)-ix_2(z_2p)]\varphi_\pi(x_{1,2}).\end{aligned} \qquad (2.7)$$

With Eq. (2.6-7) and using the Born approximation for $T^{ijkl}_{\alpha\beta\gamma\delta}$, Eq. (2.5) is then reduced to the leading term:

$$<\pi^+(p')|J_\mu(0)|\pi^+(p)> \to \frac{\alpha_s}{Q^2}(p+p')_\mu\int_0^1\varphi_\pi(y)\left[\frac{e_u}{x_2y_2}-\frac{e_d}{x_1y_2}\right]\varphi_\pi(x), \qquad (2.8)$$

with $d_2x = dx_1dx_2\delta(1-x_1-x_2)$. The factorization is now manifest. The question is then to prove the validness of the approximation to any order of α_s.

As was pointed out earlier and depicted in Figure 1 on page 10 in the vicinity of the point where the virtual photon and the pion interact, the $q\bar{q}$ pair has little to do with the final (or initial) pion. The $q\bar{q}$ components continue to interact with each other by exchanging gluons and finally evolves to the final (or initial) pion when its virtuality is decreased from Q^2 to μ^2. This process can be always described by loop corrections of perturbation theory. But the interesting point is whether or not it can be absorbed in the pion wave function and described by the dependence of the wave function on the normalization point[1] $\mu^2_{max} \sim Q^2$.

The answer to the last question, i.e. the question of factorization, is that it is true in perturbative QCD and can be generally proved. What will be demonstrated here however, is an agreement on

[1] The normalization point μ^2 is the cut-off of the integration over internal mementa in the matrix element.

accounting for the evolution of the $q\bar{q}$ pair between direct perturbative loop corrections and absorbing it in the pion wave function, i.e., factorization. If the agreement is achieved at the one loop and two-loop levels, it is strong evidence that the factorization is generally true, and, at least, it is verified up to the two-loop level. This method was used by the authors in the first papers on this approach to the proof of factorization for meson form factors [14].

The claim of factorization, in the case of meson form factor, is

$$Q^2F_\pi(Q^2) \to \alpha(Q^2)\int_0^1 d_2x d_2y \varphi_\pi(y,Q^2)\left[\frac{e_u}{x_2y_2} - \frac{e_d}{x_1y_1}\right]\varphi_\pi(x,Q^2). \tag{2.9}$$

After some rearrangement:

$$\xi = x_1 - x_2, \quad e_u = \frac{2}{3}, \quad e_d = \frac{-1}{3},$$

and also notice that $\varphi_\pi(\xi) = \varphi_\pi(-\xi)$ due to the pion's negative G-parity, Eq. (2.9) yields

$$Q^2F_\pi(Q^2) \sim \alpha_s(Q^2)I_i(Q^2)I_f^*(Q^2), \quad I_i(Q^2) = \int_{-1}^1 \frac{d\xi}{1-\xi^2}\varphi_\pi(\xi,Q^2). \tag{2.10a}$$

Here $\varphi_\pi(x,Q^2)$ is the pion wave function renormalized at the point $\mu^2_{max} \sim Q^2$. Taking $Q^2 = \mu^2$ the Born approximation of Eq. (2.10a) is obtained

$$Q^2F_\pi(Q^2) \to \alpha_s I_i^{Born} I_f^{Born*}, \quad I_i = \int_{-1}^1 \frac{d\xi}{1-\xi^2}\varphi_\pi(\xi), \tag{2.10b}$$

where $\varphi_\pi(\xi) = \varphi_\pi(\xi,Q^2)|_{Q^2=\mu^2}$. In order to make the dependence of the wave function on the normalization point explicit and to compare with the direct loop diagram calculation, the wave function should be expanded into a series of matrix elements of multiplicatively renormalizable local operators O_n. The dependence of the wave function on the normalization point is determined by the renormalization group equations:

$$< O_n >_{Q^2} = < O_n >_{\mu^2} \exp\left[- \int_{\alpha_s(\mu)}^{\alpha_s(Q)} \frac{d\alpha}{\beta(\alpha)} \gamma_n(\alpha) \right]. \tag{2.11}$$

On the base of the Gegenbauer polynomials, $C_n^{3/2}(\xi)$, eigenfunctions of the evolution equation, the expansion is

$$\varphi_\pi(\xi,Q^2) = \varphi_{asy}(\xi) \sum_{n=0}^{\infty} f_\pi^{(n)}(Q^2) C_n^{3/2}(\xi), \tag{2.12}$$

where $\varphi_{asy} = \frac{3}{4}(1 - \xi^2)$ is the wave function in the asymptotic limit. The coefficients $f_\pi^{(n)}$ are the corresponding matrix elements of the local operators O_n. The dependence of $f_\pi^{(n)}(Q^2)$ on Q^2 is given by

$$f_\pi^{(n)}(Q^2) = f_\pi^{(n)}(\mu^2) \exp\left[- \int_{\alpha_s(\mu)}^{\alpha_s(Q)} \frac{d\alpha}{\beta(\alpha)} \gamma_n(\alpha) \right] = f_\pi^{(n)}(\mu) \exp(-\varepsilon_n t), \tag{2.13}$$

$$\varepsilon_n = C_F\left[1 - \frac{2}{(n+1)(n+2)} + \sum_{j=2}^{n+1} \frac{1}{j} \right], \quad \text{and} \quad t = \frac{1}{\beta_0} \ln \frac{\alpha_s(\mu)}{\alpha_s(Q)}.$$

Substituting Eq. (2.12,13) into Eq. (2.10) yields:

$$I_l^{OE}(Q^2) = \frac{3}{4} \sum_{n=0} (1 + (-1)^n) f_\pi^{(n)}(\mu^2) \exp(-\varepsilon_n t), \tag{2.14}$$

where the superscript OE indicates *Operator Expansion.* Expanding $\exp\{-\varepsilon_n t\}$ into a power series in α_s:

$$\exp(-\varepsilon_n t) = \left[\frac{\alpha_s(Q)}{\alpha_s(\mu)} \right]^{\varepsilon_n} \cong \left[1 - \frac{\alpha_s}{4\pi} \beta_0 \ln \frac{Q^2}{\mu^2} \right]^{\varepsilon_n/\beta_0} \cong 1 - \frac{\alpha_s}{4\pi} \varepsilon_n \ln \frac{Q^2}{\mu^2} + \ldots,$$

and collecting all first order terms into f_1^{OE}, and all second order terms into f_2^{OE}, Eq (2.14) yields:

$$I_l^{OE}(Q^2) = I_l^{Born} \left\{ 1 - \left(\frac{\alpha_s}{2\pi} \ln \frac{Q^2}{\mu^2} \right) f_1^{OE} + \frac{1}{2} \left(\frac{\alpha_s}{2\pi} \ln \frac{Q^2}{\mu^2} \right)^2 f_2^{OE} + \ldots \right\}, \tag{2.16}$$

with

$$f_1^{\mathrm{OE}} = C_{\mathrm{F}}\left[x_0 \ln(1-x_0)^{-1} + (1-x_0)\ln x_0^{-1} - \frac{3}{2}\right] \tag{2.17}$$

and

$$f_2^{\mathrm{OE}} = C_{\mathrm{F}}^2 \ln^2(1-x_0)^{-1}\left[1 + O\left(\frac{1}{\ln(1-x_0)}\right)\right]. \tag{2.18}$$

This completes the calculation to the order of α_s^2 relative to the Born approximation by expanding the wave function.

For the direct loop calculation, it has been shown [17] that diagrams contributing terms of $\alpha_s \ln^2 Q^2$, $\alpha_s^2 \ln^4 Q^2$ and $\alpha_s^2 \ln^3 Q^2$ cancel in a sum. The remaining $\alpha_s \ln Q^2$ and $\alpha_s^2 \ln^2 Q^2$ terms are calculated in the following form:

$$F_\pi(Q^2) = F_\pi^{\mathrm{Born}}\left\{1 - \left(\frac{\alpha_s}{2\pi}\ln\frac{Q^2}{\mu^2}\right)\Delta_1(x_0,y_0) + \frac{1}{2}\left(\frac{\alpha_s}{2\pi}\ln\frac{Q^2}{\mu^2}\right)^2\Delta_2(x_0,y_0)\right\} \tag{2.19}$$

Summing over all contributing one-loop diagrams (see Table. 2.1 of reference [18]), one obtains

$$\begin{aligned}\Delta_1 = &\left\{C_{\mathrm{F}}\left[x_0\ln(1-x_0)^{-1} + (1-x_0)\ln x_0^{-1} - \frac{3}{2}\right] + (x_0 \to y_0)\right\} \\ &+ \frac{1}{2}\left[\frac{11}{3}C_{\mathrm{A}} - \frac{2}{3}n_f\right].\end{aligned} \tag{2.20}$$

The number of two-loop diagrams is very large so that only the result is quoted here

$$\Delta_2 = C_{\mathrm{F}}^2\left[\ln(1-x_0)^{-1} + \ln(1-y_0)^{-1}\right]^2\left[1 + O\left(\frac{1}{\ln(1-x_0)}\right)\right]. \tag{2.21}$$

Rearranging Eq. (2.19) in the form

$$F_\pi^{\text{loop}}(Q^2) = F_\pi^{\text{Born}} \frac{\alpha_s(Q^2)}{\alpha_s(\mu^2)} \Psi_i^{\text{loop}}\left(\frac{Q^2}{\mu^2}\right) \Psi_f^{\text{loop}}\left(\frac{Q^2}{\mu^2}\right), \tag{2.22}$$

where "loop" indicates loop calculation and

$$\Psi_i^{\text{loop}}\left(\frac{Q^2}{\mu^2}\right) = 1 - \left(\frac{\alpha_s}{2\pi} \ln \frac{Q^2}{\mu^2}\right) f_1^{\text{loop}}(x_0) + \frac{1}{2}\left(\frac{\alpha_s}{2\pi} \ln \frac{Q^2}{\mu^2}\right)^2 f_2^{\text{loop}}(x_0), \tag{2.23}$$

one obtains

$$f_1^{\text{loop}}(x_0) = C_F\left[x_0 \ln(1 - x_0)^{-1} + (1 - x_0) \ln x_0^{-1} - \frac{3}{2}\right],$$

which agrees with Eq. (2.17), and

$$f_2^{\text{loop}}(x_0) = C_F^2 \ln^2(1 - x_0)^{-1}\left[1 + O\left(\frac{1}{\ln(1 - x_0)}\right)\right],$$

which coincides with Eq. (2.18). Recognizing that $I_i = I_i^{\text{Born}}\Psi_i$ the factorization is, therefore, verified to the two-loop level.

Another observation that can be made is that the Q^2 -dependence of scattering reactions can now be traced to the hard scattering amplitude. It is also obvious now that the contributions of non-valence quarks and gluons are negligible. To turn each constituent of the initial hadron into the direction of the final hadron at least one gluon and one propagator of the constituent are required by the Feynman rule. This gives rise to a factor α_s/Q^2 . For high p_t scattering $Q^2 \to \infty$ so that they do not contribute.

Although the factorization statement Eq. (2.9) is only for the case of the meson form factor, it has been shown [7,9] that it is valid for other exclusive p_t processes as well. Beyond the leading order both quark scattering amplitude T_H and hadronic wave function φ can be calculated to any order

of the coupling constant α_s and Eq. (2.9) holds. Therefore, factorization is indeed valid to any order of α_s.

Chapter III

Calculating the Quark Scattering Amplitude

At large momentum transfer the quark scattering amplitudes of an exclusive hadronic process are calculable in perturbative QCD. They are distinguished by the topology and chiralities of the quarks. Figure 2 on page 21 shows a few examples. The total quark scattering amplitude is a sum of fundamental ones. A set of fundamental quark scattering amplitudes is chosen is such a way that any one in the set can not be obtained from another one in the same set by space rotation, charge conjugation, parity invariance or any other symmetry-transformation. Since QCD does not differentiate between quark flavors, for a given hadronic scattering process and a given hadron multiplet, the set of the fundamental quark scattering amplitudes constitutes a basis for the scattering amplitudes of the multiplet; i.e., the total quark scattering amplitude of any hadron in the multiplet can be expressed as a linear combination of the fundamental ones.

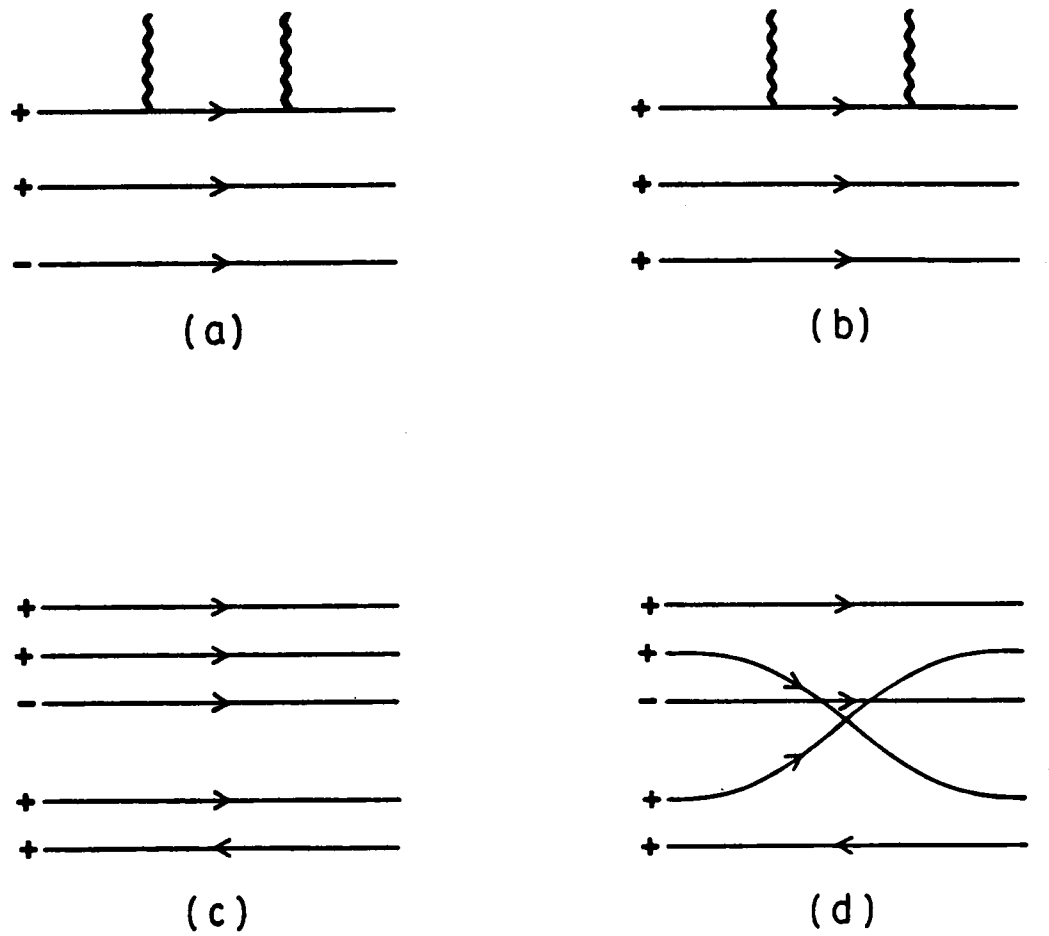

Figure 2. Examples of Quark Scattering Amplitudes: The amplitudes are distinguished by quark chiralities and topology. (a) $\gamma\gamma \to B\overline{B}$ with spin-$\frac{1}{2}$ baryon; (b) $\gamma\gamma \to B\overline{B}$ with spin-$\frac{3}{2}$ baryon; (c) $MB \to MB$ with all quarks going straight through; (d) $MB \to MB$ with one quark exchange.

In the perturbative calculation the lowest-order diagram for meson-baryon (MB) scattering is α_s^4. Thus, a minimum of four gluons is required to connect five quark lines. To find each of the fundamental amplitudes of $O(\alpha_s^4)$, 2,915 diagrams need to be evaluated. For nucleon-nucleon scattering, for which the fundamental quark scattering amplitudes contain six quark lines connected by five gluons, the number of lowest order ($O(\alpha_s^5)$) diagrams increases to 58,149 for each of the fundamental amplitudes. To predict the measurable cross sections for nucleon-nucleon scattering, literally one million diagrams must be taken into account. As the number of the diagrams becomes enormously large the complexity of individual diagrams increases rapidly as well. Such calculation is clearly not practical with traditional techniques, not even with the help of algebraic computer programs like MACSYMA, SMP, REDUCE, etc.. For such a large number of diagrams, not only the evaluation of the Feynman diagrams but also the generation of them should be computerized. A computer program specialized in generating and evaluating all required Feynman diagrams of the lowest order for exclusive hadronic scatterings has been written by Farrar [19]. It was debugged, modified, extended, and brought to operational status for many applications as part of this research. The rest of this chapter presents the development of the computer program, which will be referred to as DIAG hereafter.

3.1 The Original DIAG

Generating and evaluating Feynman diagrams are symbolic and algebraic operations. Traditional scientific computer programming languages, such as FORTRAN which is widely used in numerical calculations are not suitable for symbolic manipulations. On the other hand, symbolic and functional programming languages like LISP and PROLOG are designed for symbolic applications, but they are all lack high computing speed. DIAG is written in the C programming language which is

much more convenient for symbolic manipulation than FORTRAN and is much faster than LISP and the like.

The input to DIAG is a specification of a certain process, described in terms of chiralities and topology of the quarks and external gauge bosons if there are any. DIAG operates in the frame in which the momenta p of the hadrons all have the same magnitude. The center-of-mass (c.m.) frame for any two particles in and two particles out is a such frame, and so is the Breit frame[2] for hadronic form factors. DIAG assumes zero quark mass and evaluates in the Feynman gauge. The output is an analytic expression of the quark scattering amplitude coded as a function in the C language and can be called by other computer programs for, say, numerical integration. The quark scattering amplitude is a function of the scattering angle and momentum fractions of each external quark. Consequently, the C-function of the amplitude takes c, s, x_0, x_1,... as arguments where c and s are *cosine* and *sine* of the half scattering angle and the x_i's are momentum fractions.

DIAG is constituted by several modules. Module *main* reads input, module *gen* generates Feynman diagrams, module *mom* fixes internal momentum in terms of external momenta, module *new* evaluates Feynman diagrams and writes results to output, module *color* computes color factors, modules *u* and *unew* contain various utility functions.

The first key function of DIAG is to generate all possible Feynman diagrams once and only once. It is done by a carefully devised algorithm that generates diagrams in a consistent order. The second one is to compute color factors of diagrams. Cvitanovic's graphic rules [20] for computing color factors is implemented. Finally the last task is to evaluate spin factors of diagrams, i.e., fermion strings consisting of propagators, vertices, and spinors, which are QED Feynman diagrams by

---

[2] In the Breit frame the incident virtual photon and hadron collide head-on and the outgoing hadron moves backward with the same magnitude of momentum as the incident one.

themselves. The old technique for calculating spin factors was to square an amplitude, which is a sum of diagrams, so that a product of spinors is converted to a trace. This method requires evaluating n^2 terms and, therefore, is not suitable for a large number of diagrams. A new technique [19] has been developed for computing the spin algebra. The essentials elements are sketched below:

In the Weyl basis, the 4 × 4 Dirac matrices can be written as

$$-\gamma_5 = \begin{pmatrix} 1 & 0 \\ 0 & -1 \end{pmatrix}, \quad \gamma_0 = \begin{pmatrix} 0 & 1 \\ 1 & 0 \end{pmatrix}, \quad \text{and} \quad \vec{\gamma} = \begin{pmatrix} 0 & -\vec{\sigma} \\ \vec{\sigma} & 0 \end{pmatrix}. \tag{3.1}$$

The two-component spinors $u_\pm$ and γ-matrices $\gamma_\pm$ can then be defined by

$$u = \begin{pmatrix} u_+ \\ u_- \end{pmatrix} \quad \text{and} \quad \gamma_\mu = \begin{pmatrix} 0 & \gamma_{\mu+} \\ \gamma_{\mu-} & 0 \end{pmatrix}, \tag{3.2}$$

so that the subscript + and − acquire the meaning of + and − chirality. Introducing the basis spinors

$$|0> = \begin{pmatrix} 0 \\ 1 \end{pmatrix}, \quad \text{and} \quad |1> = \begin{pmatrix} 1 \\ 0 \end{pmatrix}, \tag{3.3}$$

the 2 × 2 γ-matrices can then be given in terms of the basis spinors

$$\begin{aligned} \gamma_{\mu\pm} = (& [|0><0| + |1><1|], \ \pm [|0><1| + |1><0|], \\ & \pm i\,[|0><1| - |1><0|], \ \mp [|0><0| - |1><1|]\,). \end{aligned} \tag{3.4}$$

Other matrices $\not{\epsilon}_\pm$ and $\not{p}_\pm$ are easy to obtain by using Eq. (3.4). Defining another two spinors by

$$|2> = \begin{pmatrix} -\sin\theta/2 \\ \cos\theta/2 \end{pmatrix}, \quad \text{and} \quad |3> = \begin{pmatrix} \cos\theta/2 \\ \sin\theta/2 \end{pmatrix}, \tag{3.5}$$

and denoting the four scattering directions by the digits 0 to 3 as illustrated in Figure 3 on page 26 all the quantities relevant to computing Feynman diagrams can be expressed in terms of the four spinors as follows:

$$\begin{aligned} u_{0+} &= \sqrt{2E}\,|1>,\ u_{1+} = \sqrt{2E}\,|0>,\quad u_{2+} = \sqrt{2E}\,|3>,\ u_{3+} = \sqrt{2E}\,|2>, \\ u_{0-} &= \sqrt{2E}\,|0>,\ u_{1-} = -\sqrt{2E}\,|1>,\ u_{2-} = \sqrt{2E}\,|2>,\ u_{3-} = -\sqrt{2E}\,|3>, \end{aligned} \tag{3.6a}$$

$$\begin{aligned} \not{p}_{0+} &= \not{p}_{1-} = 2E|1><1|,\ \not{p}_{0-} = \not{p}_{1+} = 2E|0><0|, \\ \not{p}_{2+} &= \not{p}_{3-} = 2E|3><3|,\ \not{p}_{2-} = \not{p}_{3+} = 2E|2><2|, \end{aligned} \tag{3.6b}$$

$$\begin{aligned} \varepsilon^{(0)}_{L\pm} &= \mp\sqrt{2}\,|0><1|,\ \varepsilon^{(0)}_{R\pm} = \mp\sqrt{2}\,|1><0|, \\ \varepsilon^{(1)}_{L\pm} &= \pm\sqrt{2}\,|1><0|,\ \varepsilon^{(1)}_{R\pm} = \pm\sqrt{2}\,|0><1|, \end{aligned} \tag{3.6c}$$

The inner product of spinors are

$$\begin{aligned} &<0|2> = \cos\theta/2,\quad <1|2> = -\sin\theta/2, \\ &<0|3> = \sin\theta/2,\quad <1|3> = \cos\theta/2, \\ &<0|1> = <2|3> = 0. \end{aligned} \tag{3.7}$$

The calculation of spin factors starts from the final spinor u_f, goes up though the fermion line, collects all propagators $\not{p}$ and vertices γ_μ, and finally ends at the initial spinor u_i. In the Weyl representation the product string of u, $\not{p}$, and γ_μ has a two-component form with alternating + and −. It can be generally expressed as

$$u^{\dagger}_{f\pm}\gamma^{\mu_1}_{\mp}\not{p}_{a\pm}\gamma^{\mu_2}_{\mp}\not{p}_{b\pm}\cdots u_{i\pm\,(\mp)}, \tag{3.8}$$

if it contains an even (odd) number of γ-matrices.

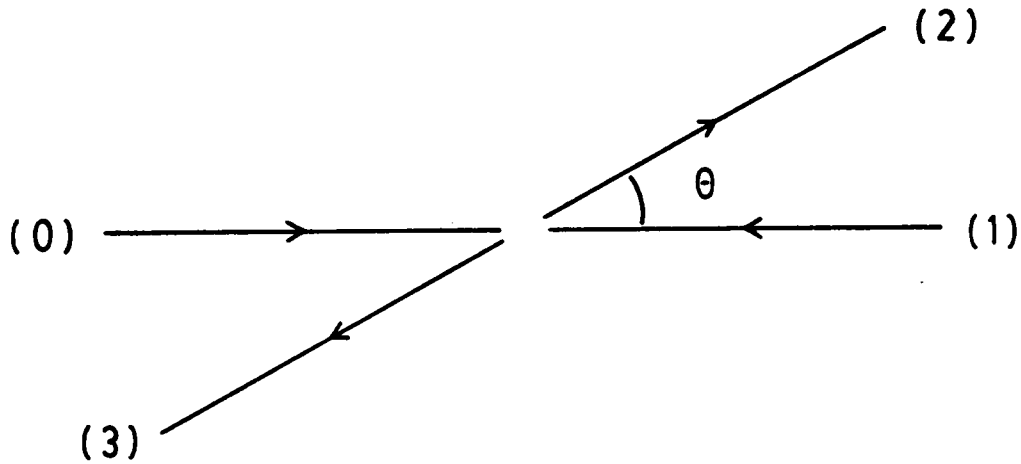

Figure 3. Scattering Directions: In c.m. frame incident particles come in from directions (0) and (1), and scattered into directions (2) and (3) with a c.m. scattering angle θ.

Contractions of γ-matrices with opposite chiralities can be performed by the identity

$$(\gamma_{\mu+})_{ij}(\gamma^{\mu}_{-})_{kl} = 1_{ij}1_{kl} + \vec{\sigma}_{ij}\cdot\vec{\sigma}_{kl} = 2\delta_{il}\delta_{jk}. \tag{3.9}$$

If the contracting γ-matrices are of the same chirality, but attached on different fermion lines, one of them may be charge conjugated as

$$[u^{\uparrow}_{f\pm}\gamma^{\mu_1}_{\mp}p_{a\pm}\cdots\gamma^{\mu_n}_{\mp}u_{i\pm}]^{T} = \tilde{u}^{\uparrow}_{i\pm}\gamma^{\mu_n}_{\pm}\cdots p_{a\mp}\gamma^{\mu_1}_{\pm}\tilde{u}_{f\pm}, \tag{3.10}$$

where $\tilde{u}_{\pm} \equiv i\sigma_2 u^{*}_{\pm}$. Contraction can then be performed in the usual way by using Eq. (3.9).

The ease of utilizing this method is now obvious. Contractions are straightforward to carry out and the rest of the calculation is nothing more than performing inner product for spinors. Furthermore, this technique is most suitable for computer-program implementation because of its simplicity and explicitness. The efficiency of DIAG is largely attributable to this.

DIAG is a complicated program that does complicate calculations. Because of the complexity, the calculation is difficult to be made error-free. Means for checking the correctness of the calculation must be provided. Checking the gauge invariance of the amplitude is a powerful method of such. It is conceivable that the amplitude will not be gauge invariant if there is a factor of 2 missing somewhere and/or a sign is missing. DIAG was provided with U(1) and SU(3) gauge invariance checking capability for processes involving external gauge bosons. The gauge group is U(1) if the gauge boson is a photon and is SU(3) is the gauge boson is a gluon. To check the gauge invariance the polarization vector of a specified gauge boson ε_μ is replaced by its 4-momentum vector k_μ, and the resulting amplitude should be identically zero. This can be easily seen in the U(1) case. Consider a plane wave for the photon, $A_\mu(x) = \varepsilon_\mu e^{-ikx}$. The Lorentz gauge $\partial_\mu A_\mu = 0$ in this case reduces to $k_\mu\varepsilon_\mu = 0$. However, one can still make $A_\mu \to A_\mu - \partial_\mu\chi$ and leave everything unchanged as long as χ satisfies the Klein-Gordon equation $\partial^2\chi = 0$. In the plane wave case, it is equivalent

to the transformation $\varepsilon_\mu \rightarrow \varepsilon_\mu + \beta k_\mu$. Therefore, gauge invariance requires that any amplitude should be vanish if ε_μ is replaced by k_μ .

The first test that DIAG met was checking its correctness in generating diagrams. DIAG performed well. It ran through quark amplitudes of *MB* and *BB* scattering. It took only about one CPU hour on a VAX-11/780 [19] for generating one quark scattering amplitude for $BB \rightarrow BB$. The generated diagrams were extensively checked and no missing nor duplicating diagrams were found.

DIAG was then used to recalculate the quark scattering amplitudes for $\gamma\gamma \rightarrow B\overline{B}$, which were first calculated by another computer program [21]. In order to obtain numerical results that can be compared with either experiment or a previous calculation, the output amplitude file must be compiled. Unfortunately, it was too long to be compiled by the C-compiler on the VAX and some other computers available at Rutgers university [22]. DIAG was then modified to code the output into the FORTRAN language and avoided the compilation difficulty. When the numerical results were obtained, they were found to be in disagreement with the previous calculation. Gauge invariance checking by replacing one of the incident photon's $\not{\varepsilon}$ with its $\not{k}$ also showed that the amplitude was not vanishing. It was concluded then that the calculation of DIAG was wrong since the amplitude it generated failed to reproduce the previous results and was not gauge invariant.

3.2 Debugging DIAG

The C version of DIAG was chosen to be worked with because of *a)* the possible bugs contained in the modified parts for the FORTRAN version can be eliminated, *b*) it is more convenient to

work with only one language, and *c*) the compilation difficulty encountered on the Rutgers VAX may not exist on the VPI&SU VAX and it is always possible to divided the amplitude function into several smaller functions and compile them separately. A simple case $\gamma\gamma \rightarrow M\overline{M}$ was selected with which to begin. It was, indeed, the simplest case of DIAG concern, with only twenty diagrams for each quark scattering amplitude of a given chirality configuration and only one topology of quarks as shown in Figure 4 on page 30.

The amplitude file produced by DIAG was hard to read. As one may expect, computer programs do things in an exactly programmed order. For example, in the evaluation of spin factors of Feynman diagrams, $\not{k}$ for quark propagators is expressed as a linear combination of external quark momenta. The product of two or more quark propagators will expand to many terms. DIAG left the evaluation at this step. Beyond it, common factors may be extracted, similar terms can be combined, relations like $c^2 + s^2 = 1$, $x_0 + x_1 = 1$, and $x_2 + x_3 = 1$ can be substituted, and, best of all, the same factors appearing in both numerator and denominator can be cancelled. These will vastly simplify the amplitude function. As a consequence, it is much easier to read, requires much less disk space and much less computer time to compile, and increases the execution speed and accuracy of numerical calculations. A symbolic simplifier was developed for DIAG, which will be described in detail in section 3.4.

A computer program as large as and as complicated as DIAG inevitably contains bugs. A distinct difficulty of debugging DIAG is that the correctness of the amplitude function is difficult to check because of the large number of diagrams involved. DIAG is aimed at scattering processes that are effectively impossible to be calculated by hand, so that it is effectively impossible to be completely checked by hand as well. Even when an amplitude function produced by DIAG is known to be incorrect, it is still difficult to locate the diagrams that cause the problem.

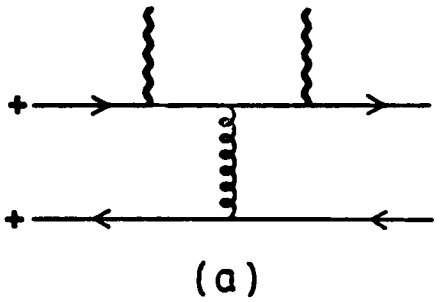

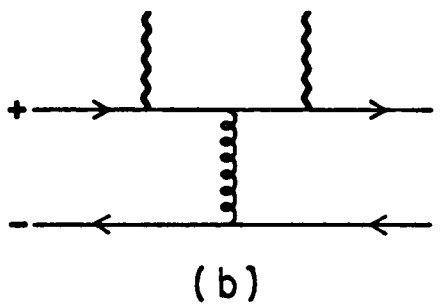

Figure 4. Fundamental Amplitudes of Photon Annihilation to Meson Pairs: Two fundamental quark scattering amplitudes for $\gamma\gamma \rightarrow M\bar{M}$ for (a) spin-0 mesons and (b) spin-1 mesons.

The strategy of checking for the correctness of the outcome of DIAG consists of three good methods. The first one is to start the checking from the simplest scattering case and moving up step by step. In general, functional parts of DIAG involved in lower-level scattering cases will be involved in higher-level cases, but it is not true *vice versa*. For example, $\gamma\gamma \rightarrow M\overline{M}$ involves the simplest manipulation, e.g., spinor inner product, contraction, charge conjugation, etc.. One level up, the process $\gamma\gamma \rightarrow B\overline{B}$ requires all the above and in addition, a spinor can be charge conjugated more than once. The three-gluon vertices already exist at this level, but they do not contribute because the color factor for these diagrams vanishes. For $MM \rightarrow MM$, not only diagrams with single three-gluon vertices, but also diagrams containing double three-gluon vertices and four-gluon vertices contribute. Beyond that, diagrams involving triple three-gluon vertices and single three-gluon plus single four-gluon vertex are encountered in $MB \rightarrow MB$. Finally in the $BB \rightarrow BB$ case, diagrams with quadruple three-gluon vertices, double four-gluon vertices, and a mix of three- and four-gluon vertices are involved. By working with DIAG step by step efforts can be concentrated in the program sections that are functioning in the current step but not before.

The second error-checking method of the strategy is to selectively check diagrams by hand. This is always the most reliable way to check but is also the most limited. With the first part of the strategy, however, it is suffice to do most of the hand checking for the diagrams that possess the new features of the step.

The last error-checking method is to utilize gauge invariance and the various symmetries of a given process. For example, in the $MM \rightarrow MM$ case some quark scattering amplitudes can be obtained from others by exchanging t and s where $t = (p'_1 - p_1)^2$, and $s = (p_1 + p_2)^2$ where p_1 and p_2 are momenta of the incident particles in the c.m. frame and p'_1 and p'_2 are momenta of the outgoing particles. DIAG is equipped with U(1) and SU(3) gauge invariance checking capabilities for external gauge bosons. It may be the most powerful method, although not conclusive. But for photonless scattering reactions, this type of gauge invariance checking does not apply. In order to

bring the powerful checking tool to reactions with no external gauge bosons another type of SU(3) gauge invariance testing was built into DIAG. In an arbitrary covariant gauge, the gluon propagator takes the form $(g_{\mu\nu} - \xi\frac{k_\mu k_\nu}{k^2})/k^2$ instead of $g_{\mu\nu}/k^2$ where ξ is referred to as the gauge parameter. The amplitude can then be expressed as a polynomial in ξ, with the highest order equal to the maximum number of gluon propagators that can be contained in a diagram. Gauge invariance requires that all terms vanish as a sum order by order in ξ except the zeroth order. This development is described in chapter 4.

When a certain amplitude is concluded to be wrong either because of its failure to reproduce the published results or its violation of gauge invariance, locating the bugs requires considerable effort. For cases as simple as $\gamma\gamma \to M\overline{M}$, the best way to locate bugs is to do hand calculations diagram by diagram until the bug is discovered. For cases as complicated as $\gamma\gamma \to B\overline{B}$ and up it is only practical to apply hand checking to a small selection of diagrams which represent new characteristics of the process. A better way to locate bugs utilizes gauge invariance checking. The amplitude produced in gauge testing mode should be identically zero. The cancellation of diagrams usually takes place within a small group of several diagrams. By checking cancellation group by group the bug can be located when cancellation fails to occur. This method, however, is also impractical without the assistance of the computer. For the case of $MB \to MB$, the amplitude for gauge testing can occupy one megabytes (one million characters) of disk space even after simplification. Two computer programs were developed to perform the cancellation task. The first one goes through the amplitude file and performs pair cancellation automatically. An amplitude file of one MBytes can be reduced to about 300 KBytes after pair cancellation. The second one then performs group cancellation with some human assistance. This method also enables the verification of the analytical zero of the gauge testing amplitude.

Some relatively simple hadronic scattering processes have been calculated in the literature. Among them are, $\gamma\gamma \to M\overline{M}$ [23], $\gamma\gamma \to B\overline{B}$ [21], meson form factors [15] and baryon form factors [9,24].

For the $\gamma\gamma \to M\overline{M}$ case, DIAG did not reproduce the published results. With the simplified amplitude and by direct hand checking a missing sign was found in the inner product of a certain pair of spinors. For the $\gamma\gamma \to B\overline{B}$ case, DIAG did not agree with the previous calculation either. By the methods described above another missing sign was located when a spinor was charge conjugated twice. The simplified amplitude file for $\gamma\gamma \to B\overline{B}$ is about 15 KBytes in size. The VAX C compiler on the VPI&SU VAX compiled it flawlessly. It also compiled the unsimplified amplitude file, which is 100 KBytes in size, with no difficulties. After correcting the bugs, both cases agreed with the previous calculations and both were gauge invariant under U(1) for external photons and SU(3) for gluon propagators.

The $MM \to MM$ scattering is the least complicated process that involves three- and four-gluon vertices and has not be calculated before. Some of the diagrams are shown in Figure 5 on page 34. Furthermore, the functional parts of DIAG that are responsible for three- and four-gluon vertex evaluation hadnot been checked nor tested after DIAG was originally written. There were some apparent errors in the code. After correcting these errors, gauge invariance testing showed that the amplitude was not gauge invariant. Because of a mistake that was made in both the program coding and the hand calculation the bug was not discovered, though a considerable portion of the diagrams were checked. However, it must be related to the three-gluon vertex because the amplitudes not containing three-gluon vertices are indeed SU(3) gauge invariant. Finally, it was observed by the cancellation method that adding a factor 2 to diagrams containing double three-gluon vertices would satisfy gauge invariance. An unwanted factor $\frac{1}{2}$ was then found.

The diagrams for $MM \to MM$ can contain at most five gluon propagators; Figure 5 on page 34 gives such an example. Therefore, in an arbitrary covariant gauge, the amplitude is a polynomial in ξ of order five. For the reason which will be made clear in chapter 4, only the linear term of ξ is nontrivial. Thus, gauge invariance is verified to the first order in ξ for $MM \to MM$.

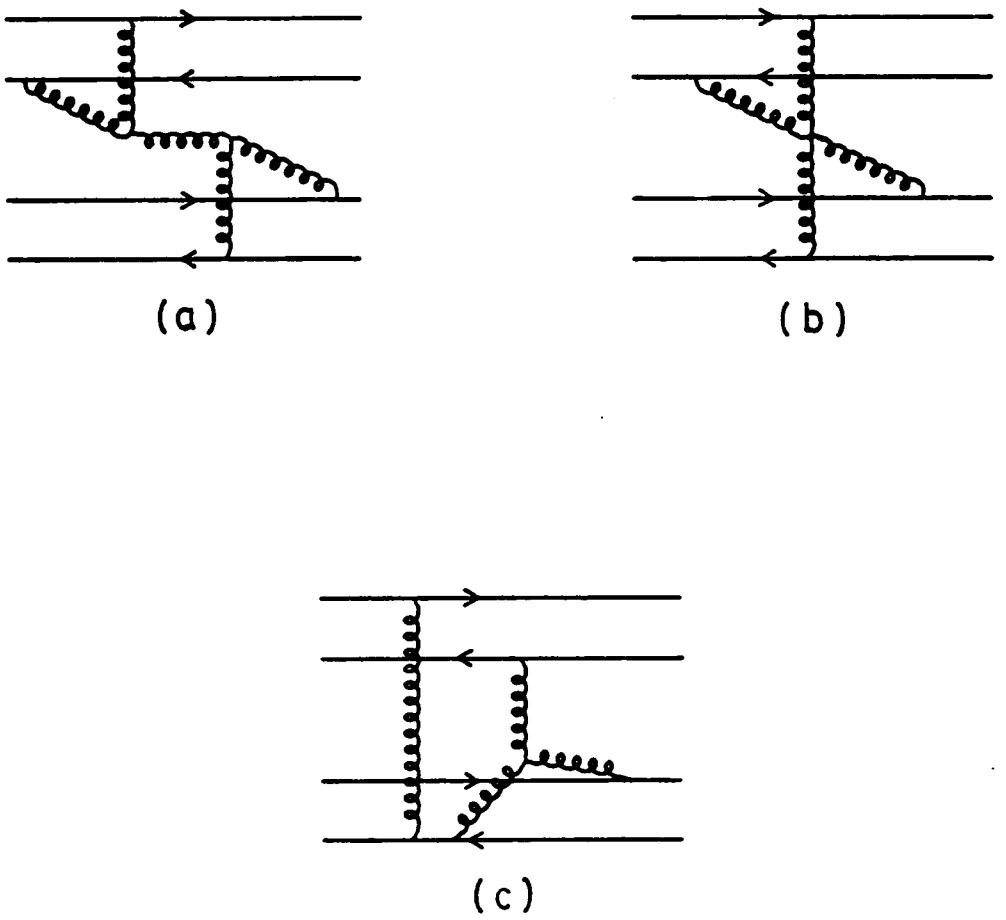

Figure 5. Multi-Gluon Vertices in Meson-Meson Scattering: Both three- and four-gluon vertices contribute in $MM \rightarrow MM$. (a) double three-gluon vertex; (b) single four-gluon vertex; (c) single three-gluon vertices.

There are only two fundamental quark scattering amplitudes for the scalar MM as shown in Figure 6(a). All the others can be obtained from symmetry considerations. Figure 6(b) illustrates a nontrivial example in which t and s are exchanged and the straight through case is transformed to the double annihilation case. It is achieved by making the following transformations:

$$\begin{aligned} &s^2 \to \frac{1}{s^2};\quad c^2 \to 1 - \frac{1}{s^2} = -\frac{c^2}{s^2}; \\ &u \to u;\quad t \to s = -\frac{t}{s^2};\quad s \to t = -s \times s^2; \end{aligned} \tag{3.11}$$

and renaming $x_2 \rightleftarrows x_3$ and $x_3 \rightleftarrows x_4$, where c and s are *cosine* and *sine* of the half scattering angle. On the other hand, the double annihilation case can be directly calculated. The agreement between the transformation and the direct calculation is another indication that the calculation is correct. The correctness of $MM \to MM$ is then supported by gauge invariance, $t \rightleftarrows s$ symmetry, and many hand evaluations of the diagrams. There were no compilation problems at this stage either.

Although $MB \to MB$ scattering involves only one more quark line than $MM \to MM$ scattering, the complexity for $MB \to MB$ increases from several ten's to one hundred times as much as for $MM \to MM$. The size of amplitude files becomes very large and much more computer time and disk space are required to work with them. For the purpose of performing cancellation, the simplifier expresses each term in a single line in the amplitude file. A term is equivalent to a diagram if the diagram has no multi-gluon vertices. A multi-gluon-vertex diagram, on the other hand, will expand to several terms. In the case of $MB \to MB$ some of the lines of the amplitude file get so long that they exceed the size of the memory buffer of all the system editors. As a result, whenever an operation on the amplitude file is needed, a program must be developed to serve the purpose. For instance, in order to compile the amplitude file it must first be cut into several pieces, since the size of it exceeds the limit that the compiler can accept, and next, all the lines that are longer than the system buffer must be wrapped.

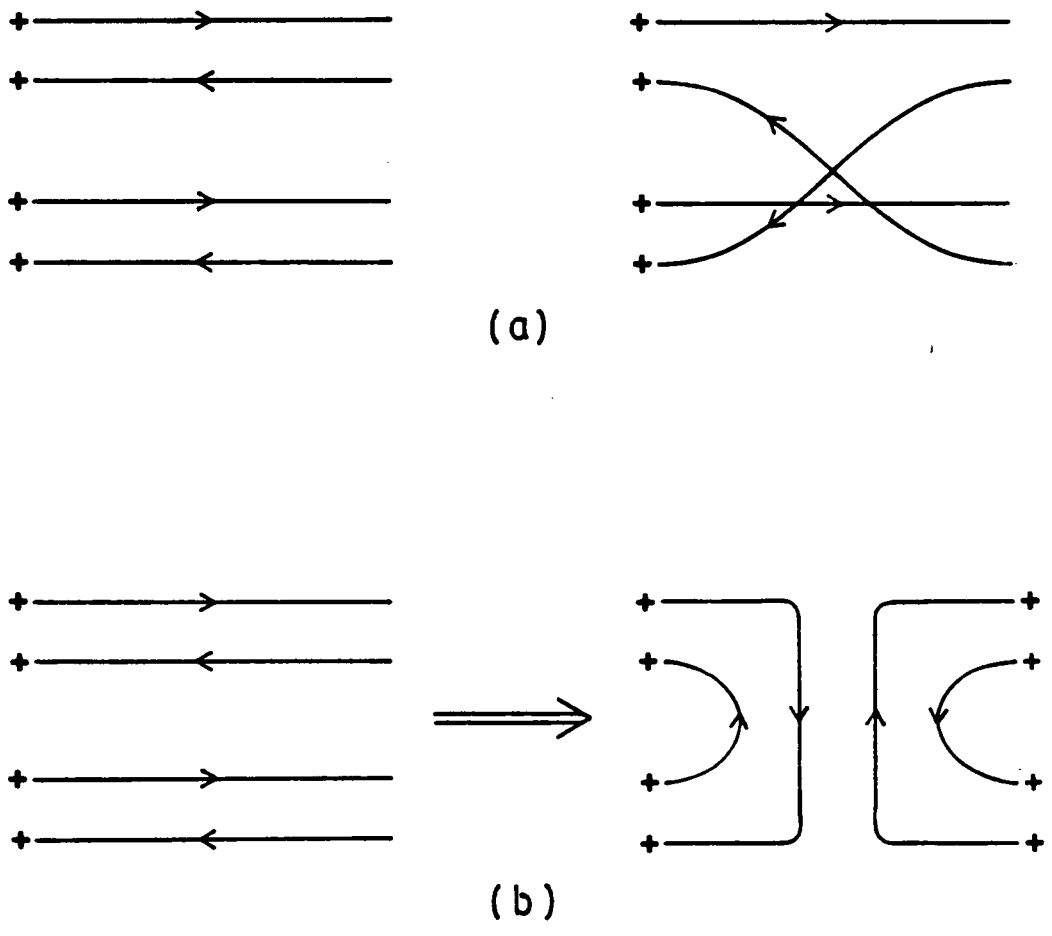

Figure 6. Fundamental Amplitudes of Meson-Meson Scattering: (a) Fundamental quark scattering amplitudes for scalar MM scattering; (b) transformation from straight-through case to double-annihilation case.

As depicted in Figure 7 on page 38, $MB \rightarrow MB$ has fifteen fundamental quark scattering amplitudes. Numerical verification showed that the amplitude A_0 was gauge invariant but amplitudes A_2 and A_4 were not. It is puzzling because DIAG works in exactly the same way for all quark topologies. By using the cancellation method the bug was located in the triple-gluon vertex evaluation. It was then discovered that all diagrams containing triple three-gluon vertices do not contribute to A_0. In contrast to $MM \rightarrow MM$, the ξ^2 term for $MB \rightarrow MB$ is also nontrivial in addition to the linear term in the ξ gauge. Therefore, gauge invariance is verified to the second order in ξ.

The correctness of diagram generating was again checked for diagrams involving more than one multi-gluon vertex, since they are the most confusing diagrams in the generating process. The correctness was confirmed.

Debugging DIAG and its applications do not end here. For the most complicated hadronic reaction $BB \rightarrow BB$, more multi-gluon vertices will get involved, especially the diagrams containing double four-gluon vertices. This is still a new territory for DIAG. Another new territory for DIAG is reactions with external gluballs and the SU(3) gauge invariance testing associated with it. Both of the applications are very interesting both experimentally and theoretically, but they will not be part of the research presented here.

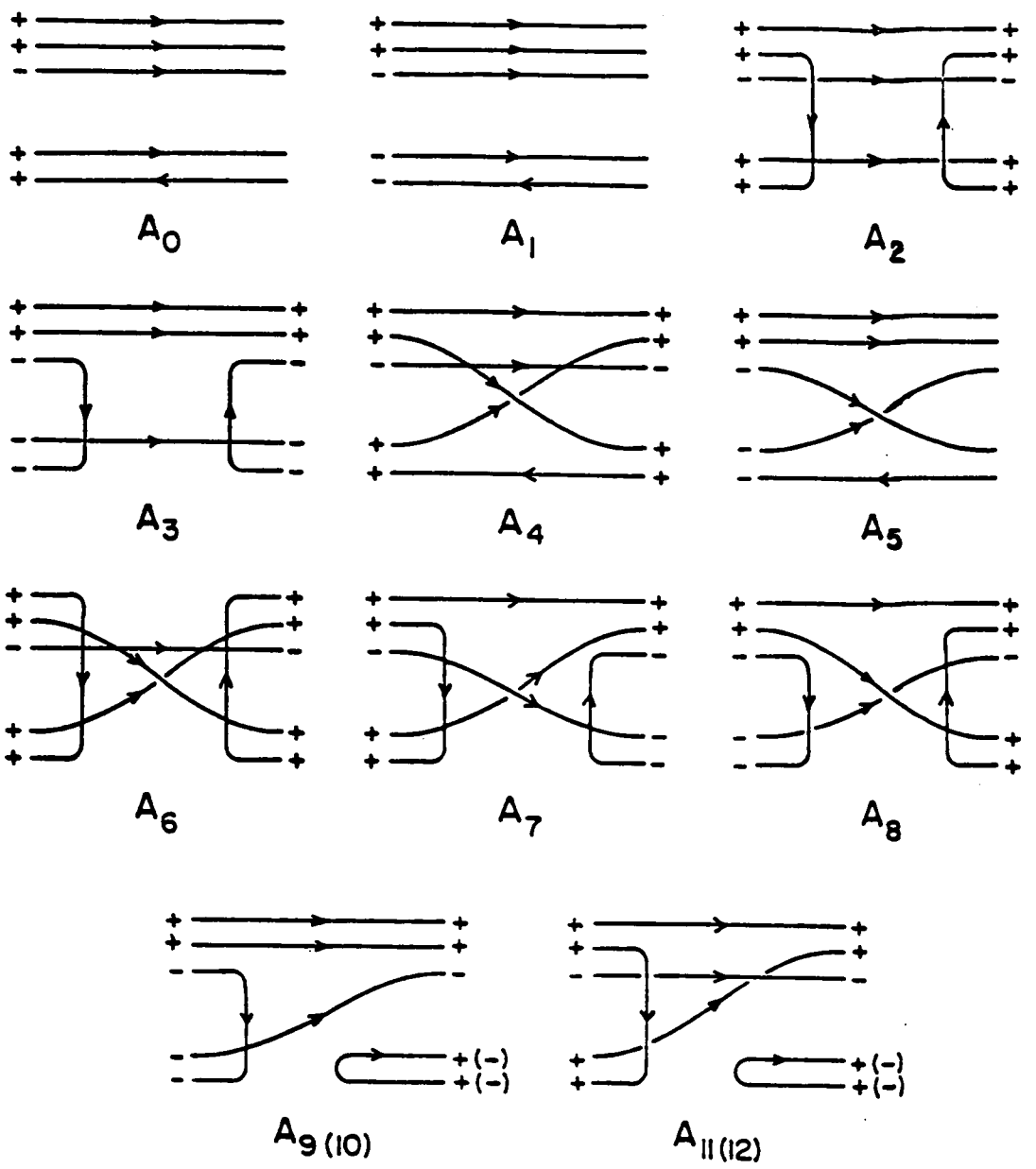

Figure 7. Fundamental Amplitudes of Meson-Baryon Scattering: spin-0 meson and spin-$\frac{1}{2}$ baryon scatterring has 15 fundamental quark scattering amplitudes.

3.3 Extending DIAG to Virtual Photons

Many hadronic scattering processes involve virtual photons. Among them the magnetic form factor of hadrons is the simplest example. With the power of DIAG it is both economical and important to extend the program to cover the class of reactions involving virtual photons. As a side benefit, DIAG calculates two more reactions, meson and baryon form factors, that can be checked against previous calculations.

With the well-built frame of DIAG it is not difficult to make the extension, at least, for form factors. Hadronic form factors can be best studied in the Breit frame. Figure 8 on page 40 illustrates the process in this frame. As far as DIAG is concerned the only difference between a virtual photon and a real one is their polarization vector ε. The polarization vector must satisfy the transverse condition

$$k^{\mu}\varepsilon_{\mu} = 0 \tag{3.12}$$

and the normalization

$$\varepsilon^{*}_{\mu}\varepsilon^{\mu} = -1\,, \tag{3.13}$$

where k^{μ} is the 4-momentum vector of the virtual photon. Since in the Breit frame, the initial and final momentum of the hadron is

$$p_i = (1,0,0,-1), \quad \text{and} \quad p_f = (1,0,0,1),$$

by momentum conservation, the momentum of the virtual photon is

$$k = (0,0,0,2). \tag{3.14}$$

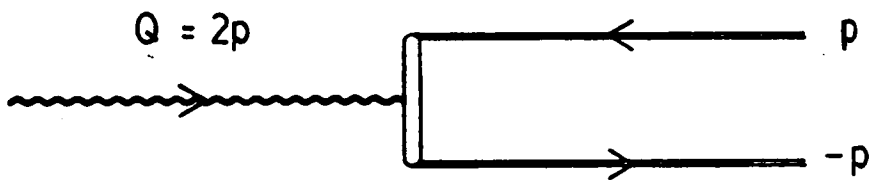

Figure 8. Hadron Form Factor in Breit Frame

Three independent ε can be chosen that satisfy both Eq. (3.12) and Eq. (3.13). Two of them are transverse and are the same as for the real photon. The third one is longitudinal which only exists if the spin-1 particle is massive. It can be written as

$$\varepsilon_{||} = \frac{i-1}{\sqrt{2}}(1,0,0,0). \tag{3.15}$$

By using Eq. (3.4) the expression in the Weyl base can be obtained

$$\not{\varepsilon}_{||\pm} = \gamma_{\mu\pm}\varepsilon^{\mu}_{||} = \frac{i-1}{\sqrt{2}}(|0><0| + |1><1|). \tag{3.16}$$

The rules of DIAG for the dot product of two 4-momentum vectors are based on the assumption that $p^2 = 0$ holds for both of the 4-vectors. Clearly, the 4-momentum vector of the virtual photon violates the assumption so that it can not be used to fix the momenta of propagators. In fact, the momentum of the virtual photon can be determined by momentum conservation, $k = p_f - p_i$, as in the form factor case. Therefore, the internal momenta can be completely determined without knowing the momentum of the virtual photon. The new scheme was incorporated into the momentum fixing part of the program.

It should be noted that the virtual photon is only allowed in the direction '0'. A general extension to allow it in all four scattering directions is possible, but one incident direction for it is sufficient for general single virtual-photon processes. For the incident virtual photon, the transverse polarization vectors of it are independent of the form of its 4-momentum vector. The longitudinal polarization vector, on the other hand, is dependent on its 4-momentum vector. Generalizing to suit any form of the momentum vector is somewhat difficult. For the current DIAG it is a safe practice to allow only transversely polarized virtual photon and always designate it in the direction '0'.

3.4 The Simplifier

The simplifier was developed at the very beginning of debugging DIAG. The immediate purpose then was to make the amplitude file directly readable. As development of DIAG progressed, the simplifier became more and more important and soon evolved to be an absolute necessity. It is difficult to imagine now how far DIAG could go without the simplifier, for it not only greatly reduces the usage of computing resources and increases computing speed, but also enables various automatic manipulations to be performed on the amplitude file, the most important among which is automatic cancellation.

The simplifier was first developed as a separate program that took the amplitude file produced by DIAG and made a simplified version out of it. This scheme was acceptable as long as the amplitude files were relatively small but became awkward when the $MB \to MB$ case was being tested. The simplifier was then built into DIAG and thus eliminated the huge intermediate amplitude file.

The simplifier was developed with no intention for general purpose usage; instead, it was tailored to the output of DIAG and the algebraic expressions of the C language. Before developing the simplifier the general purpose algebraic manipulation programs SMP and muMATH were tested. Their algebraic simplifying capability were so low that the possibility of employing them was instantly excluded. The only choice left was to write a customized algebraic simplifier.

Figure 9 on page 43 displaces a small section from the amplitude file of $\gamma\gamma \to B\overline{B}$ before simplification. It is immediately noticed that there are many redundant minus signs and parentheses in the amplitude. The first step of simplification is obviously to eliminate all these symbols along with

```
/* 1 */ t = 1;r = 0;r+ = (-x0)*1*c2;t/ = r;
r = 0;r+ = (-x0)*1*c2;r+ = (-x0)*1*s2;r+ = 1*1;t/ = r;
r = 0;r- = (-x2)*x3;r- = (-x2)*x5;t/ = r;
r = 0;r- = (-x2)*x5;t/ = r;
r = 0;r- = (-x1)*x4;t/ = r;
d = t;t = 96/1;r = 0;r+ = (-1)*x3*(-x2);t* = r;
r = 0;r- = (-1)*x4*(-1)*(-x2)*x5;t* = r;
r = 0;r+ = (-x0)*c*(-1)*1*s*(-1)*(-x0)*s*1*1*s*(-x1);
r+ = (-x0)*c*1*1*1*1*s*(-x1);t* = r;
t* = d;a- = t*q0*q0;
/* 13 */ t = 1;r = 0;r- = (-x0)*x4;r+ = (-x0)*1*c2;r- = (-x1)*x4;
r+ = (-x1)*1*c2;r- = x4*1*s2;
t/ = r;
r = 0;r- = (-x2)*x3;r- = (-x2)*x5;t/ = r;
r = 0;r- = (-x2)*x5;t/ = r;
r = 0;r- = (-x1)*x4;r+ = (-x1)*1*c2;r- = x4*1*s2;t/ = r;
r = 0;r+ = (-x1)*1*c2;t/ = r;
d = t;t = 96/1;r = 0;r+ = (-1)*x3*(-x2);t* = r;
r = 0;r+ = (-1)*x4*(-1)*(-x0)*s*1*c*(-1)*(-x2)*x5;
r+ = (-1)*x4*(-1)*(-x1)*s*1*c*(-1)*(-x2)*x5;r+ = x4*s*1*1*c*(-1)*(-x2)*x5;
t* = r;
r = 0;r+ = (-x0)*c*1*1*c*(-x1);t* = r;
t* = d;a- = t*q1*q0;
/* 172 */ t = 1;r = 0;r- = x3*1*s2;t/ = r;
r = 0;r- = (-x0)*x3;r+ = (-x0)*1*c2;r- = x3*1*s2;t/ = r;
r = 0;r+ = (-x1)*1*s2;t/ = r;
r = 0;r- = (-x2)*x4;r- = (-x2)*x5;t/ = r;
r = 0;r- = (-x2)*x5;t/ = r;
d = t;t = 96/1;r = 0;r- = x3*c*1*s*(-1)*x3*(-1)*(-x2)*x5;t* = r;
r = 0;r- = (-x1)*s*1*1*s*(-x0);t* = r;
r = 0;r+ = (-1)*(-x2)*x4;t* = r;
t* = d;a- = t*q0*q1;
/* 203 */ t = 1;r = 0;r+ = (-x0)*1*c2;t/ = r;
r = 0;r- = (-x0)*x3;r+ = (-x0)*1*c2;r- = x3*1*s2;t/ = r;
r = 0;r- = (-x0)*x3;r+ = (-x0)*1*c2;r- = (-x1)*x3;r+ = (-x1)*1*c2;r- = x3*1*s2;
t/ = r;
r = 0;r- = (-x2)*x5;r+ = (-x2)*1*s2;r- = x5*1*c2;t/ = r;
r = 0;r- = x5*1*c2;t/ = r;
d = t;t = 96/1;r = 0;r+ = (-1)*x3*(-1)*(-x0)*x5*s*(-1)*1*c*x5;
r+ = (-1)*x3*(-1)*(-x1)*x5*s*(-1)*1*c*x5;r+ = x3*s*1*s*x5*s*(-1)*1*c*x5;
r- = (-1)*x3*(-1)*(-x0)*s*1*(-1)*1*c*x5;r- = (-1)*x3*(-1)*(-x1)*s*1*(-1)*1*c*x5;
r- = x3*s*1*1*(-1)*1*c*x5;
t* = r;
r = 0;r+ = (-x1)*c*1*1*c*(-x0);t* = r;
r = 0;r+ = (-1)*(-x2)*x4;t* = r;
t* = d;a- = t*q0*q2;
```

Figure 9. Amplitude File before Simplification: A section of the amplitude file for $\gamma\gamma \to B\overline{B}$ which contains 4 diagrams.

all the blank spaces. The squeezed expressions are then stored into a linked data object term by term and, also, similar terms are combined. A list, that is a sum of terms in the binary representation, is formed. It is the primary object of the simplifier.

One of the difficulties of algebraic simplification is that it does not follow any ordered rules. There are usually many ways to simplify an algebraic expression and in general they do not reach the same simplification results. In order to avoid getting into a major battle in the algebraic computation field, yet still to have a good simplifier to serve DIAG, the major simplification method utilized by the simplifier is substitution of known identities in addition to extraction of common factors and combination of similar terms. By observing the unsimplified expressions it is also clear that most of them can be satisfatorily simplified by substitution. Different scattering processes generally have a different set of identities; the only common one is $c^2 + s^2 = 1$. Others are momentum fraction relations. For example,

$$x_0 + x_1 + x_2 = x_3 + x_4 + x_5 = 1$$

are the other two identities for $\gamma\gamma \rightarrow B\bar{B}$; For $MB \rightarrow MB$ the identities are

$$x_0 + x_1 + x_2 = x_3 + x_4 = x_5 + x_6 + x_7 = x_8 + x_9 = 1.$$

These identities are primary identities because they are not derived from any others. For a given set of the primary identities which is selected automatically by the simplifier, a set of secondary identities is generated by joining two primary ones with all possible combinations. The identity

$$c^2 + s^2 - x_0 - x_1 - x_2 = 0$$

is an example of the secondary ones for $\gamma\gamma \rightarrow B\bar{B}$. Usually a single substitution is sufficient to make the simplification, but occasionally more than one substitution are required to achieve the desired simplification. The simplifier is capable of multiple substitutions provided that the length of the list shall not increase at each one of the substitutions. In some very rare cases substitution of identities

that are a product of two primary ones is desired. However, incorporating this type of substitution increases the complexity and reduces the speed of the simplifier much more than the improvement it achieves in simplification.

Figure 10 on page 46 shows the simplified correspondent of Figure 9 on page 43. The effect of the simplifier is apparent. Table 1 on page 47 lists comparisons of various aspects of the amplitude file before and after simplification for $\gamma\gamma \rightarrow B\overline{B}$.

Similar to DIAG itself, the simplifier must also be tested and debugged step by step along with DIAG. The correctness of the simplifier was tested and ensured by numerically computing both simplified and unsimplified amplitude functions and verifying the agreement. For relatively simple cases it can be performed for the whole amplitude file. For cases as complicated as $MB \rightarrow MB$ the numerical checking is performed by randomly selecting a group of diagrams and verifying the simplification for this group. The random selective checking is also completely computerized.

In addition to the major extensions and modifications as to those of virtual photon, gauge invariance testing, and simplification, DIAG has also undergone numerous minor modifications. Some of them were made for the convenience of debugging the program while others were made for improving the efficiency of the program and of the later numerical integration. In summary, DIAG became progressively faster despite that many new features were added. However, as an expense, it became more complicated to use because of the increasing new features and therefore the increasing options to chose when running the program.

```
/* 1 */a = a-96*q0*q0/c*s*x3*(s2*x0-1)/(x0-1)/(x4-1);
/* 13 */a = a+96*q0*q1*c*s*x0*x2*x3*x4/(c2*x2+c2*x4-c2-x2*x4)/(x4-1)
/(c2*x1+s2*x4-x1*x4);
/* 172 */a = a+96*q0*q1*c/s*x0*x3*x4/(c2*x0+s2*x3-x0*x3)/(x3-1);
/* 203 */a = a-96*q0*q2/c*s*x1*x2*x3*x4*(c2*x5-x2*x5+x2)
/(c2*x0+s2*x3-x0*x3)/(c2*x2+c2*x3-c2-x2*x3)/(c2*x5+s2*x2-x2*x5);
```

Figure 10. Amplitude File after Simplification

Table 1. Comparison of Amplitudes before and after Simplification

$\gamma\gamma \rightarrow B\overline{B}$	before	after
Size of sourse	53 KByte	12 KByte
Size of object	18 KByte	6 KByte
Compilation time	146 s	25 s

The amplitude file is for $\gamma\gamma \rightarrow B\overline{B}$ for spin half baryons. Both of the photons in this case are right handed. The relatively small object size before simplification is largely due to the high optimization capability of the VAX C compiler.

Chapter IV

Testing Gauge Invariance

In the course of checking gauge invariance for MM scattering, because of some subtle mistakes, the scattering amplitude was found not to be gauge invariant. Extensive checking of the computer generated amplitude against hand calculation did not reveal any discrepancy, while the same calculation for the proton magnetic form factor and photon annihilation to hadron-antihadron pairs did satisfy gauge invariance. The following questions were then raised: first, is the gauge invariance theory formulated correctly for amplitudes involving three- and four-gluon vertices; and second, are the Feynman rules correct, especially for three- and four-gluon vertices. Most of the text books and review articles tend to restrict themselves to be very brief on these topics and still, all use different conventions for the Feynman rules. It is also not uncommon that the Feynman rules of some of them contain errors. Although it is unlikely that one may actually find anything wrong with the theory, it is very important at least to acquire a strong confidence in the theory and to make certain that the Feynman rules that DIAG implements are definitely correct.

The anwers to these questions are rooted no where but in the formulation of the theory. In the following sections of this chapter gauge theories are redeveloped with emphases on QCD and gauge invariance. For references see, for example, Abers and Lee [25], Cheng and Li [26], and Chaichian and Nelipa [27]. The implementation of gauge invariance testing is presented in the last section of this chapter.

Gauge theories are most conveniently formulated in the Feynman path integral formalism (FPI). To avoid making the lengthy derivation even longer, the FPI formalism for transition amplitudes is accepted without question. Furthermore, h = c = 1 is assumed throughout this chapter. The transition amplitude in FPI formalism is:

$$< q''_1, q''_2, \cdots, q''_n; t'' | q'_1, q'_2, \cdots, q'_n; t' > = \int \prod_{t,k} \frac{[dp_k(t)][dq_k(t)]}{2\pi} \exp[iI(t'',t')], \tag{4.1}$$

where q_t and p_t are the canonical coordinates and momenta; $I(t'',t')$ is the action of the system depending on $p_1, \cdots, p_n, q_1 \cdots, q_n$.

In quantum mechanics, transitions always take place from a state at $t = -\infty$ to a state at $t = +\infty$. In the limit of $t' \to -\infty, t'' \to +\infty$, the path integral Eq. (4.1) describes vacuum-to-vacuum transition. Therefore, as an example, for the free fermion Dirac fields for which the Lagrangian density is defined by

$$L_F(x) = i\,\overline{\psi}(x)\gamma_\mu \partial_\mu \psi(x) - m\,\overline{\psi}(x)\psi(x), \tag{4.2}$$

the transition amplitude is

$$S = \int \prod_x [d\overline{\psi}(x)][d\psi(x)] \exp[i \int dx L_F(x)]. \tag{4.3}$$

4.1 Field with Constraints

One of the advantages of the path integral formalism is that it works in the canonical Hamiltonian context and leads to quantization of the fields. As will be seen later, a gauge field is a field with constraints and the gauge fixing will be naturally introduced in solving the constrained field problem. As for now, a Hamiltonian system with constraints shall be solved and one can easily identify that the entire procedure is purely classical.

The system has n degrees of freedom described by the canonical coordinates q_i and momenta p_i. The Hamiltonian of the system is $H(p_i, q_i)$. Let *m constraints* be imposed on the system, which can be described by

$$\varphi_a(p_i, q_i) = 0, \quad a = 1,2,...,m. \tag{4.4}$$

Therefore, the variables p_i and q_i are not all independent. The most straightforward way to solve this problem is to eliminate the dependent variables by solving the constraint equations (4.4). However, this approach may not be easy and some times is even impossible. The aim here is to develop an expression in the form of a path integral which incorporates the constraints in a more convenient way.

By the means of the Lagrange multipliers λ_a, the system is then described by the Hamiltonian

$$H'(p_i,q_i) = H(p_i,q_i) + \sum_{a-1}^{m} \lambda_a \varphi_a(p_i, q_i). \tag{4.5}$$

For an arbitrary function $f(p_i, q_i)$ the equation of motion is

$$\dot{f}(p_l, q_l) = \{H, f\} + \sum_{a=1}^{m} \lambda_a \{\varphi_a, f\}, \tag{4.6}$$

where the curly braces denote the Poisson brackets:

$$\{f, g\} = \sum_{l=1}^{n} \left(\frac{\partial f}{\partial p_l} \frac{\partial g}{\partial q_l} - \frac{\partial f}{\partial q_l} \frac{\partial g}{\partial p_l} \right). \tag{4.7}$$

The constraints are clearly independent of time, and they lead to the *consistency conditions*

$$\dot{\varphi}_a(p_l, q_l) = \{H, \varphi_a\} + \sum_{b=1}^{m} \lambda_b \{\varphi_b, \varphi_a\} = 0, \tag{4.8}$$

where taking $\varphi_a = 0$ after evaluating the Poisson brackets is understood.

If both of the Poisson brackets are zero the consistency conditions are then said to be satisfied which is also to say that there are no more constraints imposed on the system. The case in which $\{H, \varphi_a\} = 0$ while $\{\varphi_b, \varphi_a\} \neq 0$ shall not be discussed because of its irrelevance here. The last case, also the most important, is that $\{H, \varphi_a\} = \Phi_{1a}$ and $\{\varphi_b, \varphi_a\} = 0$. The consistency condition requires that

$$\Phi_{1a}(p_l, q_l) = 0, \tag{4.9}$$

which also means that more constraints should be imposed on the system. Following Dirac, the constraints given by Eq. (4.4) are referred to as the *primary* constraints and the constraints given by Eq. (4.9) are the *secondary* constraints. It is also clear that the secondary constraints can not be reduced to the primary ones.

The secondary constraints Φ_{1a} are on the equal footing with the primary ones so that it should satisfy the consistency conditions similar to Eq. (4.8). It may yield additional secondary constraints $\{H, \Phi_{1a}\} = \Phi_{2a} = 0$.

Assuming that Eq. (4.4) includes all the constraints, both primary and secondary, both Poisson brackets in Eq. (4.8), the consistency condition, vanish. All the coefficients λ_a are left arbitrary. The equation of motion for a dynamic variable $f(p_i, q_i)$ described by Eq. (4.6) is not unique due the arbitrariness of the λ_a. However, all of them should be physically equivalent, because the physics is only dependent on the set of variables p_i and q_i and is independent of the choice of λ_a. The set of values of $f(p_i, q_i)$ corresponding to all possible coefficients λ_a is called an *orbit*. Since all the points on the orbit describe the same physical state, it should be suffice to consider only one of them. The point can be chosen by imposing another m conditions,

$$\chi_b(p_i, q_i) = 0, \tag{4.10}$$

which is unique for a given set of λ_a to the system. Eq. (4.10) is referred to as *subsidiary* conditions. As will be shown, it corresponds choosing a gauge when the system is a gauge field. The consistency conditions for the subsidiary conditions

$$\dot{\chi}_b = \{H, \chi_b\} + \sum_{a=1}^{m} \lambda_a \{\varphi_a, \chi_b\} = 0 \tag{4.11}$$

uniquely determine λ_a since

$$\det |\{\varphi_a, \chi_b\}| \neq 0, \quad a = b = 1,2, \ldots ,m. \tag{4.12}$$

Now a canonical transformation from p_i and q_i to P_i and Q_i can be made. Because the subsidiary conditions can be chosen in such a way that $\{\chi_a, \chi_b\} = 0$, one can chose $P_i = \chi_i$ for $i = 1,2, \ldots ,m$ and let Q_i $(i = 1,2, \ldots ,m)$ be their conjugate coordinates. The remaining canonical variables are define as

$$P_i = p'_i \quad \text{and} \quad Q_i = q'_i, \quad i = m+1, \ldots, n \tag{4.13}$$

where the variables p'_i and q'_i span a $2(n-m)$ dimensional subspace Γ'. It should be noted that they are also independent variables of the system as if the constraints of Eq. (4.4) had been solved.

According to Eq. (4.1) the transition amplitude in the $2(n-m)$ dimensional subspace Γ', after eliminating the dependent variables, can be expressed as

$$S = \int \prod_{t,i} \frac{[dp'_i][dq'_i]}{2\pi} \exp\left\{ i\int_{q'}^{t''} dt \left[\sum_{k=m+1}^{n} p'_k \dot{q}'_k - H(Q_a(p'_k, q'_k), q'_k, 0, p'_k) \right] \right\}. \tag{4.14}$$

Recalling that the goal is to avoid solving the constraints equations, Eq. (4.14) should be transformed back to the $2n$-space Γ. To achieve this, the following steps shall be followed:

1) Rewrite Eq. (4.14) equivalently into the form

$$\begin{aligned} S = \int \prod_{t,i} \frac{[dp'_i(t)][dq'_i(t)]}{2\pi} \prod_{k=1}^{m} \frac{[dP_k(t)][dQ_k(t)]}{2\pi} \delta(P_k)\delta(Q_k - Q_k(p',q')) \\ \times \exp\left\{ i\int_{t'}^{t''} dt \left[\sum_{k=1}^{m} P_k \dot{Q}_k + \sum_{l=m+1}^{n} p'_l \dot{q}'_l - H(P_k, Q_k, p'_l, q'_l) \right] \right\}. \end{aligned} \tag{4.15}$$

2) Change the variables Q_a to φ_a; then δ functions transform as

$$\prod_a \delta(Q_a, Q_a(p',q')) = \det \left| \frac{\partial \varphi_c}{\partial Q_a} \right| \prod_a \delta(\varphi_c). \tag{4.16}$$

The determinant is the Jacobian of the transformation, which can also be identified through

$$\{\chi_a, \varphi_c\}_{p,q} = \{\chi_a, \varphi_c\}_{P,Q} = \{P_a, \varphi_c\}_{P,Q} = \sum_l \delta_{al} \frac{\partial \varphi_c}{\partial Q_l} = \frac{\partial \varphi_c}{\partial Q_a}. \tag{4.17}$$

3) Make canonical transformation from P_i and Q_i to p_i and q_i; Liouville's theorem ensures that $[dP_i][dQ_i] = [dp_i][dq_i]$. Making use of the generating function $F(p,q)$ for which

$$dF = \sum_i p_i dq_i + \sum_i Q_i dP_i + (H' - H)dt\,, \tag{4.18}$$

the following relation is obtained

$$(\sum_i p_i \dot{q}_i - H)dt = (\sum_i P_i \dot{Q}_i - H)dt + d(F - \sum_i P_i Q_i), \tag{4.19}$$

where the fact that the function $F(p,q)$ does not explicitly depend on t, and thus $H' = H$, has been used. Integrating Eq. (4.19) over t from t' to t'' leaves the last term of Eq. (4.19) as a constant. Since this expression appears in an exponential, it merely contributes a constant factor. Since the amplitude is not normalized, any constant factors can be dropped.

4) Substituting Eq. (4.19) along with Eqs. (4.16-17) and $P_a = \chi_a$ into Eq. (4.15), the desired expression is obtained:

$$S = \int \prod_{i,j} \frac{[dp_i(t)][dq_i(t)]}{(2\pi)^{n-m}} \prod_{a,c} \delta(\chi_a)\delta(\varphi_c) \det|\{\chi_a, \varphi_c\}| \exp\left\{ i\int_{t'}^{t''} dt\left[\sum_i p_i \dot{q}_i - H(p_i,q_i)\right]\right\}. \tag{4.20}$$

This path integral expression absorbs the constraints into the integrand as δ functions and thus avoids solving the constraints equations. It is then readily to be applied to the gauge field.

4.2 The Yang-Mills Field

Eq. (4.20) is a general expression for fields of both Abelian and non-Abelian groups, but only the non-Abelian color gauge field is of interest here. The Yang-Mill's field will be taken as an example

to rederive the theory. From the historical view, this is what gives birth to the non-Abelian field theory; and, for the present case, the field theory for SU(2) and SU(3) are formally identical.

The symmetry described by the SU(2) group is commonly referred to as isospin. The isospin indices shall be denoted by superscript Latin letters, the Lorentz indices by subscript Greek letters and the 3-space (E_3) indices by subscript Latin letters. Summation over repeated indices is understood.

The field tensor is defined as

$$F^k_{\mu\nu} = \partial_\mu A^k_\nu - \partial_\nu A^k_\mu + g\varepsilon^{ijk} A^i_\mu A^j_\nu, \tag{4.21}$$

where A^k_μ are the fields. The Lagrangian takes the form

$$L = -\frac{1}{4} F^k_{\mu\nu} F^k_{\mu\nu} = -\frac{1}{4}(\partial_\mu A^k_\nu - \partial_\nu A^k_\mu)^2 \tag{4.22}$$

in the second order formalism and

$$L = -\frac{1}{2}\left[\partial_\mu A^k_\nu - \partial_\nu A^k_\mu + g\varepsilon^{ijk} A^i_\mu A^j_\nu - \frac{1}{2} F^k_{\mu\nu}\right] F^k_{\mu\nu} \tag{4.23}$$

in the first order formalism. Using the first order formalism, one can rewrite Eq. (4.23) in the three-dimensional form

$$L = E^k_i \dot{A}^k_i - H(E^k_i, A^k_i), \tag{4.24}$$

where

$$H(E^k_i, A^k_i) = \frac{1}{2}\left[(E^k_i)^2 + (B^k_i)^2\right], \quad E^k_i = F^k_{i0}, \quad \text{and} \quad B^k_i = \frac{1}{2}\varepsilon^{ijl} F^k_{jl}.$$

The terms with full divergence and explicit dependence on A_0 and E_0 have been omitted because they vanish either by the constraints or by the subsidiary conditions that will be chosen.

It is clear that $H(E_i^k,A_i^k)$ is the Hamiltonian and $E_i^k(x)$ and $A_i^k(x)$ are canonically conjugate momenta and coordinates. The primary constraints are obviously

$$\varphi_1^k(x) \equiv E_0^k(x) = 0, \tag{4.25}$$

which leads to the secondary constraints by

$$\varphi_2^k(x) \equiv \{\int d^3x H(E_i^k,A_i^k),E_0^k(x)\} = \partial_i E_i^k(x) - g\varepsilon^{klm}A_i^l E_i^m = 0. \tag{4.26}$$

The secondary constraints satisfy the following consistency conditions

$$\{\varphi_2^k(x), \varphi_2^l(x)\} = g\varepsilon^{klm}\varphi_2^m(x)\delta(x-y) \quad \text{and}$$
$$\{\int d^3x H(E_i^k,B_i^k), \varphi_2^l(y)\} = 0,$$

so that there are no more secondary constraints on the field.

The subsidiary conditions can now be chosen to be associated with the constraints. It is also said to choose a gauge. For the convenience of the derivation, the Coulomb gauge $\partial_i A_i^k(x) = 0$ is chosen to be associated with $\varphi_2^k(x) = 0$ and A_0^k with $E_0^k = 0$. It is straightforward to calculate the following Poisson brackets with respect to the canonical variables E_i^k and A_i^k:

$$\begin{aligned}&\{\chi_2^k, \chi_2^l\} \equiv \{\partial_i A_i^k(x), \partial_i A_i^l(y)\} = 0 \quad \text{and}\\ &\{\varphi_2^k, \chi_2^l\} \equiv \{\partial_i E_i^k(x) - g\varepsilon^{klm}A_i^l(x)E_i^m(x), \partial_i A_i^l(y)\} = M^{kl}(A_i^m)\delta(x-y),\end{aligned} \tag{4.27}$$

where

$$M^{kl}(A_i^m) = \partial_i\partial_i\delta^{kl} + g\varepsilon^{klm}A_i^m\partial_i. \tag{4.28}$$

The analysis for the other set of constraints and subsidiary conditions is even simpler. By using the fact that E_μ^k and S_ν^k are canonically conjugate variables, one obtains

$$\{\chi_1^k, \chi_1^l\} \equiv \{A_0^k(x), A_0^l(y)\} = 0 \quad \text{and}$$
$$\{\varphi_1^k, \chi_1^l\} \equiv \{E_0^k(x), A_0^l(y)\} = \delta^{kl}\delta(x - y). \tag{4.29}$$

It should be noted that δ^{kl} is a unit matrix and its determinant is 1. It should also be noted that det $|\{\varphi_a^k, \chi_c^l\}|$ is calculated as a product of det $|\{\varphi_1^k, \chi_1^l\}|$ and det $|\{\varphi_2^k, \chi_2^l\}|$. The reason is that the two sets of constraints and subsidiary conditions are independent to each other so that the matrix $\{\varphi_a^k, \chi_c^l\}$ is a direct product of two submatrices for the two sets, respectively.

With the knowledge acquired from Eq. (4.24-29), the path integral over the canonical variables, in place of Eq. (4.20), can be written for the Yang-Mill's field as

$$\begin{aligned} S = \int\prod_{x,k} & [dA_i^k(x)][dE_i^k(x)][dA_0^k(x)][dE_0^k(x)] \det |M^{kl}(A_i^m)| \\ & \times \delta(A_0^k(x))\delta(E_0^k(x))\delta(\partial_t A_i^k(x))\delta(\partial_t E_i^k(x) + g\varepsilon^{klm}A_i^l(x)E_i^m(x)) \\ & \times \exp\left\{i\int dx\left[E_i^k\dot{A}_i^k + E_0^k\dot{A}_0 - H(E_i^k, A_i^k, E_0^k, A_0^k)\right]\right\}. \end{aligned} \tag{4.30}$$

This expression can be further simplified. It is easy to identify that the expression in the exponential is the Lagrangian and can be replaced with the second order formalism Eq. (4.22). By carrying out the integration over E_μ^k, which again yields a constant factor that can singled out, the path integral over all the fields $A_\mu^k(x)$ is finally obtained:

$$S = \int\prod_{x,k} [dA_\mu^k(x)]\delta(\partial_t A_i^k(x)) \det |M^{kl}(A_i^m)| \exp[i\int dx L(x)]. \tag{4.31}$$

The Coulomb gauge has been chosen in developing the path integral Eq. (4.31) for the Yang-Mill's field because it is the most convenient one to use for deriving the theory. However, the Coulomb gauge is not invariant under the Lorentz transformation, so that the path integral Eq. (4.31) is not relativistically invariant as well. For deriving Feynman rules and performing calculations, the relativistically invariant Lorentz gauge is the most convenient one to use. To accomplish this, the

Coulomb gauge shall be transformed to the Lorentz gauge in the path integral Eq. (4.31). The transition procedure is known as the Faddeev-Popov method.

A functional $\Delta_\chi(A_\mu^k)$ shall be introduced by

$$\Delta_\chi(A_\mu^k)\int\prod[dg(x)]\delta(\chi(A_\mu^{kg}(x))) = 1, \tag{4.32}$$

where χ is any gauge condition, and the integration runs over the entire gauge group, of which g is an element. The Jocabian of a gauge transformation is unity because of the fact that the gauge group under consideration is a unitary group (SU(2) for the Yang-Mill's field). Meanwhile, the transformation of variables from A_μ^{kg} to $A_\mu^{kg'}$ in the δ function yields the same unit Jacobian. Therefore,

$$[dg(x)] = [dg'(x)] \quad \text{and } \delta(\chi(A_\mu^{kg}(x))) = \delta(\chi(A_\mu^{kg'}(x))). \tag{4.33}$$

Eq. (4.33) also implies that both $[dg]$ and $\delta(\chi)$ are gauge invariant, so that the functional Δ_χ is gauge invariant as well. For the Coulomb gauge Eq. (4.32) takes the form

$$\Delta_C(A_\mu^k)\int\prod[dg(x)\delta(\partial_i A_i^k(x))] = 1. \tag{4.34}$$

The point is to show the equivalence of the functional $\Delta_C(A_\mu^k)$ and $\det|M^{kl}(A_i^m)|$ so that the gauge factors in Eq. (4.31) correspond to Eq. (4.34), which in turn is a special case of Eq. (4.32). This will enable replacing the gauge factors in Eq. (4.31) with any desired gauge by virtue of Eq. (4.32).

The integral in Eq. (4.34) shall be calculated first. Because of the condition $\partial_i A_i^k(x) = 0$ and the δ function in the integrand, there is no contributions come from the gauge group except from the vicinity of $g(x) = 1$. In this vicinity the following expansions are valid

$$U(g) = 1 - \frac{i}{2} g u^k \tau^k, \quad dg = du^k,$$
$$A_i^{kg}(x) = A_i^k(x) + g\varepsilon^{klm} u^l(x) A_i^m(x) + \partial_i \varepsilon^k(x), \tag{4.35}$$

and

$$\partial_i A_i^{kg}(x) = g\varepsilon^{klm} A_i^m \partial_i u^l + \partial_i \partial_i u^k = M^{kl}(A_i^m) u^l. \tag{4.36}$$

Substituting Eq. (4.35,36) into the integral one obtains

$$\int \prod_{x,k} [dg(x)] \delta(\partial_i A_i^{kg}(x)) = \int \prod_{x,k} [du^k(x)] \delta(\lambda u^l) = \prod_{x,k} |\lambda^k|^{-1} = (\det |M^{kl}(A_i^m)|)^{-1}. \tag{4.37}$$

The fact that the product of eigenvalues of a matrix equals the determinant of the matrix has been used in the last step of Eq. (4.37). Thus it is proved that

$$(A_\mu^k)|_{\partial_i A_i^k = 0} = \det |M^{kl}(A_i^m)|,$$

and, indeed, the path integral with the Coulomb gauge, Eq. (4.31), is a special case of Eq. (4.32) with $\chi = \partial_i A_i$. Next, inserting the generalized Lorentz gauge in the form of Eq. (4.32),

$$\Delta_a(A_\mu^k) \int \prod_{x,k} [dg(x)] \delta(\partial_\mu A_\mu^k(x) - a^k(x)) = 1, \tag{4.38}$$

into Eq. (4.31), Keeping in mind that all the gauge factors are gauge invariant, the integration $\int [dg]$ can be switched from Lorentz gauge factors to Coulomb gauge factors and the latter can be extracted out by virtue of Eq. (4.34). The result is:

$$S = \int \prod_{x,k} [dA_\mu^k(x)] \delta(\partial_\mu A_\mu^k(x) - a^k(x)) \Delta_a(A_\mu^k) \exp(-i \int dx \frac{1}{4} F_{\mu\nu}^k F_{\mu\nu}^k). \tag{4.39}$$

Calculating the functional $\Delta_a(A_\mu^k)$ is similar to that of the functional $\Delta_C(A_\mu^k)$; one finds:

$$\Delta_a(A_\mu^k) = \det |M_a|, \quad \text{and} \quad M_a = \partial^2 \delta^{kl} + g\varepsilon^{klm}(A_\mu^m \partial_\mu + \partial_\mu A_\mu^m).$$

It should be noted that M_a is independent of $a_k(x)$. Therefore, Eq. (4.39) can be integrated over $a_k(x)$ by inserting a constant factor:

$$\exp\{-i\frac{1}{2\alpha}\int[a^k(x)]^2dx\}.$$

This leads to the desired path integral in the generalized Lorentz gauge, which is also called the α-gauge:

$$S = \int\prod_{x,k}[dA^k_\mu(x)]\det|M_a|\exp\left\{-i\int dx\left[\frac{1}{4}F^k_{\mu\nu}F^k_{\mu\nu} + \frac{1}{2\alpha}(\partial_\mu A^k_\mu)^2\right]\right\}. \tag{4.40}$$

Some comments on the factor M_a are desirable. The determinant of M_a can be expressed as a path integral over anti-commuting scalar fields and their interaction with the gauge fields. Upon some choice of gauges, though, there appear no such fields. The fields are commonly referred to as the Faddeev-Popov ghosts. They shall not be discussed in any detail here because they do not enter the calculation unless loops are encountered.

4.3 Green's Functions and S-matrix Element

What has been developed in the previous sections is the path integral formulation of the vacuum-to-vacuum transition amplitude. In practice, the *S*-matrix is what needs to be calculated. A matrix element of the *S*-matrix describes the transition amplitude of a system for which particles are free in both initial and final states. To calculate the *S*-matrix it is convenient to use a Green's function. Roughly, a Green's function describes the internal structure of the transition amplitude, that is, the *S*-matrix element. It will be shown later that the propagators and vertices are associated with Green's functions.

In this section, the path integral expression for Green's functions and the S-matrix are derived. Since path integrals are not generally analytically calculable, the method of perturbative expansion is employed to calculate the Green's function and the matrix element of the S-matrix.

A Green's function can be formulated as a path integral. Since the construction of the path integral was skipped for the vacuum-to-vacuum transition amplitude of Eq. (4.1), it should also be skipped for the Green's function. Nevertheless, it is instructive to compare Eq. (4.1) with

$$\begin{aligned} G(x_1,x_2, \ldots ,x_n) &\equiv <0|T(\varphi_1(x_1)\varphi_2(x_2) \ldots \varphi_n(x_n))|0> \\ &= \int\prod_x [d\varphi(x)]\varphi_1(x_1)\varphi_2(x_2) \ldots , \varphi_n(x_n) \exp\{i\int dx L(x)\}. \end{aligned} \tag{4.41}$$

The generating functional $W(J)$ for a Green's function can be defined as

$$W(J) = \int\prod_x [d\varphi(x)] \exp\{i\int dx[L(x) + \varphi_1(x)J_1(x) + \cdots + \varphi_n(x)J_n(x)]\}, \tag{4.42}$$

where an auxiliary current $J_i(x)$ is introduced for each field $\varphi_i(x)$. The Green's function can then be obtained by taking derivatives with respect to the currents and then setting the currents to zero:

$$G(x_1, \ldots ,x_n) = (-i)^n \frac{\delta}{\delta J_1(x_1)} \frac{\delta}{\delta J_2(x_2)} \cdots \frac{\delta}{\delta J_n(x_n)} W(J)|_{J_1 = \cdots = J_n = 0}. \tag{4.43}$$

The Green's function defined above contains both connected and disconnected diagrams. However, only connected ones are of interest. To accomplish this, another generating function $Z(J)$ shall be introduced and defined by

$$Z(J) = -i \ln W(J). \tag{4.44}$$

By differentiating both sides of the above equation with respect to J directly, it is straightforward to see that the quantity

$$G_c(x_1,x_2,\ldots,x_n) = (-i)^{n-1}\frac{\delta}{\delta J_1}\frac{\delta}{\delta J_2}\cdots\frac{\delta}{\delta J_n}Z(J)|_{J_1=\cdots=J_n=0} \tag{4.45}$$

is the connected Green's function as the subscript c denotes.

It is convenient to introduce a generating functional $\Gamma(\Phi)$ which generates the vertex Green's functions. Since the Feynman rule for vertices can also be deduced from the Green's function generated by $Z(J)$ and the S-matrix element, as will be shown later, only the the expressions of the functional and the Green's function are quoted here:

$$\Gamma(\Phi_i) = Z(J_i) - \int dx J_i(x)\Phi_i(x), \tag{4.46}$$

where

$$\Phi_i(x) = \frac{\delta Z(J)}{\delta J_i(x)}. \tag{4.47}$$

The n-point vertex Green's function is then obtained through

$$\Gamma^{(n)}_{ij\ldots} = \frac{\delta^n\Gamma(\Phi)}{\delta\Phi_i\delta\Phi_j\ldots}. \tag{4.48}$$

The functional $\Gamma(\Phi)$ can be expanded in terms of the number of loops. The leading order gives only tree diagrams and is referred to as the tree approximation. Again, without derivation, the tree approximation functional is given by

$$\Gamma_{tree}(\Phi) = I(\Phi) \tag{4.49}$$

where $I(\Phi)$ is the classical action.

Before getting to the S-matrix, the functional $W(J)$ shall be further transformed to a more convenient form for calculating the Green's functions, and thus, deducing the Feynman rules. First, by separating the Lagrangian of interacting fields from the Lagrangian of the free fields, $L(x) = L_0(x) + L_I(x)$, the functional $W(J)$ can be rewritten as

$$W(J) = \int\prod_x [d\varphi_k(x)] \exp[i\int dx L_0(x)] \exp\{i\int dx[L_I(x) + \varphi_k(x)J_k(x)]\}. \tag{4.50}$$

The last factor in the above equation can then be written as

$$\exp[i\int dx L_I(-i\frac{\delta}{\delta J_1(x)}, -i\frac{\delta}{\delta J_2(x)}, \ldots, -i\frac{\delta}{\delta J_n(x)})] \exp(i\int dx J_k\varphi_k), \tag{4.51}$$

for the obvious reason that the Lagrangian L_I is a function of the fields φ_k. In a compact form Eq. (4.50) is rewritten as

$$W(J) = \exp[i\int dx L_I(-i\frac{\delta}{\delta J_k})]\int\prod_x [d\varphi_k] \exp\{i\int dx[L_0 + \varphi_k J_k]\}. \tag{4.52}$$

The integral in the above equation containing the free Lagrangian $L_0(x)$ can be written in another form:

$$\int dx L_0(x) = \frac{1}{2}\int dx dy \varphi_i(x) K_{ij}(x - y)\varphi_j(y), \tag{4.53}$$

where $K_{ij}(x - y)$ is the differential operator determined by the free Lagrangian $L_0(x)$. Substituting Eq. (4.53) into Eq. (4.52) and making a further change of variables,

$$\varphi_i(x) = \varphi'_i(x) - \int K_{il}^{-1}(x - y)J_l(y)dy, \tag{4.54}$$

the following path integral is obtained:

$$\begin{aligned}\int\prod_x [d\varphi_k(x)] \exp\Big[\frac{i}{2}\int dx dy \varphi_i(x) K_{ij}(x - y)\varphi_j(y) + i\int dx \varphi_i(x)J_i(x)\Big] \\ = C\exp\Big[\frac{-i}{2}\int dx dy J_i(x)K_{ij}^{-1}(x - y)J_j(y)\Big],\end{aligned} \tag{4.55}$$

where

$$C = \int\prod_x [d\varphi_k(x)] \exp\left[\frac{i}{2}\int dxdy\varphi'_i(x)K_{ij}(x-y)\varphi'_j(y)\right].$$

Dropping the constant factor C and substituting Eq. (4.55) into Eq. (4.52), the desired form of $W(J)$ is finally achieved:

$$W(J) = \exp\left[i\int dxL_I(-i\frac{\delta}{\delta J_k(x)})\right]\exp\left[\frac{i}{2}\int dxdyJ_i(x)K_{ij}^{-1}(x-y)J_j(y)\right]. \tag{4.56}$$

The generating functional for the S-matrix element can now be constructed with the functional $W(J)$ of Eq. (4.56):

$$\begin{aligned} S(\varphi_k^0) = & \exp\left[i\int dxL_I(-i\frac{\delta}{\delta J_k(x)})\right] \\ & \times \exp\left[-i\int dx\varphi_k^0(x)J_k(x) - \frac{i}{2}\int dxdyJ_i(x)K_{ij}^{-1}(x-y)J_j(y)\right]|_{J_1=\cdots=J_n=0}. \end{aligned} \tag{4.57}$$

The matrix element, for example, for m initial free particles scattering into n free final particles can be obtained by

$$\begin{aligned} S_{m\to n} = & \varphi_{i,1}(x)\frac{\delta}{\delta\varphi_1^0(x)}\varphi_{i,2}(x)\frac{\delta}{\delta\varphi_2^0(x)}\cdots\varphi_{i,m}\frac{\delta}{\delta\varphi_m^0(x)}\varphi_{f,m+1}(y)\frac{\delta}{\delta\varphi_{m+1}^0(y)} \\ & \times \varphi_{f,m+2}(y)\frac{\delta}{\delta\varphi_{m+2}^0(y)}\cdots\varphi_{f,m+n}(y)\frac{\delta}{\delta\varphi_{m+n}^0(y)}S(\varphi_k^0)|_{\varphi_1^0=\cdots=0}. \end{aligned} \tag{4.58}$$

In Eq. (4.57) and (4.58), $\varphi_k^0(x)$ are arbitrary functions and served as external free points to which the external free fields can be attached. The external free fields are denoted as $\varphi_{i,k}(x)$ for initial free fields and $\varphi_{f,k}(x)$ for final free fields.

By far, various Green's functions and the S-matrix element have been derived in the exact path integral form. In order to calculate them, perturbation theory shall be applied. The perturbative expansion is obtained by expanding the interacting term $\exp[i\int dxL_I(x)]$ in the path integral

$$\exp[i\int dx L_I(x)] = \sum_{n=0}^{\infty} \frac{i^n}{n!}\int dx_1 \int dx_2 \ldots \int dx_n L_I(x_1)L_I(x_2)\ldots L_I \ldots L_I(x_n). \tag{4.59}$$

All the Green's functions, as well as the *S*-matrix elements, can then be calculated order by order. Outlined below are such calculations for QCD to the leading order.

4.4 Feynman Rules for QCD

To each order of the perturbative expansion there exists a set of Green's functions such that any member in the set can not be decomposed into a product combination of two or more members of the set and any Green's function which is not in the set can be decomposed into a product combination of two or more members of the set. This set is commonly referred to as the Feynman rules of the same order.

Deriving Feynman rules is a very tedious and lengthy procedure. Although it is the utmost goal of this study, the detailed derivation will not be shown. However, some cautions will be pointed out for the derivation.

The QCD Lagrangian is given by

$$L = -\frac{1}{4}F^k_{\mu\nu}F^k_{\mu\nu} + \bar{\psi}^a(i\gamma_\mu D_\mu - m)\psi^b, \tag{4.60}$$

where

$$F^k_{\mu\nu} = \partial_\mu A^k_\nu - \partial_\nu A^k_\mu + g f^{ijk} A^i_\mu A^j_\nu \quad \text{and}$$
$$D_\mu = \partial_\mu - \frac{i}{2} g \lambda^k A^k_\mu. \tag{4.61}$$

The color indices are denoted by superscript Latin letters and the Lorentz indices by subscript Greek letters. A^k_μ are the gluon fields, ψ^a are the quark fields, λ^k are the Gell-Mann matrices, f^{ijk} is the structure constant of the SU(3) group, and g is the coupling constant.

By imposing the generalized Lorentz gauge condition and omitting all the terms containing the ghost field, the free Lagrangian and the interacting Lagrangian can be written, respectively, as

$$L_0 = -\frac{1}{4}(\partial_\mu A^k_\nu - \partial_\nu A^k_\mu)^2 - \frac{1}{2\alpha}(\partial_\mu A^k_\mu)^2 + \bar{\psi}^a(i\partial\!\!\!/ - m)\psi^a \quad \text{and}$$
$$L_I = -g f^{ijk}(\partial_\mu A^i_\nu) A^j_\mu A^k_\nu - \frac{1}{4} g^2 f^{ijk} f^{imn} A^j_\mu A^k_\nu A^m_\mu A^n_\nu + \frac{g}{2} \bar{\psi}^a \gamma_\mu A^k_\mu (\lambda^k)^{ab} \psi^b. \tag{4.62}$$

The generating functional $W(J)$, according to Eq. (4.56), is

$$W(J^i_\mu, \bar{\eta}^a, \eta^a) = R \exp\{-i\int dx dy [\frac{1}{2} J^i_\mu(x)(K^{ij}_{\mu\nu}(x-y))^{-1} J^j_\nu(y) + \bar{\eta}^a(x) K^{-1}_{ab}(x-y)\eta^b]\}, \tag{4.63}$$

where

$$R = \exp\{i\int dx L_I(-i\frac{\delta}{\delta J^i_\mu(x)}, -i\frac{\delta}{\delta \bar{\eta}^a(x)}, -i\frac{\delta}{\delta \eta^a(x)})\}. \tag{4.64}$$

Following Eq. (4.59) R can be expanded into a power series:

$$R = 1 + i\int dx L_I(-i\frac{\delta}{\delta J^i_\mu(x)}, \dots) + \frac{i^2}{2}\int dx \int dy L_I(-i\frac{\delta}{\delta J^i_\mu(x)}, \dots) L_I(-i\frac{\delta}{\delta J^i_\mu(y)}, \dots) + \cdots, \tag{4.65}$$

where the fields in $L_I(x)$ are substituted according to

$$A^k_\mu \to -i\frac{\delta}{\delta J^k_\mu}, \quad \bar{\psi}^a \to -i\frac{\delta}{\delta \eta^a}, \quad \text{and} \quad \psi^a \to -i\frac{\delta}{\delta \bar{\eta}^a}. \tag{4.66}$$

The propagator of the free quark and gluon fields are found through

$$\frac{\delta^2}{\delta\eta^a(x)\delta\bar{\eta}_b(y)} Z_0(J^k_\mu, \ldots)|_{J^k_\mu = \ldots = 0} = -K^{ab}(x-y)^{-1}, \tag{4.67}$$

and

$$\frac{\delta^2}{\delta J^k_\mu(x)\delta J^l_\nu(y)} Z_0(J^k_\mu, \ldots)|_{J^k_\mu = \ldots = 0} = -K^{kl}_{\mu\nu}(x-y)^{-1}, \tag{4.68}$$

respectively. Here $Z_0(J) = Z(J)|_{L_I = 0}$. The gluon propagator $(K^{kl}_{\mu\nu})^{-1}$, the only gauge dependent Feynman rule, can be calculated now. As is stated in Eq. (4.53) the gluon propagator is determined by the form of the free Lagrangian which, for the gluon fields, is

$$L_0(x) = -\frac{1}{4}(\partial_\mu A^k_\nu - \partial_\nu A^k_\mu)^2 - \frac{1}{2\alpha}(\partial_\mu A^k_\mu)^2. \tag{4.69}$$

Integrating by parts gives

$$\int dx L_0(x) = \frac{1}{2}\int dx A^k_\mu \Big[g_{\mu\nu}\partial^2 - (1 - \frac{1}{\alpha})\partial_\mu\partial_\nu \Big] A^k_\nu. \tag{4.70}$$

According to Eq. (4.53) one can identify immediately that

$$K^{kl}_{\mu\nu}(x-y) = \delta^{kl}\delta(x-y)\Big[g_{\mu\nu}\partial^2 - (1 - \frac{1}{\alpha})\partial_\mu\partial_\nu \Big]. \tag{4.71}$$

In momentum space Eq. (4.71) becomes:

$$K^{kl}_{\mu\nu}(k) = \Big[-g_{\mu\nu}k^2 + (1 - \frac{1}{\alpha})k_\mu k_\nu \Big] \delta^{kl}. \tag{4.72a}$$

Upon direct verification one finds that

$$K^{kl}_{\mu\nu}(k)^{-1} = \frac{1}{k^2}\Big[-g_{\mu\nu} + (1-\alpha)k_\mu k_\nu \Big] \delta^{kl} \tag{4.72b}$$

is the inverse of Eq. (4.72a). Finally, in the α-gauge, the gluon propagator is abtained:

$$-i\frac{\delta^2}{\delta J_\mu^k(x)\delta J_\nu^l(y)}Z_0|_{J=0} = -i\frac{\delta_{kl}}{(2\pi)^4}\int\frac{dk}{k^2}\left[g_{\mu\nu} - (1-\alpha)\frac{k_\mu k_\nu}{k^2}\right]e^{ik(x-y)}. \tag{4.73}$$

The quark-gluon vertex, the three-gluon vertex, and the four-gluon vertex are determined to the leading order as follows:

$$i\Gamma_\mu^{kab}(x,y,z) = i\frac{\delta^3}{\delta A_\mu^k(x)\delta\psi^b(z)\delta\overline{\psi}^a(y)}\Gamma_{\text{tree}}(A_\mu^k, \dots)|_{A=\dots=0}, \tag{4.74}$$

$$i\Gamma_{\mu\nu\lambda}^{klm}(x,y,z) = i\frac{\delta^3}{\delta A_\mu^k(x)\delta A_\nu^l(y)\delta A_\lambda^m(z)}\Gamma_{\text{tree}}(A_\mu^k \dots)|_{A=\dots=0}, \tag{4.75}$$

and

$$i\Gamma_{\mu\nu\lambda\rho}^{jklm}(x,y,z,u) = i\frac{\delta^4}{\delta A_\mu^j(x)\delta A_\nu^k(y)\delta A_\lambda^l(z)\delta A_\rho^m(u)}\Gamma_{\text{tree}}(A_\mu^k, \dots)|_{A=\dots=0}, \tag{4.76}$$

where

$$\Gamma_{\text{tree}} = \int dx L(A_\mu^k(x), \psi^b(x), \overline{\psi}^a(x)) \tag{4.77}$$

as given in Eq. (4.49).

In momentum space these Feynman rules are derived as

$$i\Gamma_\mu^{kab}(p,q,r) = -\frac{i}{2}g\gamma_\mu(\lambda^k)^{ab}, \tag{4.78}$$

$$i\Gamma_{\mu\nu\lambda}^{ijk} = gf^{ijk}[(q-p)_\lambda g_{\mu\nu} + (q-r)_\mu g_{\mu\lambda} + (r-q)_\mu g_{\lambda\nu}], \tag{4.79}$$

$$
\begin{aligned}
i\Gamma^{jklm}_{\mu\nu\lambda\rho} = ig^2[& f^{jnm}f^{kln}(g_{\mu\nu}g_{\lambda\rho} - g_{\mu\lambda}g_{\nu\rho}) \\
& + f^{jkn}f^{lmn}(g_{\rho\mu}g_{\mu\lambda} - g_{\mu\lambda}g_{\nu\rho}) \\
& + f^{jnl}f^{kmn}(g_{\mu\nu}g_{\lambda\rho} - g_{\rho\mu}g_{\nu\lambda})\,]
\end{aligned}
\tag{4.80}
$$

In the multi-gluon-vertex cases all indices circulate counter-clockwise and are associated in order. For example, k, μ, and p are the color index, Lorentz index and the momentum of one gluon as in Eq. (4.79). Furthermore, all momenta are out of the vertices.

In order to define the Feynman rules a convention needs to be chosen. There are several conventions for defining Feynman rules. For example, one can change the coupling constant $g \rightarrow -g$ without changing the physics. Furthermore, each propagator and vertex is normally associated with a factor (i) or (-i) so that collectively a diagram consistint of propagators and vertices would have the correct sign and the phase (i). There are various ways to assign these factors to propagators and vertices. The convention used here is to assign a factor (-i) to each propagator and a factor (i) to each vertex, as is shown in deriving the gluon propagator and vertices in Eq. (4.73-76). This convention is verified by directly evaluating the S-matrix element containing a certain diagram by using Eq. (4.58), and the overall factor agrees with what should be obtained from calculating the same diagram by using the Feynman rules.

It is noteworthy to point out that directly calculating the matrix element containing a certain diagram is much more complicated than using the Feynman rules. In order to get a complete diagram the calculation has to be done at higher order while the Feynman rules are only elements of a diagram so that its calculation can be done at the lowest order.

4.5 Implementation of Gauge Invariance Testing

As mentioned earlier, DIAG can check gauge invariance by replacing the polarization 4-vector ε_μ of a specified external gauge boson with its momentum 4-vector k_μ. This checking scheme, obviously, can not apply to processes that do not involve external gauge bosons. For such a class of processes the most convenient method to check for gauge invariance is to calculate an amplitude under an arbitrary covariant gauge and verify that the result of the calculation is gauge-invariant. In an arbitrary covariant gauge characterized by the gauge parameter $\xi = 1 - \frac{1}{\alpha}$, as demonstrated in the previous section, the only gauge-dependent Feynman rule is that for the gluon propagator. The amplitude in the ξ-gauge, as discussed before, is a polynomial in ξ. Gauge invariance is equivalent to ξ-independence here and, therefore, coefficients of any non-zero order of ξ vanish identically. To incorperate this scheme into DIAG the most suitable and general approach is to calculate the amplitude-coefficient for a specified order of ξ by replacing a specified number (equal to the specified order of ξ) of $g_{\mu\nu}$'s with $k_\mu k_\nu/k^2$'s. This replacement and calculation must be allowed for any order of ξ.

Unlike gauge invariance testing performed on external gauge bosons where the replacement $k_\mu \rightarrow \varepsilon_\mu$ takes place for and only for a specified external boson, the replacement $k_\mu k_\nu/k^2 \rightarrow g_{\mu\nu}$ for that testing performed on internal gluons takes place a certain number of times for each diagram with all possible combinations. Taking $MB \rightarrow MB$ as an example and assuming that the amplitude of ξ^2 is in question, for simple diagrams that do not contain multi-gluon vertices there are four internal gluons for each diagram. In order to collect all ξ^2 terms two of the four gluons' $g_{\mu\nu}$ should be replaced by $k_\mu k_\nu/k^2$ and the diagram must be calculated for all possible $C_4^2 = 6$ double replacements. For diagrams with triple three-gluon vertices in which seven internal gluons are involved, each diagram has $C^{21} = 21$ possible double replacements.

The implementation of this scheme is very sophisticated and complicated, especially when more then one three-gluon vertex is involved. Since DIAG was designed for calculations under Feynman gauge, the spin-factor evaluation part of it must be redesigned and rewritten. The program must be capable of:

- generating all possible combinations of the replacement $k_\mu k_\nu / k^2 \rightarrow g_{\mu\nu}$ for gluon propagators once and only once for a given order of ξ,

- remembering and identifying the gluons having the replacement in effect and applying different computing rules accordingly,

- tracking a gluon "tree" if two or more multi-gluon vertices are present since, in that case, the computing rule for a certain gluon propagator is dependent on its neighbouring multi-gluon vertices.

This type of gauge invariance checking was expected to be a very powerful one since, still taking $MB \rightarrow MB$ for example, the vanishing of the amplitude-coefficients can be checked order by order up to ξ^7. It was later discovered that high-order amplitude coefficients are trivially zero. It can be easily seen as follows:

Suppose that a quark line is attached by one and only one gluon propagator; then the momentum of the gluon can be assigned as $k_i - k_f$ where k_i is the momentum of the incident quark and k_f is that of the outgoing quark. If the gauge replacement is in effect for this gluon, the quark line then evaluates to a factor $u\dagger_f(k_f)(\not{k}_i - \not{k}_f)u_i(k_i) = 0$ because of the fact that $\not{k}u(k) = 0$. For the $MM \rightarrow MM$ case at most one gluon can attach both of its ends to quark lines that also have other gluons attached on them. Therefore only single gauge replacement yields a non-trivial amplitude.

For the $MB \rightarrow MB$ case the amplitude of ξ^2 is also non-trivial, and finally for $BB \rightarrow BB$ only the amplitudes for the first three orders of ξ are non-trivial.

It should be noticed that the trivially vanishing amplitudes are not results of gauge invariance, which always reveals itself as cancellations in a sum of diagrams. In the $MM \rightarrow MM$ case, for example, a diagram with a four-gluon vertex does not contribute in gauge invariance testing so that the testing can not discover any mistake within the calculation for the four-gluon vertex. Fortunately there is only one diagram with a four-gluon vertex for $MM \rightarrow MM$. Caution must be taken, though, should a similar situation arise in other scattering reactions. Although the trivial amplitudes of higher order ξ make the gauge invariance checking less complete and powerful than it was expected, it is still the best available method to ensure the correctness of DIAG's calculation.

Chapter V

Hadron Wavefunctions

Factorization separates the non-perturbative part of a scattering reaction from the perturbative part and absorbs it into hadronic wave functions. In the asymptotic limit $Q^2 \to \infty$, the form of hadron wave functions is purely perturbative and is independent of its Q^2-evolutionary history [10] and, therefore, is universal for baryons or mesons. It can also be easily derived [18] for baryons that $\varphi_{asy}(x) \sim x_1 x_2 x_3$ where x_1, x_2, and x_3 are momentum fractions of the valance quarks. At the scale of momentum transfer that is experimentally accessible, however, the asymptotic form resembles little the true hadron wave functions. Although the Q^2-dependence of hadron wave functions is also determined by perturbative QCD, the wave functions themselves are determined by non-perturbative QCD.

QCD sum rules provide a very promising approach to determine these wave functions. With the sum-rule derived wave functions QCD calculations for the nucleon magnetic form factors and for the branching ratio of $\mathrm{br}(\psi \to p\bar{p})/\mathrm{br}(\psi \to e^+e^-)$ [10] give good agreement with experiments. On

the other hand, the perturbative QCD calculation for $\gamma\gamma \to p\bar{p}$ is about an order of magnitude smaller than the experimentally measured cross section at $W_{\gamma\gamma} \sim 2.5$GeV, even when the sum-rule derived wave functions are used [21]. Although such a barely above threshold center-of-mass energy may be too low to justify the application of perturbative QCD, it is interesting and important to get an assessment of the accuracy of the wave functions and the sensitivity of perturbative QCD predictions to variations in the wave functions.

5.1 Sum-Rule Derived Wave Functions

The wave function for the proton, for instance, is the amplitude for finding the three-quark valence state in which the momentum partition of the three quarks is $(x_1p,\ x_2p,\ x_3p)$ where p is the longitudinal momentum of the proton and $x_1 + x_2 + x_3 = 1$. The transverse momentum of the quarks in the proton state can be neglected in the leading twist approximation since they are very small relative to the momentum transfer Q^2 and, hence, the longitudinal momentum p of the proton. As mentioned earlier at momentum scales relevant for experiments ($Q^2 = 15 \sim 20$ GeV for the nucleon magnetic form factors) the proton wave function differs significantly from its asymptotic form $\varphi_{asy} \sim x_1x_2x_3$. This is mainly due to the extremely slow evolution of the wave function with Q^2 when Q^2 is large. The dependence on Q^2 of the wave function can be determined by the evolution equation [9]

$$Q^2\frac{\partial}{\partial Q^2}\varphi(x,Q) = \frac{\alpha_s(Q^2)}{4\pi}\int_0^1 d_3y\ V(x,y)\,\varphi(y,Q), \tag{5.1}$$

in the leading order, where V can be evaluated from a single-gluon-exchange kernel. Following reference [9] the general solution of the evolution equation takes the form

$$\varphi(x,Q) = f_N \varphi_{asy}(x) \sum_{n=0}^{\infty} C_n \left[\frac{\alpha_s(Q^2)}{\alpha_s(\mu^2)} \right]^{\gamma_n} P_n(x), \tag{5.2}$$

where f_N is the decay constant, $\varphi_{asy}(x) \sim x_1 x_2 x_3$ is the asymptotic wave function, $P_n(x)$ are Appel polynomials (eigensolutions of the evolution equation), γ_n are associated anomalous dimensions and C_n are coefficients to be determined, which contain all non-perturbative information of the wave function.

The moments of the wave function,

$$< x_1^{n_1} x_2^{n_2} x_3^{n_3} >_{\mu^2} = \int_0^1 d_3 x x_1^{n_1} x_2^{n_2} x_3^{n_3} \varphi(x, \mu^2), \tag{5.3}$$

can be studied by QCD sum rules. At present only $p = n_1 + n_2 + n_3 \leq 2$ moments have been determined so that further approximation must be made to Eq. (5.2). Since there are six independent $p \leq 2$ moments, all the coefficients C_n can be uniquely determined if only the first six terms of Eq. (5.2) are kept. Further setting $Q^2 = \mu^2 \sim 1\text{GeV}^2$ at which the moments are evaluated, Eq (5.2) is reduced to

$$\varphi(x, \mu^2) = \varphi_{asy}(x) \sum_{0}^{5} C_n P_n(x). \tag{5.4}$$

The determination of the six C_n by the six $p \leq 2$ moments is then straightforward linear algebra.

To illustrate how the moments could be calculated the familiar example of the π-meson should be taken. Following Chernyak and Zhitnitsky [18] the leading twist matrix element of the π-meson is determined by:

$$
\begin{aligned}
&<0|\bar{d}(z)\not{z}\gamma_5 \exp\Big[ig\int_{-z}^{z} d\sigma_\lambda A_\lambda(\sigma)\Big]u(-z)|\pi^+(p)> \\
&\quad \equiv \sum_n \frac{i^n}{n!} <|\bar{d}\not{z}\gamma_5(iz_\nu \overleftrightarrow{D}_\nu)^n u(0)|\pi^+(p)> \\
&\quad = i(zp)f_\pi \int_{-1}^{1} d\zeta\, e^{i\zeta(zp)}\varphi^\pi(\zeta),
\end{aligned}
\tag{5.5}
$$

where

$$
\overleftrightarrow{D} = \overrightarrow{D} - \overleftarrow{D},\ \ \overrightarrow{D} = \overrightarrow{\partial} - igA^a(\lambda^a/2),
$$

and $\zeta = x_1 - x_2$ is the relative momentum fraction. At large Q^2($z^2 \sim 1/Q^2 \to 0$) the left side of Eq. (5.5) can be evaluated to the form:

$$
<0|\bar{d}\not{z}\gamma_5(iz\overleftrightarrow{D})^n u|\pi(p)> = z_\nu z_{\mu_1}\ldots z_{\mu_n} <0|\bar{d}\gamma_\nu\gamma_5 i\overleftrightarrow{D}_{\mu_1}\ldots i\overleftrightarrow{D}_{\mu_n} u|pi> = (zp)^{n+1}D_n, \tag{5.6}
$$

where D_n are some constants. Expanding the exponential in the right side of Eq. (5.5) yields

$$
i(zp)f_\pi \int_{-1}^{1} d\zeta e^{i\zeta(zp)}\varphi_\pi(\zeta) = f_\pi \sum_n \frac{i^{n+1}}{n!}(zp)^{n+1}\int_{-1}^{1} d\zeta\, \zeta^n \varphi_\pi(\zeta) = f_\pi \sum_n \frac{i^{n+1}}{n!}(zp)^{n+1} <\zeta^n>. \tag{5.7}
$$

By relating Eq. (5.6) and (5.7) through Eq. (5.5) it can be found easily that

$$
D_n = if_\pi <\zeta^n>. \tag{5.8}
$$

The matrix elements of Eq. (5.6) can be calculated with the assistance of the QCD sum rules so that the moments can be determined.

To construct the proton wave function of the leading twist, for example, the following three-local operator matrix element [10] should be defined:

$$
\begin{aligned}
&<0|u_\alpha^i(z_1)u_\beta^j(z_2)d_\gamma^k(z_3)|p>\varepsilon^{ijk} \\
&\quad = \frac{1}{4}f_N\Big\{(\not{p}C)_{\alpha\beta}(\gamma_5 N)_\gamma V(z_ip) + (\not{p}\gamma_5 C)_{\alpha\beta}N_\gamma A(z_ip) - (\sigma_{\mu\nu}p_\nu C)_{\alpha\beta}(\gamma_\mu\gamma_5 N)_\gamma T(z_ip)\Big\},
\end{aligned}
\tag{5.9}
$$

where, as before, Latin letters denote color indices and Greek letters denote Lorentz indices, $|p>$ is the proton state with momentum p, C is the charge conjugation matrix, N is the proton spinor and u and d are quark fields. The general proton state (spin up) takes the form:

$$|p_+> = \left[\psi_1(x)|u^l_+ u^m_+ d^n_- > + \psi_2(x)|u^l_+ u^m_- d^n_+ > + \psi_3(x)|u^l_- u^m_+ d^n_+ >\right]\frac{\varepsilon^{lmn}}{\sqrt{6}}, \tag{5.10}$$

where '+' denotes spin-up and '−' denotes spin-down. In terms of Lorentz indices '+' and '−' correspond to 0 and 3 respectively. Transforming the quark fields in Eq. (5.9) into momentum space and substituting Eq. (5.10) into Eq. (5.9) yields

$$\begin{aligned}
\psi_1(x) &= -\frac{f_N}{2\sqrt{24}}T(x), \\
\psi_2(x) &= \frac{f_N}{2\sqrt{24}}\frac{V(x)-A(x)}{2}, \\
\psi_3(x) &= \frac{f_N}{2\sqrt{24}}\frac{V(x)+A(x)}{2},
\end{aligned} \tag{5.11}$$

where $T(x)$, $V(x)$, and $A(x)$ are momentum-space representations of their counterparts in Eq. (5.9). The proton state can then be given in terms of T, V, and A as

$$\begin{aligned}
|p_+> = &\frac{f_N}{2\sqrt{24}}\frac{\varepsilon^{lmn}}{\sqrt{6}} \\
&\times\left[T(x)|u^l_+ u^m_+ d^n_- > + \frac{V(x)-A(x)}{2}|u^l_+ u^m_- d^n_+ > + \frac{V(x)+A(x)}{2}|u^l_- u^m_+ d^n_+ >\right],
\end{aligned} \tag{5.12}$$

The two u-quark symmetry requires

$$T(1,2,3) = T(2,1,3), \quad V(1,2,3) = V(2,1,3), \quad \text{and} \quad A(1,2,3) = -A(2,1,3), \tag{5.13}$$

and the fact that the isospin of the proton equals $\frac{1}{2}$ leads to

$$\begin{aligned}
&2T(1,2,3) = \varphi_N(1,3,2) + \varphi_N(2,3,1), \quad \text{and} \\
&\varphi_N(1,2,3) = V(1,2,3) - A(1,2,3),
\end{aligned} \tag{5.14}$$

where the arguments 1,2,3 represent x_1, x_2, and x_3. respectively. Therefore, there is only one independent wave function for the proton. For definiteness φ_N shall be chosen to be the independent one.

For the wave functions given above two sources of uncertainty are studied. First, the moments calculated by QCD sum rules have associated errors. How do the errors manifest themselves in wave functions and how do they affect the perturbative QCD predictions is a question to be answered. Second, the model wave function contains only quadratic terms and thus accounts only for $p \leq 2$ moments. The contributions from $p \geq 3$ moments are totally unknown and uncontrolled. Is there any clue that one can get some control on these uncertainties is another question to explore. Two simple reactions, $\psi \to p\bar{p}$ and the nucleon magnetic form factor $G_M^{p,n}$, are chosen for this analysis because 1) they are simple and easy to calculate and 2) measurements are available for the momentum scale that justifies a perturbative QCD calculation.

In the rest of the analysis, if not otherwise specified, all calculations for $\psi \to p\bar{p}$ and $G_M^{p,n}$ are normalized to the measurements. They are calculated in the form

$$\left[(\frac{1}{2}m_\psi)^4 e^2\right]^2 \frac{\mathrm{br}(\psi \to p\bar{p})}{\mathrm{br}(\psi \to e^+e^-)} = 0.00834\mathrm{GeV}^8,$$
$$Q^4 G_M^p = 1.17\mathrm{GeV}^4, \text{ and } G_M^n = -\frac{1}{2}G_M^p$$

where the corresponding data are also given. $\gamma\gamma \to p\bar{p}$ is calculated as $s^6\frac{d\sigma}{dt}$ in the unit of $\mu b \cdot \mathrm{GeV}^{10}$. If not otherwise specified its value is given at $\cos\theta = 0.4$ which is an approximation of the average of the cross section over the " wide angle " region $\cos = 0.0 \to 0.6$.

5.2 *Uncertainties of Sum-Rule Derived Moments*

Knowing the moments of the nucleon wave functions, the asymptotic form to which the wave functions will evolve in the limit of $Q^2 \to \infty$ and the overall normalization $\int_0^1 d_3x\, \varphi_N(x,Q^2) = 1$, one can construct a model wave function in the form of Eq. (5.4) that possesses all these properties. Chernyak and Zhitnitsky (CZ) [10] first did the sum-rule calculation and proposed a model wave function. King and Sachrajda (KS) [28] redid the calculation and found some changes to CZ's original calculation. The KS moments and wave function is used in this analysis. Within errors these moments agree with those now obtained by CZ [29]. Table 2 on page 80 lists these moments and their errors.

For $p \leq 2$ there are ten moments out of which six moments are independent because of the relation $x_1 + x_2 + x_3 = 1$. The overall normalization factor, physically the decay constant, f_N is determined by setting $<000>$ to 1 where $<n_1n_2n_3>$ is an abbreviated notation for moment $<x_1^{n1}x_2^{n2}x_3^{n3}>$. For the analysis of uncertainties the errors of independent moments are assumed to be independent, also. Noting that $<000>$ must be chosen as one of the independent moments, since it is the only $p = 0$ moment and also that it has no error, there are five independent errors contributing to the uncertainty. To avoid overestimating the uncertainty five independent moments with the least error ranges are chosen, and the error ranges of two of them are reduced by half to ensure that the remaining four dependent moments are within their error ranges when they are determined by the six independent ones.

Since the five errors are assumed to be independent, each of them will introduce an independent error for the wave function. The wave function, with the uncertainty, can be written as

Table 2. Moments of the Nucleon Wave Functions

	CZ (original)		KS		CZ (new)	
$n_1 n_2 n_3$	sum rules	model	sumrules	model	sum rules	model
000	1	1	1	1	1	1
100	0.60-0.75	0.63	0.49-0.59	0.55	0.54-0.62	0.579
010	0.09-0.16	0.15	0.18-0.21	0.21	0.18-0.20	0.192
001	0.18-0.24	0.22	0.22-0.26	0.24	0.20-0.25	0.229
200	0.25-0.40	0.40	0.27-0.37	0.35	0.32-0.42	0.369
020	0.03-0.08	0.03	0.08-0.09	0.09	0.065-0.088	0.068
002	0.08-0.12	0.08	0.10-0.12	0.12	0.09-0.12	0.089
110	0.07-0.12	0.11	0.08-0.10	0.10	0.08-0.10	0.097
101	0.09-0.14	0.12	0.09-0.11	0.10	0.09-0.11	0.113
011	−0.03-0.03	0.03	unreliable	0.02	−0.03-0.03	0.027

Three calculations are listed. The sum rule column gives the ranges of moments determined by sum rules and the model column gives the values chosen for constructing the model wave functions.

$$
\begin{aligned}
\varphi(x) &= \varphi_N(x) \pm \varphi_1(x) \pm \varphi_2(x) \pm \varphi_3(x) \pm \varphi_4(x) \pm \varphi_5(x) \\
&= 20.16x_1^2 + 15.12x_2^2 + 22.68x_3^2 + 8.4x_1 + 5.04x_2 - 11.76 \\
&\pm [-1.26x_1^2 - 3.78(x_2^2 + x_3^2) - 2.52x_1 + 2.1] \\
&\pm [2.52(x_1^2 - x_2^2) - 1.68(x_1 - x_2)] \\
&\pm [2.52x_1^2 - 7.56x_2^2 - 12.6x_3^2 - 11.76x_1 - 3.36x_2 + 7.56] \\
&\pm [8.82x_1^2 + 3.78(x_2^2 - x_3^2) - 9.24x_1 - 5.88x_2 + 3.78] \\
&\pm [-7.56(x_1^2 - x_2^2) + 5.88(x_1 - x_2)]
\end{aligned}
\tag{5.15}
$$

The moments of the five wave function errors, the central part of the wave function (KS), and the sum-rule calculation are presented in Table 3 on page 82. The errors of the moments $<001>$, $<020>$, $<002>$, $<110>$, and $<101>$ are chosen to be independent and the error ranges of $<001>$ and $<110>$ are reduced by half.

The effects of the uncertainties on perturbative QCD predictions are calculated for $\psi \to p\bar{p}$ and the magnetic form factor of the proton. The result can be represented as a matrix whose elements are

$$
M_{ij} = \int_0^1 \int_0^1 d_3x\, d_3y\, \varphi_i^*(x)\, T_H(x,y,Q^2)\, \varphi_j(x). \tag{5.16}
$$

where $\varphi_0 = \varphi_N$. The results are presented in Table 4 on page 84 and Table 5 on page 85 with the symmetric part left blank and normalized to 1 with respect to the measurements. The total error ε is defined by

$$
\varepsilon^2 = \sum_{i+j>0} M_{ij}^2,
$$

and is about 4% for $\psi \to p\bar{p}$ and 40% for G_M^p.

Table 3. Moments of KS Wave Function and Its Error Wave Functions

$n_1n_2n_3$	sum rules	φ_N	φ_1	φ_2	φ_3	φ_4	φ_5
000	1	1	0	0	0	0	0
100	0.49-0.59	0.55	−.02	0.01	−.02	0.01	0.01
010	0.18-0.21	0.21	0.01	−.01	0.02	−.01	−.01
001	0.22-0.26	0.24	0.01	0.00	0.00	0.00	0.00
200	0.27-0.37	0.35	−.02	0.01	−.02	0.02	0.00
020	0.08-0.09	0.09	0.00	−.01	0.00	0.00	0.00
002	0.10-0.12	0.12	0.00	0.00	−.02	0.00	0.00
110	0.08-0.10	0.10	0.00	0.00	0.00	−.01	0.00
101	0.10-0.11	0.10	0.00	0.00	0.00	0.00	0.01
011	unreliable	0.02	0.01	0.00	0.02	0.00	−.01

As can be seen from Table 3 on page 82, the uncertainty is still somewhat overestimated because, when the contributions from all five error terms to a certain moment are combined it will be big enough to exceed the error range of the moment. Nevertheless, it gives a reasonable upper bound of the uncertainties.

5.3 Uncertainties from High Moments

Unlike the uncertainties of the $p \leq 2$ moments which are well understood and under control, the uncertainties due to $p \geq 3$ moments are totally unknown. Since the sum-rule calculation is very difficult, it is not anticipated that the $p \geq 3$ moments will be calculated soon. What can be done in the absence of high sum-rule moments then? Firstly, the sensitivity of perturbative QCD predictions to the contributions of high moments, $p = 3$ in particular, can be studied. Secondly, one can impose some constraints based on physically reasonable guesses for the high moments; and finally, the contributions of the high moments can be parametrized to fit the existing data. In any case the cubic Appel polynomials must be derived for these analyses.

There are ten $p = 3$ moments of which four are independent. Correspondingly, there are four orthogonal cubic Appel polynomials. A general method of deriving Appel polynomials has been given in reference [9] but only quadratic Appel polynomials have been derived. Defining $\widetilde{\varphi}(x,Q)$

Table 4. Uncertainties for the Branching Ratio of ψ Decay

wfn	φ_N	φ_1	φ_2	φ_3	φ_4	φ_5
φ_N	0.9389	0.0073	0.0002	0.0278	0.0077	0.0002
φ_1		0.0001	0.0000	0.0002	0.0001	0.0000
φ_2			0.0000	0.0000	0.0000	0.0000
φ_3				0.0010	0.0002	0.0000
φ_4					0.0001	0.0000
φ_5						0.0000

$\varepsilon \sim 4.2\%$

Table 5. Uncertainties for the Proton Form Factor

wfn	φ_N	φ_1	φ_2	φ_3	φ_4	φ_5
φ_N	1.0683	−0.1136	0.0442	−0.1787	0.1539	−0.0838
φ_1		0.0121	0.0046	0.0190	−0.0163	0.0085
φ_2			0.0018	−0.0074	0.0060	−0.0035
φ_3				0.0299	−0.0258	0.0138
φ_4					0.0219	−0.0109
φ_5						0.0072

$\varepsilon \sim 40\%$

by $\varphi(x,Q) \equiv x_1x_2x_3\tilde{\varphi}(x,Q)$ and $\xi \equiv \ln\ln\frac{Q^2}{\Lambda^2}$, the evolution equation for baryon wave functions can be written as

$$x_1x_2x_3\left(\frac{\partial}{\partial\xi} + \frac{3}{2}\frac{C_F}{\beta_0}\right)\tilde{\varphi}(x,Q) = \frac{C_B}{\beta_0}\int_0^1 d_3y V(x,y)\tilde{\varphi}(y,Q), \tag{5.17}$$

where

$$C_B = \frac{n_c + 1}{2n_c}, \quad C_F = \frac{n_c^2 - 1}{2n_c}, \quad \text{and} \quad n_c = 3$$

and the potential V is given by

$$\begin{aligned} V(x,y) &= 2x_1x_2x_3\sum_{i\neq j}\theta(y_i - x_i)\delta(x_k - y_k)\frac{y_i}{x_i}\left[\frac{\delta_{h_i\bar{h}_j}}{x_i + x_j} + \frac{\Delta}{y_i - x_i}\right] \\ &= V(y,x), \end{aligned} \tag{5.18}$$

where $\Delta\tilde{\varphi}(y,Q) \equiv \tilde{\varphi}(y,Q) - \tilde{\varphi}(x,Q)$ and $\delta_{h_i\bar{h}_j} = 1(0)$ if the helicities of quark i and quark j are antiparallel (parallel). Assuming that the eigenfunction of Eq. (5.17) takes on the form:

$$\tilde{\varphi}(x,Q) = \tilde{\varphi}_n(x)e^{-\gamma_n\xi} = \tilde{\varphi}_n(x)\left[\ln\frac{Q^2}{\Lambda^2}\right]^{-\gamma_n},$$

the ξ-dependent part can then be factored out, which leaves

$$x_1x_2x_3\left(\frac{3}{2}\frac{C_F}{\beta_0} - \gamma_n\right)\tilde{\varphi}_n(x) = C_B\int_0^1 d_3y V(x,y)\tilde{\varphi}_n(y). \tag{5.20}$$

The eigenfunctions of Eq. (5.20) are referred to as Appel polynomials. Because of the fact that $V(x,y)$ is real and symmetric, $V(x,y) = V(y,x)$, the eigenvalues γ_n are real and, therefore, it can be easily shown that $\{\tilde{\varphi}_n(x)\}$ form a complete and orthogonal basis with weight $w(x) = x_1x_2x_3$. Expanding V in a polynomial basis $\{x_1^{n_1}x_2^{n_2}\}$ by virtue of Eq. (5.18), one obtains:

$$
\begin{aligned}
&\frac{1}{2x_1x_2x_3}\int_0^1 d_3y V(x,y) y_1^m y_3^n \\
&= \left[\frac{\delta_{h_2\bar{h}}}{(m+1)}(m+2) - 3\sum_{j=2}^{m+1}\frac{1}{j} + \frac{\delta_{h_2\bar{h}}}{(n+1)}(n+2) - 3\sum_{j=2}^{n+1}\frac{1}{j}\right] x_1^m x_3^n \\
&+ \left[\sum_{i=1}^{m}\frac{m-i+1+\delta_{h_2\bar{h}}}{i}(m+2)x_1^{m-i}\sum_{j=0}^{i}\binom{i}{j}(-1)^j x_3^{n+j} + \binom{1\leftrightarrow 3}{m\leftrightarrow n}\right] \\
&- \left[\sum_{i=1}^{n} x_1^{m+i}x_3^{n-i}\sum_{j=0}^{i}\binom{n}{j}\binom{n-j}{n-i}(-1)^j\sum_{k=2}^{m+j+1}\frac{1}{k} + \binom{1\leftrightarrow 3}{m\leftrightarrow n}\right] \\
&= \sum_{i,j}(x_1^i x_3^j)U_{ij,mn},
\end{aligned}
\tag{5.21}
$$

where $\delta_{h_2\bar{h}} = 1(0)$ for spin-$\frac{1}{2}$($\frac{3}{2}$) baryons. Substituting Eq. (5.21) into Eq. (5.20) yields an eigenvalue system:

$$
\left(\frac{3}{2}\frac{C_F}{\beta_0} - \gamma_k\right)\left[x_1^m x_3^n\right] = \frac{2C_B}{\beta_0}\sum_{i,j}\left[x_1^i x_3^j\right]U_{ij,mn}. \tag{5.22}
$$

The anomalous dimension γ_n can be found readily

$$
\gamma_n = \left(\frac{3}{2}C_F - 2C_B\lambda_n\right)/\beta_0, \tag{5.23}
$$

where λ_n are the eigenvalues of the matrix U determined by

$$
U\chi = \lambda\chi, \quad \chi^T = (1, x_1, x_3, x_1^2, \ldots). \tag{5.24}
$$

For $m + n \leq 3$ and in the basis $\{m,n\} \equiv \{x_1^m x_3^n\}$ defined by

{00 10 01 20 11 02 30 21 12 03}

the matrix U for a spin-$\frac{1}{2}$ baryon can be calculated directly from Eq. (5.21):

$$\begin{bmatrix}
1 & \frac{2}{3} & \frac{2}{3} & \frac{1}{4} & 0 & \frac{1}{4} & \frac{2}{15} & 0 & 0 & \frac{2}{15} \\
0 & -\frac{5}{6} & -\frac{1}{6} & \frac{3}{4} & \frac{2}{3} & -\frac{1}{2} & \frac{3}{10} & 0 & \frac{1}{4} & -\frac{2}{5} \\
0 & -\frac{1}{6} & -\frac{5}{6} & -\frac{1}{2} & \frac{2}{3} & \frac{3}{4} & -\frac{2}{5} & \frac{1}{4} & 0 & \frac{3}{10} \\
0 & 0 & 0 & -\frac{23}{12} & -\frac{1}{3} & \frac{5}{12} & \frac{4}{5} & \frac{2}{3} & -\frac{1}{2} & \frac{2}{5} \\
0 & 0 & 0 & \frac{1}{4} & -\frac{8}{3} & \frac{1}{4} & -\frac{3}{5} & \frac{3}{4} & \frac{3}{4} & -\frac{3}{5} \\
0 & 0 & 0 & \frac{5}{12} & -\frac{1}{3} & -\frac{23}{12} & \frac{2}{5} & -\frac{1}{2} & \frac{2}{3} & \frac{4}{5} \\
0 & 0 & 0 & 0 & 0 & 0 & -\frac{27}{10} & -\frac{5}{12} & \frac{1}{3} & -\frac{1}{20} \\
0 & 0 & 0 & 0 & 0 & 0 & \frac{7}{10} & -\frac{15}{4} & -\frac{1}{12} & \frac{4}{5} \\
0 & 0 & 0 & 0 & 0 & 0 & \frac{4}{5} & -\frac{1}{12} & -\frac{15}{4} & \frac{7}{10} \\
0 & 0 & 0 & 0 & 0 & 0 & -\frac{1}{20} & \frac{1}{3} & -\frac{5}{12} & -\frac{27}{10}
\end{bmatrix}. \tag{5.25}$$

The matrix can be decomposed into orthogonal subspaces characterized by degree $M = m + n$ and of dimension $M + 1$. For any given $M = m + n$ the eigenvalue problem can be solved with only the corresponding sub-matrix. Taking $M = 1$ as an example, the submatrix in question is

$$\begin{pmatrix} -\frac{5}{6} & -\frac{1}{6} \\ -\frac{1}{6} & -\frac{5}{6} \end{pmatrix}$$

which has $M + 1 = 2$ eigenvalues.

Solving the eigenvalues for the $M = 3$ submatrix (4×4) is quite straightforward, but to completely determine the eigenvector involves the entire 10×10 matrix. The results, i.e., the $M = 3$ Appel polynomials, are listed in Table 6 on page 89 along with the $M < 3$ Appel polynomials.

Table 6. Appel Polynomials of Degrees up to Three

n	$-\lambda_n$	c_{00}	c_{10}	c_{01}	c_{20}	c_{11}	c_{02}	c_{30}	c_{21}	c_{12}	c_{03}
0	-1	1									
1	$\frac{2}{3}$		1	-1							
2	1	2	-3	-3							
3	$\frac{5}{3}$	2	-7	-7	8	4	8				
4	$\frac{7}{3}$		1	-1	$-\frac{4}{3}$		$\frac{4}{3}$				
5	$\frac{5}{2}$	2	-7	-7	$\frac{14}{3}$	14	$\frac{14}{3}$				
6	2.58	-0.119	0.715	0.715	-1.52	-1.89	-1.52	1	1.58	1.58	1
7	2.88	-0.447	2.68	2.68	-3.48	-13.7	-3.48	1	11.4	11.4	1
8	3.70	0	0.394	-0.394	-1.18	0	1.18	1	$-.0921$	.0921	-1
9	2.58	0	0.497	-0.497	-1.49	0	1.49	1	1.45	-1.45	-1

$$\tilde{\varphi}_n \sim \sum_{i,j} c_{ij} x_1^i x_3^j$$

If the $p = 3$ moments were known the nucleon wave function could be uniquely determined up to cubic terms. One of the properties of Appel polynomials is zero projection on lower moments. For example, $p \leq 2$ moments of level-3 Appel polynomials (cubic) are all zero. Therefore, adding high level polynomials to the model wave function will not affect its $p \leq 2$ moments. For the analysis of $p = 3$ moments the best model wave function to use is naturally

$$\varphi_{\Lambda}(x) = \varphi_N(x) + \varphi_{asy}(x) \sum_{6}^{9} C_n P_n(x), \tag{5.26}$$

where $\varphi_N(x)$ is the quadratic (KS) wave function.

The quadratic wave function $\varphi_N(x)$ has finite $p = 3$ moments. If the coefficients $C_6 - C_9$ are selected such that $p = 3$ moments for φ_{Λ} vanish, it will result in a very huge correction to the wave function and explode all predictions. A careful study of each independent $p = 3$ moment shows that the perturbative QCD predictions cannot afford a 10% change in $p = 3$ moments. Table 7 on page 91 contains the results. It is inevitably true that QCD predictions are very sensitive to $p = 3$ moments. In contrast, they are quite insensitive to $p \leq 2$ moments as is shown in Section 5.2.

There is no forcible way to put any constraint on the $p = 3$ moments unless it comes from an established theory or experiment. On general physical grounds, though, one expects that the true wave function should be smooth rather than bumpy. With this consideration, $C_6 - C_9$ can be uniquely determined by maximizing the smoothness of φ_{Λ}. Mathematically, it is equivalent to minimizing the following expression:

$$I(C_6, C_7, C_8, C_9) = \int_0^1 d_3x |\nabla \varphi_{\Lambda}(x)|^2. \tag{5.27}$$

The following wave function

Table 7. Sensitivity of Predictions to p = 3 Moments

Moment	$\Delta(\psi \to p\bar{p})$	$\Delta(G_M^p)$	$\Delta(G_M^n)$
300	0.33	0.71	1.47
030	0.03	0.03	0.09
210	0.15	0.28	0.76
120	0.04	0.07	0.21

The percentage variation of perturbative QCD predictions due to 10% change of $p = 3$ moments.

$$\varphi_{ms}(x) = \varphi_{asy}(x)\{12.28 - 46.18x_1 - 44.8x_3 + 65.52x_1x_3 - 16.8x_1x_3(x_1 + x_3) + 69.72x_1^2 - 19.6x_3^3 + 44.52x_3^2 - 2.8x_3^3\} \quad (5.28)$$

is obtained when one minimizes Eq. (5.27).

Table 8 on page 93 presents the $p = 3$ moments for both φ_N and φ_{ms} and Table 9 on page 94 presents predictions of them. It can be seen from Table 8 on page 93 that φ_N and φ_{ms} have nearly the same $p = 3$ moments. Noting the sensitivity on $p = 3$ moments, the slight differences could still be significant. Table 9 on page 94 shows that with φ_{ms} and $\alpha_s = 0.32$ the predictions for $\mathrm{br}(\psi \to p\bar{p})/\mathrm{br}(\psi \to e^+e^-)$ and $G_M^{p,n}$ differ slightly from the predictions with φ_N and $\alpha_s = 0.3$. It also shows a 20% improvement in $\gamma\gamma \to p\bar{p}$ prediction.

The maximum-smoothness wave function φ_{ms} could be an alternative to the quadratic wave function. It accounts for $p = 3$ moments in some way and contains all cubic terms. One must be cautious, however, since it is only a fine version of the quadratic wave function because truncating high order terms also implies smoothness. Furthermore, the maximum-smoothness is just a general physical consideration. The smoothest wave function, though, is the asymptotic form $x_1x_2x_3$ in which one only needs the first Appel polynomial $P_0(x) = 1$. The true wave function is obviously not as smooth as φ_{asy}. The $p \leq 2$ moments introduced asymmetry into the wave function. It is intuitively helpful to determine at which level of p the moments contribute most of the asymmetry to the wave function. Supposing that only $p \leq 1$ moments are known, it is interesting to see what $p = 2$ moments one can get from the same maximum-smoothness procedure. If the $p = 2$ moments obtained from the maximum-smoothness constraint agree well with that from sum-rule cal-

Table 8. The p = 3 moments of KS and Its Alternative Wave Functions

$n_1n_2n_3$	φ_N	φ_{ms}	φ_{fit}
300	2.33e−1	2.32e−1	2.33e−1
030	5.73e−2	5.77e−2	6.81e−2
003	8.13e−2	8.19e−2	8.57e−2
210	5.93e−2	5.99e−2	6.09e−2
201	5.73e−2	5.79e−2	5.65e−2
120	3.00e−2	2.96e−2	2.36e−2
102	3.20e−2	3.15e−2	2.80e−2
021	2.67e−3	2.79e−3	−1.71e − 3
012	6.67e−3	6.63e−3	6.27e−3
111	1.07e−2	1.06e−2	1.54e−2

Table 9. Predictions with KS and the Maximum-Smooth Wave Functions

wfn\proc	α_s	$\psi \to p\bar{p}$	G_M^p	G_M^n	$\gamma\gamma \to p\bar{p}$
φ_N	0.30	0.94	1.07	0.88	0.545
φ_{ms}	0.30	0.96	1.20	1.04	0.509
φ_{ms}	0.31	1.00	1.01	0.77	0.580
φ_{ms}	0.32	1.09	1.07	0.82	0.659

Table 10. The p = 2 Moments of KS and Linear Wave Functions

$n_1n_2n_3$	φ_N	φ_{linear}	φ_{ms2}
200	3.50e−1	3.05e−1	3.09e−1
020	9.00e−2	5.04e−2	5.18e−2
002	1.20e−1	7.29e−2	7.17e−2
110	1.00e−1	1.19e−1	1.15e−1
101	1.00e−1	1.26e−1	1.25e−1
011	2.00e−2	4.11e−2	4.29e−2

The linear wave function is obtained by truncating quadratic terms from φ_N. φ_{2ms} is determined by the maximum-smoothness procedure from the linear wave function.

culation, the $p = 3$ moments obtained this way may be more trustworthy. However, the calculation does not show a good agreement, as presented in Table 10 on page 95.

QCD predictions with the quadratic wave function for $\psi \to p\bar{p}$ and $G_M^{p,n}$ agree well with experiment, but not for $\gamma\gamma \to p\bar{p}$. Is it possible that the $p = 3$ moments are responsible for this? To explore this possibility, the coefficients $C_6 - C_9$ for the level-3 Appel polynomials are parametrized to fit $\psi \to p\bar{p}$, $G_M^{p,n}$, and $\gamma\gamma \to p\bar{p}$ simultaneously. A 30% error has been attached to the amplitude not to account the experimental error but for reflecting the uncertainties in the theoretical calculation. For the cross sections of $\psi \to p\bar{p}$ and $\gamma\gamma \to p\bar{p}$, this yields a 60% error. With the effective coupling constants, 0.300, 0.306, 0.303 for $\psi \to p\bar{p}$, $G_M^{p,n}$, and $\gamma\gamma \to p\bar{p}$ respectively, the best fit obtained yields a χ^2 of 4.9. The fit is presented in Table 11 on page 97. The reason for using different coupling constant α_s will be discussed in the next chapter. The wave function giving the best fit is

$$\begin{aligned}\varphi_{\text{fit}}(x) = \varphi_{\text{asy}}(x)\{ &-1.70 - 76.65x_1 - 30.64x_2 + 379.49x_1x_2 \\ &+ 148.81x_1^2 - 4.32x_2^2 + 22.68x_3^2 - 310.47x_1^2x_2 \\ &- 322.01x_1x_2^2 - 55.46x_1^3 + 69.87x_2^3\}.\end{aligned} \tag{5.29}$$

The moments of φ_{fit} are given in Table 8 on page 93. Figure 11 on page 98 shows the theoretical predictions with the quadratic and the best-fit cubic wave functions for $\gamma\gamma \to p\bar{p}$. The data [30] is virtually independent of the scattering angle. It is $\sim 36 \pm 12\mu$b GeV[10] in the $2.0 < W_{\gamma\gamma} < 2.4$ GeV range and is $\sim 12 \pm 6\mu$b Gev[10] in the $2.4 < W_{\gamma\gamma} < 2.8$ GeV range. It should be noticed that although the χ^2 value is reasonably good, $\gamma\gamma \to B\bar{B}$ is the major contributor and its predicted value is still below data.

Table 11. Fitting Cubic Wave Function to Existing Data

Process	α_s	Experiment	Theory
$\psi \to p\bar{p}$	0.300	0.00834	0.00630
G_M^n	0.306	−0.585	−0.457
G_M^p	0.306	1.17	1.52
$\gamma\gamma \to p\bar{p}$	0.303	12 ± 6	1.13

$C_6 = 40.47$ $C_7 = -33.26$ $C_8 = -62.67$ $C_9 = 0$

$\chi^2 = 4.9$

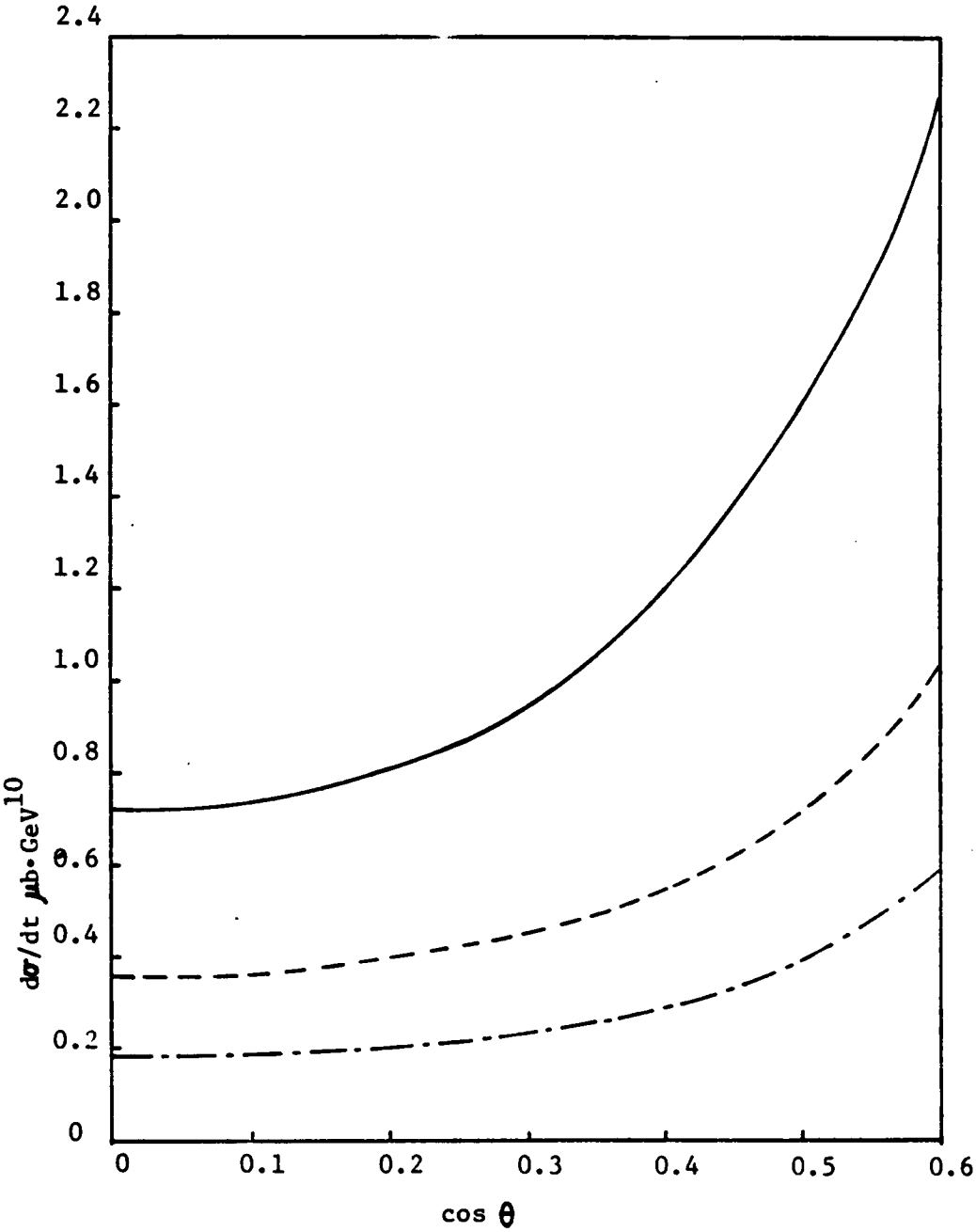

Figure 11. **Predictions for Photon Annihilation to Baryon Pairs:** $s^6 d\sigma/dt$ in $\mu b \cdot GeV^{10}$ for $\gamma\gamma \to p\bar{p}$ using the quadratic (KS) wave function (dashed line), using the best-fitted cubic wave function (solid line), and for $\gamma\gamma \to \Delta^{++}\bar{\Delta}^{++}$ (dot-dashed) line.

While the prediction for $\gamma\gamma \to p\bar{p}$ is below data, it is important and interesting to study the cross sections for $\gamma\gamma \to \Delta^{++}\bar{\Delta}^{++}$ and other hyperon pairs and the ratios of those cross sections to that of the proton. When the prediction of absolute cross sections is not accurate enough to match data, relative ratios of cross sections for a family of reactions can also provide important information of the theory. Naively, the ratio of the cross sections of $\gamma\gamma \to \Delta^{++}\bar{\Delta}^{++}$ and $\gamma\gamma \to p\bar{p}$ is expected to be $\left[\frac{\text{charge of the } \Delta^{++}}{\text{charge of the proton}}\right]^4 = 16$. By using SU(6) symmetric wave functions the ratio is found to be as large as 50 [21]. With the sum-rule derived wave functions for the Δ's [11]:

$$
\begin{aligned}
|\Delta^{++}_{\frac{1}{2}}> &= \frac{1}{4\sqrt{24}} f_\Delta^{(1/2)} T_\Delta(x)|u_+u_+u_->\\
|\Delta^{++}_{\frac{3}{2}}> &= \frac{1}{6\sqrt{48}} f_\Delta^{(3/2)} \varphi_\Delta^{(3/2)}(x)|u_+u_+u_+>
\end{aligned}
\tag{5.30}
$$

where

$$
\begin{aligned}
&f_\Delta^{(1/2)} = (1.2 \pm 0.2) \times 10^{-2}\text{GeV}^2, \quad f_\Delta^{(3/2)} = 1.4 \times 10^{-2}\text{GeV}^2,\\
&T_\Delta(x) = \varphi_{asy}(x)\left[4.2(x_1^2 + x_2^2) + 2.52x_3^2 - 6.72x_1x_2 + 0.43x_3(x_1 + x_2)\right]\\
&\varphi_\Delta^{(3/2)}(x) \sim \varphi_{asy}(x) = 120x_1x_2x_3,
\end{aligned}
\tag{5.31}
$$

the ratio is found to be as small as 0.5 while experiment [31] gives an upper bound of 3. The result is also shown in Figure 11 on page 98. The dramatic difference between the SU(6) symmetric wave functions and the sum-rule derived wave functions for the ratio of $\sigma(\gamma\gamma \to \Delta^{++}\bar{\Delta}^{++})/\sigma(\gamma\gamma \to p\bar{p})$ indicates some thing of interest but it is still necessary to have the rest of the $\gamma\gamma \to B\bar{B}$ reactions be predicted with sum-rule wave functions before further conclusions can be drawn.

The analysis of the sensitivity of predictions to the nucleon wave function can be summarized as follows: With the quadratic (CZ, KS) wave function and a reasonable choice of the coupling constant, the predictions agree very well with the data on $\psi \to p\bar{p}$ and the nucleon form factors. The same agreement can clearly still be achieved with a cubic wave function of the form of Eq. (5.26) with four free parameters. The question is whether the agreement between the prediction

and the data for $\gamma\gamma \to p\bar{p}$ can be improved by using the cubic wave function, compared to the quadratic wave function, while maintaining agreement within errors for $\psi \to p\bar{p}$ and the form factors. The maximum prediction for $\gamma\gamma \to p\bar{p}$ with a parametrized cubic wave function is found to be about twice as large as the prediction with the quadratic wave function, but still below data. Therefore:

- The uncertainty in the perturbative QCD prediction for $\gamma\gamma \to p\bar{p}$, due to the uncertainty in the nucleon wave function, is at the factor-of-two level. Determination of the next set of moments would therefore be very useful. Since there is no known reason that $\gamma\gamma \to p\bar{p}$ is unusually sensitive to the wave function, without better control of the wave functions, future perturbative QCD predictions for the magnitudes of hadron scattering cross-sections can be trusted at no better than the factor-of-four level, assuming that the contribution to the overall uncertainty due to the wave function is comparable for each of the hadrons.

- The uncertainty in the nucleon wave function is probably not enough to render the theoretical predictions for $\gamma\gamma \to p\bar{p}$ in agreement with the presently available data. However with the best-fitted cubic wave function discussed above, the data are not so far from the prediction as to warrant alarm, considering the proximity of the threshold. Improving the error bars on the differential cross section measurements, studying the energy dependence at fixed angle with $t \sim 2\text{GeV}^2$, resolving the question of the possible importance of resonances, and making the measurements available for all $\gamma\gamma \to B\bar{B}$ reactions will be the crucial experimental contributions to the question of whether perturbative QCD predictions apply to $\gamma\gamma \to p\bar{p}$ and, in general, to $\gamma\gamma \to B\bar{B}$ in these ranges of energy.

Chapter VI

The Running Coupling Constant

The strength of any interaction is described by a coupling constant. In QCD there are fermion-gluon and gluon-gluon interactions and an effective coupling constant $\bar{g}$ is associated with each vertex for both of them. The QCD effective coupling constant has been discussed in the introduction. Collectively the equations for $\bar{g}^2$ are written again as follows:

$$\begin{aligned}
&\frac{d\bar{g}^2}{dt} = \bar{g}\beta(\bar{g}), \quad \bar{g}(t=0) = g, \quad t = \ln(Q^2/\mu^2), \\
&\beta(g) = -\beta_0\frac{g^3}{16\pi^2} - \beta_1\frac{g^5}{(16\pi^2)^2} - \ldots, \\
&\beta_0 = 11 - \frac{2}{3}n_f, \text{ and } \beta_1 = 102 - \frac{38}{3}n_f.
\end{aligned} \tag{6.1}$$

As depicted in Figure 12 on page 102 a fermion-gluon vertex as well as a gluon-gluon vertex can have one or more loop corrections and they are associated with g, g^3, and g^5, respectively. These

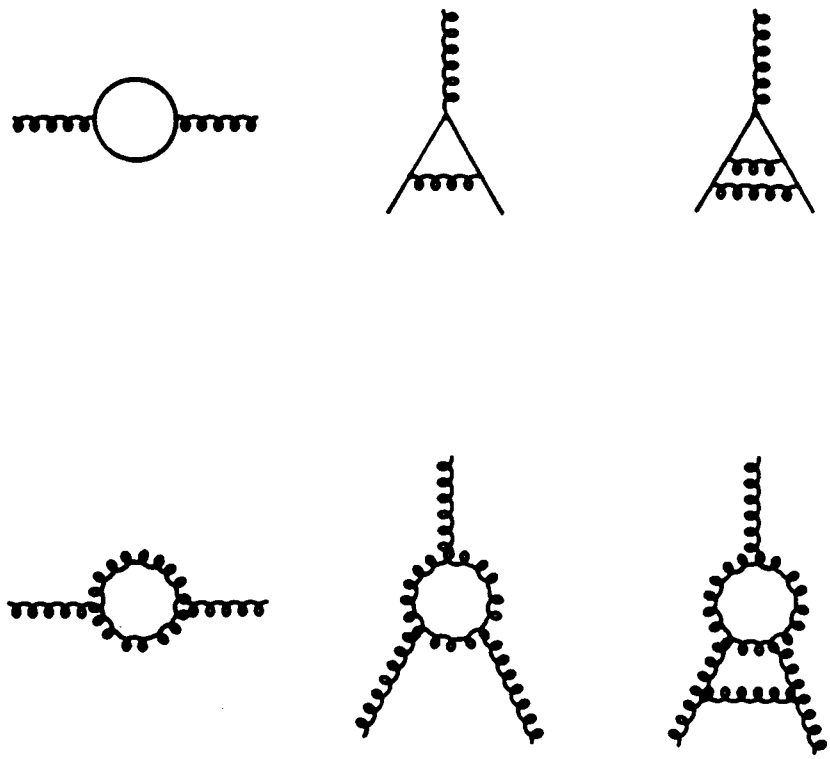

Figure 12. Loop Corrections to Vertices

corrections are described by the perturbation series of the function β of Eq. (6.1). To the first order in g, $\beta = 0$, so that $\bar{g} = g$ and is Q^2-independent. Working to the first and second loop corrections and recalling the definition $\alpha_s = \bar{g}^2/4\pi$, one obtains

$$\begin{aligned} \alpha_s(Q^2) &= \frac{4\pi}{\beta_0 \ln(Q^2/\Lambda^2)} \quad \text{and} \\ \alpha_s(Q^2) &= \frac{4\pi}{\beta_0 \ln(Q^2/\Lambda^2) + (\beta_0/\beta_1) \ln \ln(Q^2/\Lambda^2)}, \end{aligned} \tag{6.2}$$

respectively, and the scale parameter Λ is defined by

$$\Lambda^2 = \mu^2 \exp[-(16\pi^2/\beta_0 g^2)]. \tag{6.3}$$

With the running coupling constant defined, one can work with perturbative QCD expansions to all orders of it. It is instructive to distinguish the QCD prediction's order of $\bar{g}$ and the order of corrections contained in $\bar{g}$ itself. The coupling constant $\bar{g}$ is associated with a vertex; it can constrain one or more loop corrections of the vertex. The high order corrections for a QCD prediction are contributed by, e.g., the one loop correction to fermion or gluon propagator, or non-valence "sea" quarks.

In perturbation theory an observable ρ can generally be written as

$$\rho = C_0 \alpha_s(Q^2) \left[1 + C_1(Q^2) \frac{\alpha_s(Q^2)}{\pi} + C_2(Q^2) \frac{\alpha_s^2(Q^2)}{\pi^2} + \ldots \right]. \tag{6.4}$$

The coefficients $C_i(Q^2)$ are dependent on the form of α_s (renormalization scheme) and the scale of Q. The calculation for an observable must be independent of the choices of the scheme and scale if all perturbation orders are kept and this requirement uniquely defines the coefficients C_i. For finite-order analysis, on the other hand, the calculation is scheme- and scale-dependent. In fact,

one can set $C_i(Q^2)$ to any value simply by rescaling Q^2 or redefining α_s. Therefore, for a consistent calculation both the scheme and the scale must be fixed.

There are several schemes to choose from and the modified minimum subtraction [31] $\overline{\text{MS}}$ is chosen in this study, which is characterized by

$$\Lambda_{\text{QCD}} = \Lambda_{\text{MS}}.$$

As pointed out in the introduction the Λ_{QCD} dependence of the predictions is unknown for exclusive processes involving baryons. Because of the lack of loop calculations for these processes, it is not yet possible to determine Λ_{QCD}. On the other hand, there have been several calculations to determining Λ_{QCD} from $e^+e^- \rightarrow$ three-jets measurement [32]. It is interesting to see, in the absence of a Λ_{QCD} directly determined from the baryon processes, what value of Λ_{QCD} gives the best predictions to those well-studied reactions such as $\psi \rightarrow p\bar{p}$ and the nucleon magnetic form factors, and if it agrees with the Λ_{QCD} determined from three-jets.

Before studying the Λ_{QCD}-dependence the scale ambiguity must be solved. A procedure for fixing the scale of Q has been suggested by Brodsky, Lepage, and Mackenzie [33]. The essence of the procedure is to choose a scale Q^* such that both Q^* and C_i^* are independent of the number of flavors n_f. The perturbation expansion, Eq. (6.4), is then replaced by:

$$\rho = C_0\alpha_s(Q^{*2})\left[1 + C_1^*\frac{\alpha_s(Q^{*2})}{\pi} + C_2^*\frac{\alpha_s^2(Q^{*2})}{\pi^2} + \ldots\right]. \tag{6.5}$$

Physically, it has an interpretation of absorbing quark vacuum polarization into Q^{*2}. For exclusive processes and the $\overline{\text{MS}}$ scheme Brodsky *et al* found that $Q^* = e^{-5/6}Q \sim 0.43Q$ so that

$$\alpha_s(Q^2) = \alpha_{s\overline{\text{MS}}}(e^{-5/3}Q^2) \sim \alpha_{s\overline{\text{MS}}}(0.18Q^2), \tag{6.6}$$

where $\alpha_{s\overline{MS}}$ is the same one as given in Eq. (6.2). It should be warned that this method does not apply to gluon-gluon vertices.

Unlike QED where the running coupling constant has an upper bound $\frac{1}{137}$, the QCD running coupling constant does not have an upper bound. Furthermore, the functional form of the running coupling constant, Eq.(6.2), is only meaningful at large Q^2. When one integrates the scattering amplitude over the quark momentum distribution amplitude, the momentum fraction of each quark goes from 0 to 1 and, thus, Q^2 for gluon propagators are not large at some points. Although there are more elegant means to treat this problem and it is also a topic for future study, the simplest way to treat this is to impose an effective upper bound for the running coupling constant. Therefore, where should the upper bound be is the question that must be answered before the running coupling constant can be used for predictions.

In order to study these questions the running coupling constant is rewritten in a more suitable form:

$$\alpha_s(Q^2) = \frac{4\pi}{\beta_0 \ln(Q^2/c_1 s)}, \tag{6.7a}$$

or, including the next order correction to the vertex,

$$\alpha_s(Q^2) = \frac{4\pi}{\beta_0 \ln(Q^2/c_1 s) + (\beta_0/\beta_1) \ln \ln(Q^2/c_1 s)}, \tag{6.7b}$$

when $\alpha_s \leq c_2$ or $\alpha_s = c_2$ otherwise. Here, $c_1 = \kappa \Lambda^2/s$ and κ is the value that fixes the scaling ambiguity and c_2 is the effective upper bound.

Table 12. Predictions with different choices of the coupling constant

c_1	c_2	$\psi \to p\bar{p}$	G_M^2	Λ(MeV)	k_c^2/s
0.004	0.310	0.77	1.14	85	0.104
0.009	0.305	0.85	1.10	130	0.243
0.016	0.300	0.90	1.07	170	0.448
0.020	0.300	0.92	1.07	190	0.560
f.c.c.	0.300	0.94	1.07	—	—

Four sets of $\{c_1,c_2\}$ are listed. The prediction with a fixed coupling constant (f.c.c.) is also listed in the last line.

QCD predictions for $\psi \to p\bar{p}$ and $G_M^{p,n}$ are calculated with different set values of c_1 and c_2. For $\psi \to p\bar{p}$, α_s is fixed at 0.18 for gluons attached on the charm quark [21]. Table 12 on page 106 presents several sets which give good agreement with data. Taking $\kappa \sim \frac{1}{0.18} \sim 5.6$ as advocated in reference [33], $c_1 = 0.02$ corresponds to $\Lambda \cong 190$Mev at $s = 10\text{Gev}^2$, which agree very well with $\Lambda = 200$Mev measured from three-jets experiment.

The running coupling constant is an approximation for loop corrections. It has the advantage of including some higher order effects in a very convenient way and provides a path for studying the Λ-dependence of baryon processes. On the other hand, it creates integration problem so that an artificial upper bond has to be imposed on it. Furthermore, it destroys the gauge invariance of the amplitude because the amplitude is composed of only tree diagrams. The amplitude is indeed gauge invariant with a fixed coupling constant. Attaching a running coupling constant is equivalent to partially including loop diagrams so that the amplitude can no longer be gauge invariant. Fortunately, Table 12 on page 106 shows that fixing the coupling constant at its cut-off (upper bound) yields equivalently good predictions. It indicates that the running coupling constant does not really run at energies of $s \sim 10\text{GeV}^2$. Therefore, the running coupling constant can be well replaced by a fixed effective coupling constant.

Since the running coupling constant is a function of k^2 of the gluon propagator, the effective coupling constant must be related to the average of k^2 for a given process. The simplest way to estimate the averaged k^2 is to set all momentum fractions of external quarks to $\frac{1}{2}$ or $\frac{1}{3}$ if the quark is a constituent of a meson or a baryon, respectively. The averaged k^2 can then be obtained since it is always an expression in terms of the momentum fractions of external quarks. With all the diagrams evaluated for a given process, however, the averaged k^2 can be determined in a much more precise fashion.

The first method gives a simple averaged absolute value of k^2 for all gluon propagators of all diagrams. It first adds up $|k^2|$ for all gluons of each diagram, sums them over all diagrams, finds the average by dividing by the total number of gluon propagators, and then integrates the average over momentum fractions of external quarks. The average obtained this way is noted as $\overline{|k^2|}$. The second method gives a weighted average of $|k^2|$ for all gluons. Suppose that an amplitude is given by

$$\int d_3x d_3y[\varphi_0(x)\varphi_0(y)A_0(x,y) + \varphi_1(x)\varphi_1(y)A_1(x,y) + ...]$$

and the weighted average is defined as

$$<|k^2|> \sim \int d_3x d_3y[\varphi_0(x)\varphi_0(y)k^2_{A0}(x,y) + \varphi_1(x)\varphi_1(y)k^2_{A1}(x,y) + ...], \tag{6.7}$$

where k^2_{Ai} is the averaged $|k^2|$ for all gluon propagators of the quark amplitude A_i.

Table 13 on page 109 contains both weighted and unweighted $|k^2|$ and also the averages of both k_{min} and k_{max} of each diagram. Comparing the averaged $|k^2|$ with the onset of α_s listed in the last column, k_c^2/s, of Table 12 on page 106, it can be seen again that the averaged $|k^2|$ are well below the onset of α_s and it is confirmed that the running coupling constant does not run.

The fixed effective coupling constant for different processes and with different k^2 averaging regimes are presented in Table 14 on page 110. It is set to 0.3 for $\psi \rightarrow p\bar{p}$ to serve as a reference point since the value of Λ_{QCD} is assumed unknown. The coupling constants obtained from the unweighted average, $\overline{|k^2|}$, are used in the fit discussed in the last chapter.

Table 13. Averaged k^2 of Gluon Propagators

Process	s/GeV^2	$\overline{\lvert k^2\rvert}/s$	$<\lvert k^2\rvert>/s$	$\overline{\lvert k^2_{\min}\rvert}/s$	$<\lvert k^2_{\min}\rvert>/s$	$\overline{\lvert k^2_{\max}\rvert}/s$	$<\lvert k^2_{\max}\rvert>/s$
$\psi \to p\bar{p}$	9.6	0.11	0.12	0.02	0.011	0.24	0.31
$G_M^{J^{PC}}$	10	0.095	0.064	0.041	0.018	0.15	0.11
$\gamma\gamma \to p\bar{p}$	5.76	0.18	0.16	0.094	0.068	0.28	0.25
$\gamma\gamma \to p\bar{p}$	4	0.18	0.16	0.094	0.068	0.28	0.25

$k^2_{\min}$ and $k^2_{\max}$ for $\gamma\gamma \to p\bar{p}$ are averaged at cos = 0.4.

Table 14. Fixed Effective Coupling Constant

		$\alpha_s(\ )$					
Process	s/GeV^2	$\overline{\lvert k^2\rvert}$	$<\lvert k^2\rvert>$	$\overline{\lvert k^2_{min}\rvert}$	$<\lvert k^2_{min}\rvert>$	$\overline{\lvert k^2_{max}\rvert}$	$<\lvert k^2_{max}\rvert>$
$\psi \to p\bar{p}$	9.6	0.300	0.300	0.300	0.300	0.300	0.300
$G_M^{p,n}$	10	0.306	0.363	0.248	0.261	0.344	0.429
$\gamma\gamma \to p\bar{p}$	5.76	0.303	0.322	0.233	0.220	0.336	0.383
$\gamma\gamma \to p\bar{p}$	4	0.339	0.363	0.253	0.237	0.383	0.448

To conclude this chapter, the running coupling constant is effectively fixed at $s \sim 10\text{GeV}^2$ for the best choice of parameters $c_1 = 0.02$ and $c_2 = 0.3$; the value of c_1 indicates $\Lambda_{QCD} = 190\text{MeV}$. The fixed effective coupling constants determined by the averaged $|k^2|$ gives a more tailored treatment for the coupling strength process by process and also yields good agreement of the predictions with the data on $\psi \to p\bar{p}$ and the nucleon form factors. There remain some questions that must be studied further, though. Table 14 on page 110 clearly shows that different averaging regime for $|k^2|$ yields different values of the effective α_s. It is important to understand and determine which one can best represent the actual physical situation. On the running coupling constant side, more understanding must be acquired on the origin of the cut-off c_2 and its dependence on s and Q^2. When the running coupling constant is attached to diagrams the meaningfulness of the functional form of it, Eq. (6.2), and the treatment of it must be studied at low $|k^2|$ values. Only with the understanding of all these questions can the running coupling constant really run and provide a more reliable method for studying the Λ_{QCD}-dependence of baryon processes.

Chapter VII

Meson-Baryon Wide-Angle Scattering

The development of the computer program DIAG has permitted perturbative QCD calculations for quark scattering amplitudes for a wide range of exclusive reactions. To obtain cross sections for any of these reactions, however, requires integration of the quark amplitudes over the wave functions of the hadrons involved in the scattering. For any scattering process that involves four or more quark lines the quark scattering amplitudes contain singularities. As depicted in Figure 13 on page 113, when the external momenta of both mesons are symmetrically configured, the momentum of the marked gluon vanishes and, therefore, causes the amplitude to be infinit. For example, the diagram is singular if all the external momenta have a fraction of $\frac{1}{2}$. This type of singularities are identified as Lanshoff singularities.

Solving the integration problem by itself is theoretically interesting because the zero-momentum propagator is a result of free quarks. It, in turn, is a result of the fact that perturbative QCD does

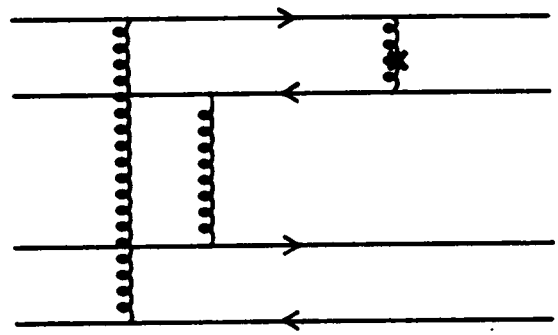

Figure 13. Lanshoff Singularity

not enforce confinement [34]. To understand the theory underlying the treatment of the singularities requires much more theoretical effort and progress. Nevertheless, the integration can be carried out by simply cutting off the propagator momenta and many important questions can be studied even without such theoretical progress.

The least complicated scattering reaction that has not been previously calculated and involves Lanshoff singularities is meson-meson scattering. Although it is very simple and convenient to work with, the information that can be obtained from studying it is far from adequate. For spin-0 mesons there are only two independent quark scattering amplitudes as depicted in Figure 6 on page 36 in Chapter 3. Before the singularities can be well treated, predictions for absolute cross sections are not possible and only ratios can be calculated. For a set of two quark amplitudes only one ratio exists. Experimentally, it is also difficult to reach very high energies for meson-meson scattering and to extract ratios of the quark amplitudes. Meson-baryon scattering, on the other hand, has a much richer set of reactions and quark amplitudes. For example, there are sixty-six reactions of the type $\{\pi^{\pm}, K^{\pm,0}\} + p \rightarrow \{\pi, K, \eta, \eta', \varphi\} + \{B_8, B_{10}\}$ [35]. Figure 7 on page 38 in Chapter 3 contains these quark amplitudes. The cross sections of eleven reactions out of the sixty-six have been measured at $s = 20GeV^2$ and $-t = 9GeV^2$ and ratios of quark amplitudes have been extracted [36]. With this rich set of quark amplitudes and measurements many interesting questions can be studied concerning testing perturbative QCD.

Solving the integration problem is also practically difficult. For the meson-baryon scattering case the integration is six dimensional with a huge integrand function for the amplitude formula. For the presently accessible computing power it is practically impossible to reach high numerical precisions such as 10%. For instance, an integration with the four-point Gauss formula for each dimension takes twenty-five cpu minutes to complete on a VAX-11/780. Therefore, the first important question is if the integrations are numerically reliable. It is conceivable that the ampli-

tudes are not smooth functions because they are singular although regulated. No physics can be extracted from a such calculation unless the reliability is established.

The next important question to study is the sensitivity of the calculation to the cut-off values. Without further and deeper theoretical understanding the physical cut-off cannot be obtained from theory. However, it can be argued that the propagator cut-off should be related to the quark mass or Λ_{QCD}. Supposing that Λ_{QCD} is between 0.1 GeV $\sim$ 0.3 GeV and the cut-off $k_c^* \sim \Lambda_{QCD}$, the dimensionless cut-off, k_c^*/s, should be in the range of $5 \times 10^{-4} \sim 5 \times 10^{-3}$ for $s = 20\text{GeV}^2$. By using the scale-fixing argument advocated in reference [33] and discussed in Chapter 6, $k^{*2} \sim 0.18k^2$, so that k_c^2/s is of $3 \times 10^{-3} \sim 3 \times 10^{-2}$. This argument is, of course, far from adequate to reveal the underlying physics, but it sets a cut-off reference for numerical integrations which, in turn, if reliable, can yield important information on questions such as at which cut-off values the singular part of the amplitude dominates, at what cut-off values the singular and non-singular parts are comparable, and when the ratios of amplitudes are relatively insensitive to the cut-off values.

The sensitivity of physical predictions to the choices of hadronic wave functions has long been interesting in perturbative QCD. As discussed in chapter 5 the theoretical predictions for the nucleon form factor and photon annihilation to baryon-antibaryon pairs are very much dependent on the choices of the wave functions. It is certainly very interesting to see if the predictions for meson-baryon scattering are wave function sensitive. Since different wave functions differ significantly from each other, it is also interesting to see how the cut-off dependence of the predictions is altered by using different wave functions.

The flavor-spin state for an SU(6) symmetric wave function for the proton can be written as

$$|p_+> = \frac{1}{\sqrt{6}}[2|u_+u_+d_-> - |u_+d_+u_-> - |d_+u_+u_->]. \tag{7.1}$$

Projecting relevent quark amplitudes for a given process onto the SU(6) flavor-spin state Equation (7.1), the scattering amplitudes can be obtained. For $\pi^+p \to \pi_+p$ and $\pi^-p \to \pi^-p$ the scattering amplitudes are, respectively:

$$\begin{aligned} A_{\pi^+p} &= \frac{1}{12}[6A_0 + 6_0 + 1A_2 + 4A_3 + 5A_4 + 2A_5 + 1A_6 + 2A_7 + 2A_8] \text{ and} \\ A_{\pi^-p} &= \frac{1}{12}[6A_0 + 6_0 + 5A_2 + 2A_3 + 1A_4 + 4A_5 + 1A_6 + 2A_7 + 2A_8]. \end{aligned} \tag{7.2}$$

A complete scattering amplitudes for all the sixty-six reactions can be found in reference [35]. The sum-rule derived wave function for the proton is not SU(6) symmetric [10]; it can be written in the form

$$|p_+> \sim T(x)|u_+u_+d_-> + B(x)|u_+d_+u_-> + C(x)|d_+u_+u_->. \tag{7.3}$$

For the pions the sum-rule wave functions are

$$\begin{aligned} |\pi^+> &\sim \varphi_\pi[|u_+\bar{d}_+> + |u_-\bar{d}_->] \text{ and} \\ |\pi^-> &\sim \varphi_\pi[|d_+\bar{u}_+> + |d_-\bar{u}_->]. \end{aligned} \tag{7.4}$$

Projections of the quark scattering amplitudes $A_0 - A_8$ onto the wave function Equations (7.3,4) for elastic π^+p and π^-p scatterings are presented in Table 15 on page 117. The scattering amplitude is obtained by summing up the amplitudes of the corresponding column. The difference between the sum-rule scattering amplitudes and the SU(6) symmetric scattering amplitudes can be immediately recognized.

Finally and most interesting is the question of which topologies of the quark amplitudes contribute dominantly and how the ratios of the quark amplitudes compare with experiment. As mentioned

Table 15. Projection of Quark Amplitudes onto Sum-Rule Wave Functions

$\pi^+p \to \pi^+p$	$\pi^-p \to \pi^-p$
$<p,\pi^+\|A_0\|p,\pi^+> = \int(TT + BB + CC)\varphi_\pi\varphi_\pi A_0[dx] = <p,\pi^-\|A_0\|p,\pi^->$	
$<p,\pi^+\|A_1\|p,\pi^+> = \int(TT + BB + CC)\varphi_\pi\varphi_\pi A_1[dx] = <p,\pi^-\|A_1\|p,\pi^->$	
$<p,\pi^+\|A_2\|p,\pi^+> = \int BB\varphi_\pi\varphi_\pi A_2[dx]$	$<p,\pi^-\|A_2\|p,\pi^-> = \int(TT + CC)\varphi_\pi\varphi_\pi A_2[dx]$
$<p,\pi^+\|A_3\|p,\pi^+> = \int TT\varphi_\pi\varphi_\pi A_3[dx]$	$<p,\pi^-\|A_3\|p,\pi^-> = \int(BB + CC)\varphi_\pi\varphi_\pi A_3[dx]$
$<p,\pi^+\|A_4\|p,\pi^+> = \int(TT + CC)\varphi_\pi\varphi_\pi A_4[dx]$	$<p,\pi^-\|A_4\|p,\pi^-> = \int BB\varphi_\pi\varphi_\pi A_4[dx]$
$<p,\pi^+\|A_5\|p,\pi^+> = \int(BB + CC)\varphi_\pi\varphi_\pi A_5[dx]$	$<p,\pi^-\|A_5\|p,\pi^-> = \int TT\varphi_\pi\varphi_\pi A_5[dx]$
$<p,\pi^+\|A_6\|p,\pi^+> = \int CC\varphi_\pi\varphi_\pi A_6[dx]$	$<p,\pi^-\|A_6\|p,\pi^-> = \int(TT + BB)\varphi_\pi\varphi_\pi A_6[dx]$
$<p,\pi^+\|A_7\|p,\pi^+> = \int BT\varphi_\pi\varphi_\pi A_7[dx]$	$<p,\pi^-\|A_7\|p,\pi^-> = \int TB\varphi_\pi\varphi_\pi A_7[dx]$
$<p,\pi^+\|A_8\|p,\pi^+> = \int TB\varphi_\pi\varphi_\pi A_8[dx]$	$<p,\pi^-\|A_8\|p,\pi^-> = \int BT\varphi_\pi\varphi_\pi A_8[dx]$

$$\text{Amp} = \sum_i <p,\pi|A_i|p,\pi>$$

earlier, the cross sections of eleven meson-baryon scattering reactions have been measured at $s = 20\text{GeV}^2$. As pointed out in reference [36], the cross section of $\pi^+p \to \pi^+p$ is two and half times as large as the cross section for $\pi^-p \to \pi^-p$, and the cross section for $\pi^+p \to \pi^+\Delta^+$ is large. Both of the data disagree with the predictions based on the Massive Quark Model formulation [37]. It is very interesting to see if perturbative QCD calculations can produce these observations. The authors of reference [36] grouped the thirteen quark amplitudes into four groups: gluon exchange (A_0 and A_1), quark interchange (A_4 and A_5), annihilation (A_2 and A_3) and combinations of annihilation and quark interchange (A_{6-12}). By using the symmetric SU(6) flavor-spin state for the baryon and assuming $A_0 \sim A_1$, $A_2 \sim A_3$, $A_4 \sim A_5$, and $A_6 \sim A_7 \sim ... \sim A_{12}$, it is concluded that only the quark interchange and gluon exchange quark topologies are significant and the quark interchange is three times as large as the gluon exchange.

The quark amplitude A_1 is integrated with a wide range of cut-off values. As shown in Table 16 on page 120 the integrated amplitude is inversely proportional to the cubic of the cut-off at small cut-off's. Since most of the diagrams have three factors in the denominator, it is clear that the singular diagrams dominate the small cut-off region. While the cut-off increases the singular part becomes comparable with the nonsingular part and the amplitude reverses sign. Since a the dimensionless cut-off should be $0.003 \sim 0.03$ and a reasonable cut-off will not let the singular part dominate and let the ratios of amplitudes be very sensitive to it, a range from 0.005 to 0.06 is chosen for the dimensionless cut-off for integrating the quark amplitudes. Table 17 on page 121 presents the numerical integrations of $A_0 - A_8$ with sum-rule wave functions for $\pi^\pm p \to \pi^\pm p$ at 90 degree in the c.m. frame. Table 18 on page 122 contains the same integration with asymptotic wave functions, and Table 19 on page 123 lists the integrations with equipartition wave functions. All integrations are evaluated by the Gauss formula with four points for each dimension. The numerical reliability is checked by using the eight points per dimension Gauss formula for the same integrations. Since an eight points per dimension integration takes eight and one-half cpu hours on a VAX 8600, only A_0 is integrated with sum-rule wave functions for cut-off 0.01, 0.03 and 0.05. The

results are -5.35×10^3, 4.89×10^4 , and 2.29×10^5 respectively. Comparing them with their counterparts in Table 17 on page 121, the discrepancy at cut-off equals 0.01 is huge and is 92% and 40% for cut-off equals 0.03 and 0.05 respectively.

For the lower cut-off's the calculation can not be trusted. For the upper ones the numerical precision of 40% is not good enough for a more precise and detailed study but is still acceptable for the preliminary analysis given here. The integration results clearly show that amplitude ratios are less sensitive at large cut-off values. Although the underlying theory governing the cut-off is not clear, the calculations give a lower bound of $\sim$ 0.02 for the dimensionless cut-off at $s = 20\text{GeV}^2$.

The integrated amplitudes are also dependent on the choices of wave functions significantly. Both sum-rule and asymptotic wave functions predict an unexpected considerable difference between A_0 and A_1. Unfortunately this inequality can not be resolved by experiment since for any meson-baryon reactions they either both contribute or both do not. The equipartition wave function predicts A_0 and A_1 dominance and the asymptotic wave function predicts A_0 dominance. Although the predictions with the asymptotic wave function accounts for the inequality of the π^+p and π^-p cross section, it can not explain the the large cross section of $\pi^+p \to \rho^+p$ and $\pi^+p \to \pi^+\Delta^+$, which do not contain contributions from A_0 and A_1. The predictions with sum-rule wave functions are most rich in structure. The integration shows dominance of A_4 and A_0 for π^+p and A_2 and A_0 for π^-p. It also agrees with the measured π^+p and π^-p inequality.

Table 16. The Cut-off Spectrum of A1

cut-off	$<\pi,p\|A_1\|\pi,p>$
1.0e − 6	−1.38e + 18
1.0e − 5	−1.39e + 15
1.0e − 4	−1.45e + 12
1.0e − 3	−1.63e + 09
5.0e − 3	−1.18e + 07
7.0e − 3	−3.10e + 06
9.0e − 3	−4.78e + 05
9.5e − 3	−1.46e + 05
9.8e − 3	1.07e + 04
1.0e − 2	1.05e + 05
5.0e − 2	3.55e + 04
7.5e − 2	2.00e + 04
1.0e − 1	9.62e + 03

Table 17. Integrated Amplitudes with Sum-Rule Wave Functions

cut-off	$<\pi^{\pm}\|A_0\|\pi^{\pm}>$	$\frac{<\pi^{\pm}\|A_1\|\pi^{\pm}>}{<A_0>}$	$\frac{<\pi^{+}\|A_2\|\pi^{+}>}{<A_0>}$	$\frac{<\pi^{-}\|A_2\|\pi^{-}>}{<A_0>}$
$5e-3$	$-3.52e+6$	3.35	0.22	1.08
$1e-2$	5.84e+5	0.18	−0.36	−2.67
$2e-2$	1.02e+6	0.86	−0.09	−0.86
$3e-2$	5.84e+5	0.76	−0.12	−1.10
$4e-2$	2.46e+5	0.51	−0.15	−1.30
$5e-2$	1.37e+5	0.26	−0.18	−1.40
$6e-2$	1.05e+5	0.23	−0.16	−1.20

$\frac{<\pi^{+}\|A_3\|\pi^{+}>}{<A_0>}$	$\frac{<\pi^{-}\|A_3\|\pi^{-}>}{<A_0>}$	$\frac{<\pi^{+}\|A_4\|\pi^{+}>}{<A_0>}$	$\frac{<\pi^{-}\|A_4\|\pi^{-}>}{<A_0>}$	$\frac{<\pi^{+}\|A_5\|\pi^{+}>}{<A_0>}$
0.23	0.11	7.73	0.57	−0.38
−0.32	−0.15	−6.59	−0.27	
−0.10	−0.05	0.19	0.07	0.20
−0.13	−0.07	1.25	0.16	0.28
−0.16	−0.08	1.50	0.20	0.28
−0.18	−0.08	1.61	0.21	0.26
−0.14	−0.06	1.25	0.17	0.22

$\frac{<\pi^{-}\|A_5\|\pi^{-}>}{<A_0>}$	$\frac{<\pi^{+}\|A_6\|\pi^{+}>}{<A_0>}$	$\frac{<\pi^{-}\|A_6\|\pi^{-}>}{<A_0>}$	$\frac{<\pi^{\pm}\|A_7\|\pi^{\pm}>}{<A_0>}$	$\frac{<\pi^{\pm}\|A_8\|\pi^{\pm}>}{<A_0>}$
−0.42	−0.07	−0.09	0.26	0.25
1.30	0.07	0.09	−0.25	−0.24
0.32	0.02	0.02	0.03	0.03
0.52	0.03	0.02	0.06	0.06
0.55	0.04	0.02	0.10	0.10
0.58	0.05	0.02	0.13	0.14
0.57	0.03	.004	0.13	0.14

The flavor-spin state $|\pi^{\pm}>$ is actually $|\pi^{\pm}p>$; the notation p has been dropped for simplicity.

Table 18. Integrated Amplitudes with Asymptotic Wave Functions

cut-off	A_0	A_1/A_0	A_2/A_0	A_3/A_0
$5e-3$	5.76e+5	−2.07	−0.21	−0.10
$1e-2$	3.14e+5	0.03	−0.12	−0.11
$2e-2$	1.00e+5	0.35	−0.16	−0.19
$3e-2$	3.82e+4	0.16	−0.28	−0.30
$4e-2$	2.36e+4	0.14	−0.29	−0.30
$5e-2$	1.75e+4	0.14	−0.31	−0.27
$6e-2$	1.48e+4	0.22	−0.29	−0.24

A_4/A_0	A_5/A_0	A_6/A_0	A_7/A_0	A_8/A_0
−0.65	−1.30	−0.06	−0.06	−0.06
0.05	−0.10	−0.08	−0.00	0.00
0.23	0.16	−0.08	0.02	0.03
0.42	0.31	−0.09	0.05	0.05
0.37	0.21	−0.12	0.05	0.05
0.27	0.13	−0.14	0.05	0.05
0.19	0.07	−0.15	0.05	0.06

Table 19. Integrated Amplitudes with Equipartition Wave Functions

cut-off	A_0	A_1/A_0	A_2/A_0	A_3/A_0
$5e-3$	$-2.98E+09$	0.89	$5e-4$	-0.03
$1e-2$	$-2.98E+09$	0.89	$-1e-3$	-0.03
$2e-2$	$-1.12E+09$	0.88	-0.09	-0.10
$3e-2$	$-3.59E+08$	0.87	-0.18	-0.17
$4e-2$	$-1.14E+08$	0.83	-0.16	-0.15
$5e-2$	$-4.38E+07$	0.80	-0.10	-0.10
$6e-2$	$-1.90E+07$	0.77	-0.03	-0.04

A_4/A_0	A_5/A_0	A_6/A_0	A_7/A_0	A_8/A_0
-0.36	-0.57	0.17	0.04	0.04
-0.36	-0.57	0.17	0.04	0.04
-0.26	-0.44	0.13	0.03	0.03
-0.13	-0.29	0.08	0.02	0.02
-0.01	-0.21	0.08	0.02	0.02
0.02	-0.22	0.12	0.04	0.04
0.04	-0.26	0.15	0.06	0.06

Table 20. Ratio of Pion-Proton Scattering Amplitudes

cut-off	Sum-rule	Asymptotic	Equipartition
$5e-3$	0.50	1.05	1.04
$1e-2$	0.18	0.88	1.04
$2e-2$	0.64	0.90	1.00
$3e-2$	0.44	0.81	0.95
$4e-2$	0.34	0.79	0.93
$5e-2$	0.26	0.79	0.93
$6e-2$	0.44	0.83	0.93

Ratios of $\mathrm{Amp}(\pi^+p \to \pi^+p)/\mathrm{Amp}(\pi^-p \to \pi^-p)$ evaluated with sum-rule, asymptotic and equipartition wave functions.

Since the ratios of the quark amplitudes extracted from the data in Reference [36] are based on the SU(6) symmetric wave function and the assumption that $A_0 \sim A_1$, $A_2 \sim A_3$, $A_4 \sim A_5$, and $A_6 \sim A_7 \sim A_8$, it is not meaningful to compare them with the calculations now. It is very interesting to see if sum-rule wave functions can predict the large cross section of $\pi^+ p \to \pi^+ \Delta^+$. Besides, the numerical precision of 40% can barely resolve the difference between the $\pi^+ p$ and $\pi^- p$ cross sections. The calculations need to be improved in precision which can only be achieved with supercomputing power. A final conclusion can be drawn after the meson-baryon scattering spectrum is fully analyzed and the numerical accuracy is improved.

Chapter VIII

Conclusion

This dissertation involved the following:

- The computer program DIAG was extensively debugged and tested. Perturbative QCD calculations for quark scattering amplitudes for a wide range of exclusive reactions can now be done with the program. The meson-baryon scattering system is one of the most interesting reactions. To make the amplitude file useful, i.e., compilable, integrable and manageable was made possible with the assistance of the symbolic simplifier which was developed specifically for DIAG. DIAG was also modified and extended to include virtual photons and to test for gauge invariance within arbitrary covariant gauges. The correctness of the computer-generated amplitudes was ensured by extensive hand checking, gauge invariance testing and various symmetry testing.

- The sensitivity of physical predictions to the nucleon wave function was systematically studied. The SU(6) symmetric wave functions were found to be generally not acceptable. The sum-rule derived wave functions yielded good agreement with experiments on the nucleon form factors and the branching ratio of Ψ decay. The uncertainties of the $p \leq 2$ moments were found to be not significant but the undetermined $p \geq 3$ moments yield a factor-of-two difference for the cross section of $\gamma\gamma \rightarrow B\overline{B}$. The cross section for $\gamma\gamma \rightarrow \Delta^{++}\overline{\Delta}^{++}$ was calculated with sum-rule wave functions for Δ^{++}. Calculating the full set of $\gamma\gamma \rightarrow B\overline{B}$ and making corresponding measurements available will be an important test for perturbative QCD.

- The running coupling constant was found to be effectively constant at the current accessible energies and momentum transfer (t = 10GeV^2 ~ 20GeV^2). The value for Λ_{QCD} found from this study is ~ 200 MeV.

- Quark scattering amplitudes for meson-meson scattering and meson-baryon scattering were evaluated. Integrations of the meson-baryon amplitudes were carried out with a series of cut-off values. Three wave functions, sum-rule, asymptotic, and equipartition, were used for the integrations. The numerical precision for four-point Gauss integration is marginal for large cut-off's but is unacceptable for small cut-off's. The dimensionless cut-off, k_c^2/s, was determined to be not smaller then 0.02. Both asymptotic and sum-rule wave functions yield agreement with experiment on the inequality of the π^+p and π^-p cross sections but the computational error is large. While the SU(6) symmetric wave functions can not explain the observed large Δ^+ production, it will be interesting to see if it can be explained by sum-rule wave functions in the future.

In order to be able to predict the absolute cross sections for meson-baryon scattering, the integration problem must be solved. Much theoretical effort is required before the treatment of the

singularity can be understood. Meanwhile, the numerical precision for the integration must also be improved and the full set of all meson-baryon scattering system should be analyzed. With the numerous reactions in the set, many testings can be done for perturbative QCD and much important information and understanding can be obtained from the study.

References

1. E.D. Bloom *et al*, Phys. Rev. Let. **23**, 930 (1969); M. Breidenbach *et at*, Phys. Rev. Let. **23** , 93 (1969).
2. R.P. Feynman, Phys, Rev. Let. **23**, 1415 (1969).
3. M. Gell-Mann, Phys. Rev. **125**, 1067 (1962); G. Zweig, CERN report (unpublished); M. Gell-Mann, Phys. Let. **8**, 214 (1964).
4. D. Gross and F. Wilczek, Phys. Rev. Let. **30**, 1343 (1973); Phys. Rev. **D 8**, 1067 (1962);
5. H.D. Politzer, Phys. Rev. Let. **30**, 1346 (1973); Phys. Rep. **14C**, 129 (1974).
6. *For a review, see* A.J. Buras, Rev. Mod. Phys. **52**, 199 (1980) *and references therein.* **185**, 1975
7. A.H. Mueller, Phys. Rep. **73**, 237 (1981).
8. A. Zee, Phys. Rev. **D 8**, 4038 (1973); *see also* ref. 7.
9. G.P. Lepage and S.J. Brodsky, Phys. Rev. **D 22**, 2157 (1980).
10. V.L. Chernyak and I.R. Zhitnitsky, Nucl. Phys. **B 246**, 52 (1984).
11. G.R. Farrar, H. Zhang, A.A. Ogloblin and I.R. Zhitnitsky, *to be published.*
12. N. Christ, B. Hasslacher and A.H. Mueller, Phys. Rev. **D 6** , 3543 (1972); D.J. Gross and F. Wilczek, Phys. Rev. **D 8** , 3633 (1973); Phys. Rev. **D 9**, 980 (1974); H. Georgi and H.D. Politzer, Phys. Rev. **D 9**, 416 (1974).
13. S. Gupta and A.H. Mueller, Phys. Rev. **D 20**, 118 (1979).
14. V.L. Chernyak and I.R. Zhitnitsky, Yad. Fiz. **31**, 1053 (1980);
15. G.R. Farrar and D.R. Jackson, Phys. Rev. Lett. **43**, 246 (1979).
16. K.G. Wilson, Phys. Rev. **179**, 1499 (1969).
17. J.M. Cornwall and G. Tiktopoulos, Phys. Rev. **D 13**, 3370 (1976).
18. V.L. Chernyak and I.R. Zhitnitsky, Phys. Rep. **112**, 173 (1984).
19. G.R. Farrar and F. Neri, Phys. Lett. **130B**, 109 (1983).
20. P. Cvitanovic, Phys. Rev. **D 14**, 1536 (1976).
21. G.R. Farrar, E. Maina and F. Neri, Nucl. Phys. **B 259**, 720 (1985).
22. G.R. Farrar, *Private communication.*
23. S.J. Brodsky and G.P. Lepage, Phys. Rev. **D 24**, 1808 (1981).
24. G.P. Lepage and S.J. Brodsky, Phys. Rev. Lett. **43**, 545 (1979).
25. E.S. Abers and B.W. Lee, Phys. Rep. **9C**, 1 (1973).
26. T.P. Cheng and L.F. Li, *Gauge Theory of Elementary Particle Physics*, Oxford University Press, (1984).
27. M. Chaichian and N.F. Nelipa, *Introduction to Gauge Field Theories*, Springer-Verlag, (1984).

28. I.D. King and C.T. Sachrajda, *Preprint* SHEP 85/86 - 15 (1986).

29. V.L. Chernyak, A.A. Ogloblin and I.R. Zhitnitsky, *Private communication.*

30. M. Althoff *et al*, Phys. Lett. **130B**, 449 (1983).

31. M Althoff *et al*, DESY preprint 84-015.

32. W. Bardeen, A.J. Buras and T. Muta, Phys. Rev. **D 18**, 3998 (1978).

33. JADE Collab., W. Bartel *et al*, Phys. Lett. **119B**, 239 (1982); MARK J Collab., B Adeva *et al*, Phys. Rev. Lett. **50**, 2051 (1983); G. Wolf, *talk presented at the XIVth International Symposium on Multiparticle Dynamics, Lake Tahoe, Calif. (1983).*

34. S.J. Brodsky, G.P. Lepage and P.B. Mackenzie, Phys. Rev. **D 28**, 228 (1983).

35. G.R. Farrar, *Invited Lecture presented at the Conference on the Intersections between Particle and Nuclear Physics*, May 23-30, 1984.

36. G.R. Farrar, Phys. Rev. Lett. **53**, 28 (1984).

37. A.S. Carroll *et al, Talk presented at the Meeting of APS Division of Particles and Fields*, Jan 14-17, 1987; A.S. Baller, *University of Minnesota dissertation.*

38. G. Nardulli, G. Preparata and J. Soffer, Nuovo Cim. **83A**, 361 (1980), Phys. Rev. **D31**, 626 (1985).

The vita has been removed from the scanned document